National Library of Canada
Canadian Theses Service
Ottawa, Canada
K1A 0N4

Bibliothèque nationale du Canada
Services des thèses canadiennes

CANADIAN THESES

THÈSES CANADIENNES

NOTICE

The quality of this microfiche is heavily dependent upon the quality of the original thesis submitted for microfilming. Every effort has been made to ensure the highest quality of reproduction possible.

If pages are missing, contact the university which granted the degree.

Some pages may have indistinct print especially if the original pages were typed with a poor typewriter ribbon or if the university sent us an inferior photocopy.

Previously copyrighted materials (journal articles, published tests, etc.) are not filmed.

Reproduction in full or in part of this film is governed by the Canadian Copyright Act, R.S.C. 1970, c. C-30.

AVIS

La qualité de cette microfiche dépend grandement de la qualité de la thèse soumise au microfilmage. Nous avons tout fait pour assurer une qualité supérieure de reproduction.

S'il manque des pages, veuillez communiquer avec l'université qui a conféré le grade.

La qualité d'impression de certaines pages peut laisser à désirer, surtout si les pages originales ont été dactylographiées à l'aide d'un ruban usé ou si l'université nous a fait parvenir une photocopie de qualité inférieure.

Les documents qui font déjà l'objet d'un droit d'auteur (articles de revue, examens publiés, etc.) ne sont pas microfilmés.

La reproduction, même partielle, de ce microfilm est soumise à la Loi canadienne sur le droit d'auteur, SRC 1970, c. C-30.

THIS DISSERTATION HAS BEEN MICROFILMED EXACTLY AS RECEIVED

LA THÈSE A ÉTÉ MICROFILMÉE TELLE QUE NOUS L'AVONS REÇUE

NL-339 (r.86/06)

Canada

THE UNIVERSITY OF ALBERTA

Magnetic Signatures of Precursors to Substorm Expansive Phase Activiy

by

Catherine D. de Groot-Hedlin

A THESIS

SUBMITTED TO THE FACULTY OF GRADUATE STUDIES AND RESEARCH

IN PARTIAL FULFILMENT OF THE REQUIREMENTS FOR THE DEGREE

OF Master of Science

IN

Geophysics

Department of Physics

EDMONTON, ALBERTA

FALL 1986

Permission has been granted to the National Library of Canada to microfilm this thesis and to lend or sell copies of the film.

The author (copyright owner) has reserved other publication rights, and neither the thesis nor extensive extracts from it may be printed or otherwise reproduced without his/her written permission.

L'autorisation a été accordée à la Bibliothèque nationale du Canada de microfilmer cette thèse et de prêter ou de vendre des exemplaires du film.

L'auteur (titulaire du droit d'auteur) se réserve les autres droits de publication; ni la thèse ni de longs extraits de celle-ci ne doivent être imprimés ou autrement reproduits sans son autorisation écrite.

ISBN 0-315-32504-6

D. Reidel
publishing
company

a member of the Kluwer academic publishers group
Dordrecht / Boston / Lancaster / Tokyo

Spuiboulevard 50
P.O. Box 17
3300 AA Dordrecht
The Netherlands

Bankers: ABN Bank, Dordrecht
Account Number 50.80.11.817
Postal Cheque Account Number 172579

Telex: 29245
Telefax: (0)78-334254

Telephone: (0)78- 334212

Ms Catherine de Groot-Hedlin
Department of Physics
University of Alberta
Edmonton, Alberta
Canada T6G 2J1

May 16th, 1986

Re: Carovillano/Forbes (eds): Solar-Terrestrial Physics
ISBN 90-277-1632-3, ASSL 104, © 1983 DR.

Dear Ms de Groot,

This is to acknowledge receipt of your recent (undated) letter asking permission to include figures 1 (page 244), 1 (page 266) and 5 (page 304) in your M. Sc. thesis. I am pleased to grant you herewith permission - free of charge - to do so.

Concerning figure 7 of Akasofu's Polar and Magnetospheric Substorms: also in this case permission is granted.

Trusting to have been of service and wishing you success with your studies, I am,

Yours sincerely,

Ernst den Hoet
Rights & Permissions

conoco

Research & Development Department

Conoco Inc.
P.O. Box 1267
Ponca City, OK 74603
(405) 767-3456

May 2, 1986

Catherine de Groot-Hedlin
Department of Physics
University of Alberta
Edmonton, Alberta
Canada T6G 2J1

Dear Ms. de Groot-Hedlin:

I give you permission to include diagrams 2.2 and 2.13 (Ph.D. thesis "The dynamical development of the polar electrojets") in your M.Sc. thesis. You also have my permission to include any of the other figures if the need arises.

Please give my regards to Gordon and John.

Sincerely yours,

J. L. Kisabeth
Research Associate
Exploration Research & Development Division

bw

THE UNIVERSITY OF ALBERTA

RELEASE FORM

NAME OF AUTHOR Catherine D. de Groot-Hedlin

TITLE OF THESIS Magnetic Signatures of Precursors to Substorm Expansive Phase Activiy

DEGREE FOR WHICH THESIS WAS PRESENTED Master of Science

YEAR THIS DEGREE GRANTED FALL 1986

Permission is hereby granted to THE UNIVERSITY OF ALBERTA LIBRARY to reproduce single copies of this thesis and to lend or sell such copies for private, scholarly or scientific research purposes only.

The author reserves other publication rights, and neither the thesis nor extensive extracts from it may be printed or otherwise reproduced without the author's written permission.

(SIGNED) C. de Groot-Hedlin

PERMANENT ADDRESS:

10821 - 137 street

Edmonton, Alberta

T5M 1M9

DATED July 17 1986

THE UNIVERSITY OF ALBERTA

FACULTY OF GRADUATE STUDIES AND RESEARCH

The undersigned certify that they have read, and recommend to the Faculty of Graduate Studies and Research for acceptance, a thesis entitled Magnetic Signatures of Precursors to Substorm Expansive Phase Activity submitted by Catherine D. de Groot-Hedlin in partial fulfillment of the requirements for the degree of Master of Science in Geophysics.

.....

Supervisor

.....

.....

.....

Date.. April 21, 1986..

Dedication

to my parents, Adrian and Nell de Groot

Abstract

The expansive phase of a magnetospheric substorm involves a number of discrete episodes of enhanced energy release into the vicinity of the Harang discontinuity in the ionosphere. This energy release involves the formation of a substorm current wedge which consists of downward field-aligned current flow into the dawnside auroral ionosphere, westward current in the ionosphere, and upward field-aligned current flow out of the ionosphere on the evening side. The magnetic field lines threading the disturbed portion of the ionosphere map to the interface between the central plasma sheet and the low latitude boundary layer in the deep magnetotail. The velocity shear at this interface suggests that the MHD Kelvin-Helmholtz instability causes the formation of the substorm current wedge. Based on this hypothesis, data from a network of ground-based magnetometers were examined for the purpose of finding current structures which may be interpreted in terms of the growth of the Kelvin-Helmholtz instability. Model current system calculations were carried out in order to find three-dimensional current systems giving rise to the observed magnetic perturbations. Differential longitude and latitude profiles were examined with the object of finding current patterns set up in the few minutes before expansive phase onset. It was found that, prior to the expansive phase onset, a current structure resembling a weak substorm current wedge appeared to the north of, and in the

longitudinal sector of the eventual expansive phase onset.

Acknowledgements

I wish to thank Dr. G. Rostoker for his supervision and many useful discussions throughout the course of this research. I am indebted to Dr. J.L. Kisabeth and Martin Connors for the development of the program used in modelling the data. I also wish to extend my thanks to Maureen Yeremy for her help in providing the programs for handling the data.

Finally, this project could not have been completed without the constant encouragement and moral support of my husband, Michael.

Table of Contents

Chapter		Page
I.	INTRODUCTION	1
	A. The Magnetosphere	1
	B. Solar Wind-Magnetosphere Dynamics	10
	C. The Auroral Oval	14
	D. Magnetospheric Substorms	18
	E. Previous Studies into Substorm Precursors	25
	F. Purpose of Thesis	26
II.	DATA COLLECTION AND HANDLING	29
	A. Sources of Data	29
	B. Data Presentation	33
	C. Method of Analysis	35
	D. Selection of Events	40
III.	DATA INTERPRETATION AND MODELLING OF CURRENT SYSTEMS	42
	A. Event Analysis-Day 231	42
	Development of the Event	42
	Modelling the Current Systems	51
	Summary of Day 231	62
	B. Event Analysis-Day 59, 1979	63
	Development of the Growth Phase	63
	Modelling the Current Systems	70
	Summary of Day 59	79
	C. Event Analysis-Day 20, 1978	81
	Development of the Event	81
	Modelling the Current Systems	89
	Summary for day 20	99

IV. DISCUSSION AND CONCLUSIONS 100

A. Summary of Results 100

B. Limitations of the Modelling Program 101

C. Kelvin-Helmholtz Instability 103

D. Generation of Field-aligned Current 106

E. Conclusions 111

BIBLIOGRAPHY 116

APPENDIX 122

A. MHD Analysis of the Kelvin-Helmholtz instability 122

List of Tables

Table		Page
II.1	Coordinates of magnetometer stations	30
III.1	Model parameters for the day 231 event	52
III.2	Model parameters for day 59, 1979	71
III.3	Model parameters for day 20, 1978	90

List of Figures

Figure		Page
I.1	Noon-midnight cross section of the Earth's magnetosphere	5
I.2	Cutaway view of the Earth's magnetosphere showing the various plasma domains	7
I.3	Proton drift paths for ions with finite kinetic energy	9
I.4	Velocity streamlines for the viscous interaction model	11
I.5	Dungey model of the interaction between the interplanetary and geomagnetic fields	13
I.6	Average position of the auroral oval	15
I.7	Mapping of electric fields and currents from the magnetotail to the auroral ionosphere	17
I.8	Average positions of the electrojets and the Harang discontinuity	19
I.9	Development of a canonical auroral substorm	21
I.10	Sketch of the substorm current wedge	24
II.1	Map of Canada showing locations of magnetic observatories	31
II.2	Elementary current loops for westward and southward ionospheric currents	36
II.3	Theoretical latitude profiles for a westward electrojet	38
III.1	Stacked magnetograms for day 231, 1978	43
III.2	Pi2 pulsations for day 231, 1978	44
III.3	Riometer data for day 231, 1978	46
III.4	Latitude profiles of the Alberta line for the interval preceding onset	48
III.5	Latitude profiles of the Churchill line for the interval preceding onset	49

Figure		Page
III.6	Longitude profiles for the interval preceding onset	50
III.7	Profiles taken one minute after expansive phase onset indicating region of substorm enhanced activity	53
III.8	Profiles for the background current system at 0812	54
III.9	Model current system for day 231	55
III.10	Profiles based on model current system	56
III.11	Observed differential profiles at 0816, day 231	59
III.12	Differential profiles based on the current model	61
III.13	Stacked magnetograms for the day 59,1979 event	64
III.14	Pi2 pulsations for day 59, 1979	65
III.15	Riometer data for day 59, 1979	66
III.16	Latitude profiles of the Alberta line for the interval preceding onset	68
III.17	Latitude profiles of the Churchill line for the interval preceding onset	69
III.18	Longitude profiles for the interval preceding onset	72
III.19	Profiles for the background current system	73
III.20	Model current system for day 59, 1979	74
III.21	Profiles base on the model current system	76
III.22	Observed differential profiles for day 59, 1979	78
III.23	Differential profiles based on the current model	80
III.24	Stacked magnetograms for day 20, 1978	82
III.25	Pi2 pulsations for day 20, 1978	83

Figure		Page
III.26	Riometer data for the day 20, 1978 event	85
III.27	Latitude profiles of the Alberta line for the interval preceding onset	86
III.28	Latitude profiles of the Churchill line for the interval preceding onset	88
III.29	Longitude profiles for the interval preceding onset	91
III.30	Observed profiles taken at 0600, day 20	92
III.31	Current model for the event of day 20, 1978	93
III.32	Background profiles based on the current model	95
III.33	Observed differential profiles for day 20, 1978	97
III.34	Differential profiles for day 20 based on the current model	98
IV.1	Streaklines for the Kelvin-Helmholtz instability	109
IV.2	Mapping of Kelvin-Helmholtz waves from the CPS/LLBL interface to surge forms in the auroral ionosphere	113

I. INTRODUCTION

This study was conducted for the purpose of investigating variations in the Earth's magnetic field occurring prior to a period of geomagnetic disturbance called a geomagnetic substorm. These disturbances are a manifestation of the solar-terrestrial interaction. The solar wind, which is a gas of charged particles, interacts with, and is deflected by the Earth's magnetic field. This creates a magnetic cavity around the Earth, called the magnetosphere. Some of the solar wind energy penetrates the magnetosphere, where part of it is degraded to heat in the earth's atmosphere, and some of it is stored. The stored energy is released intermittently in episodes called polar magnetic substorms. These intermittent outbursts appear to reflect plasma instabilities in the magnetotail. Any instability includes a period of growth; thus this study was conducted to find precursors in the geomagnetic field which are indicative of that growth.

A. The Magnetosphere

Until the early part of this century it was believed that the Earth's dipole field extended into space without distortion. The concept of the geomagnetic field being altered by the sun was first put forward in a paper by Chapman and Ferraro (1931). In it they suggested that the Earth's field would be confined to a cavity during the passage of a hot gas emitted from a solar flare; thus the

distortion of the magnetosphere was considered to be an intermittent phenomenon connected with geomagnetic storms. From his study of comet tails Biermann (1957) concluded that the interplanetary medium was filled with corpuscular radiation that was being continually emitted from the sun. Parker (1958) called this corpuscular radiation the solar wind because of its hydrodynamic characteristics and pointed out that the Earth's magnetosphere is continually exposed to a solar wind which is both supersonic and super-Alfvénic so that the magnetosphere is continually distorted by the solar wind.

The solar wind is effectively a magnetized plasma since the Debye length($\simeq$10m) of the individual particles in the solar wind and the proton and electron gyroradii ($\simeq$50km, 1.5km respectively) (Kavanagh, 1972) are much less than the dimensions of the magnetosphere so that an analogy to fluid flow may be made in discussing the solar-terrestrial interaction. Since the solar wind is both supersonic and super-Alfvénic the Earth acts as an obstacle to its path, causing a bow shock to be formed on the dayside of the Earth. The solar wind plasma just Earthward of the bow shock is compressed and thermalized, then deflected around the magnetosphere by the geomagnetic field. This region of plasma is called the magnetosheath.

In order to come to an understanding of the magnetospheric dynamics it is first necessary to understand the motion of a single charged particle in the presence of

electric and magnetic fields. For mathematical simplicity the motion of a charged particle is decoupled into two components, the gyrational motion about the magnetic field and the drift motion. In general the drift velocity of a charged particle is given by

$$\underline{v}=\underline{F}x\underline{B}/qB^2 \qquad 1.1$$

where $\underline{B}$ is the magnetic field, q is the charge, and $\underline{F}$ is the force which the particle experiences. A charged particle under the influence of the Earth's magnetic field will experience a guiding centre drift given by

$$\underline{v}=\frac{\underline{E}x\underline{B}}{B^2}+\epsilon_\perp\frac{\underline{B}x\nabla\underline{B}}{qB^3}+2\epsilon_{\|}\frac{\underline{B}x\nabla\underline{B}}{qB^3} \qquad 1.2$$

where $\underline{E}$ is the electric field, and $\epsilon_\perp$ and $\epsilon_{\|}$ refer to components of the kinetic energy perpendicular and parallel to the magnetic field, respectively. The first term, called the convective velocity, results from the force due to the electric field. The second term, called the gradient drift, is a result of a gradient in the magnetic field, and the last term, the curvature drift, is caused by the curvature of the Earth's field lines.

The generalized Ohm's law is given by the expression

$$\underline{J}=g(\underline{E}+\underline{v}x\underline{B}) \qquad 1.3$$

where $\underline{J}$ is the current, and g is the conductivity. In the magnetohydrodynamic (MHD) approximation, the conductivity is taken to be infinite parallel to the magnetic field lines and zero perpendicular to the field lines. Since infinite current cannot flow along the field lines we must have the

condition

$$\underline{E}=-\underline{v}x\underline{B} \qquad 1.4$$

A consequence of the infinite conductivity is the frozen field condition, i.e. the plasma remains on a given flux tube.

Using as a first approximation the frozen field condition, it can be seen that plasma flowing past the Earth is divided into two regions. In the exterior region the plasma is influenced by magnetic field lines rooted in the sun. In the interior region, called the magnetosphere, the magnetic field lines are connected to the Earth. The boundary between the two regions is called the magnetopause. This is shown schematically in figure 1.1. However the MHD condition is just a first approximation; the magnetosphere is not completely impenetrable as the frozen field conditions imply. This allows for interchange of energy between the solar wind and the magnetosphere.

The interaction of the solar wind with the Earth's magnetic field involves a dynamic pressure which causes a compression of the basically dipolar field, and a combination of Maxwell and hydrodynamic stresses which distends the field on the nightside to form the magnetotail. Transverse to the solar wind flow, the magnetotail is cylindrical in shape with a diameter of approximately 50 Re and a length of more than 1000 Re (Ness et al,1967). The tangential stress which the solar wind exerts on the magnetosphere in order to stretch it is balanced by a

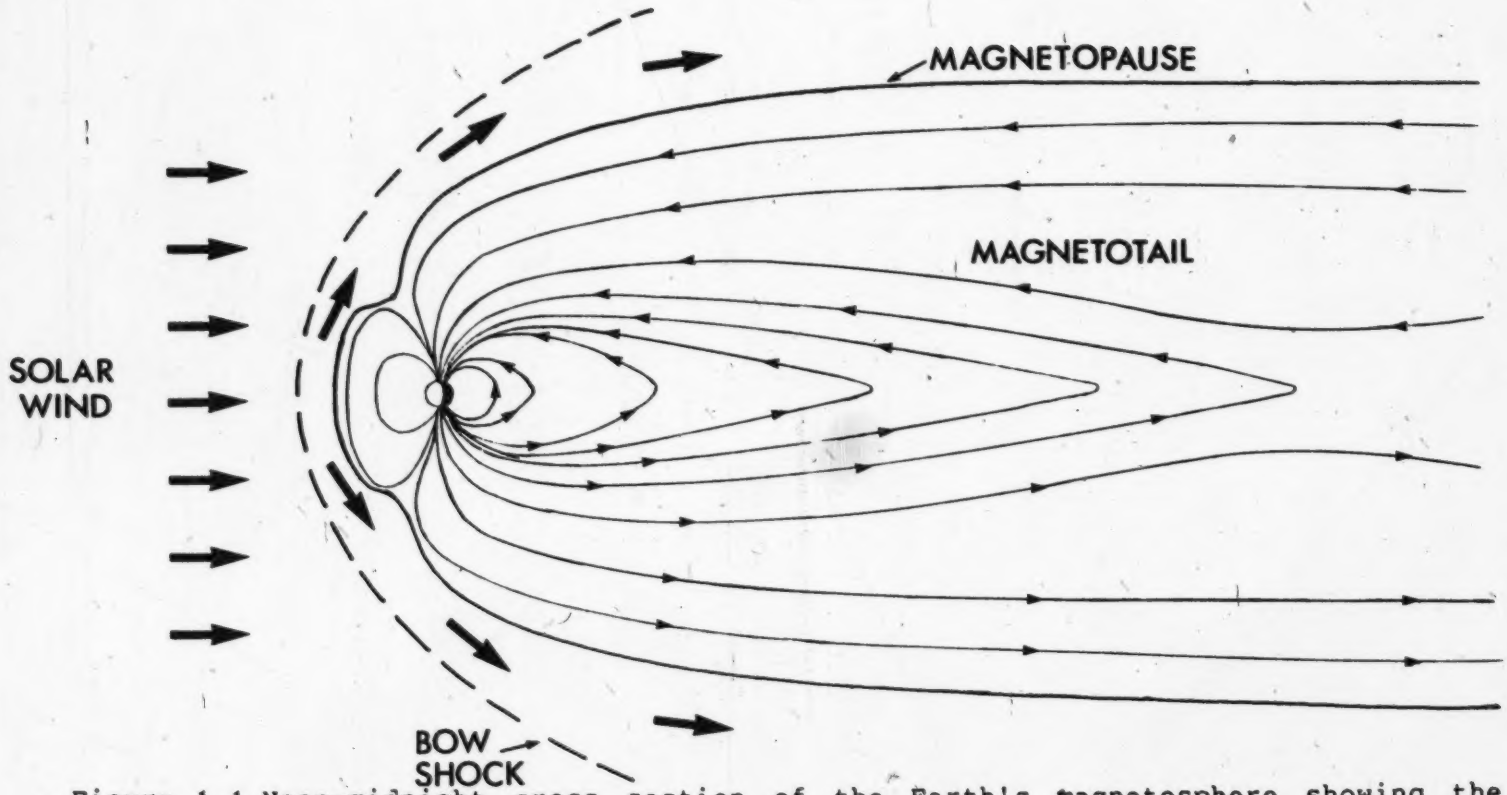

Figure 1.1 Noon-midnight cross section of the Earth's magnetosphere showing the distortion of the dipolar field inside the magnetosphere and the solar plasma flow outside.

magnetic field line tension within the magnetotail.

The geomagnetic field line direction on the night side is reversed between the northern and southern hemispheres. By Maxwell's equation the current $\underline{J}$ is given by

$$\mu_o \underline{J} = \nabla \times \underline{B} \qquad 1.5$$

neglecting the displacement current. This implies the existence of a current sheet in the magnetotail flowing from dawn to dusk across the plasma sheet.

The plasma domains of the magnetosphere are shown in figure 1.2. The plasma mantle and low latitude boundary layer (LLBL) are regions of magnetosheath-like plasma controlled by the Earth's magnetic field. All energy, momentum, and mass transfer from the solar wind to the magnetosphere occurs across these boundary layers. This is discussed further in section 1.B. The plasma mantle and the LLBL are sources of plasma to the plasma sheet which provides the energetic particles that precipitate into the auroral ionosphere.

The central plasma sheet (CPS) is a region of hot plasma in the centre of the magnetotail which carries most of the cross tail current. The particle density is $\simeq 1/cm^3$, much higher than that of the tail lobe region surrounding it but lower than that of the magnetosheath where densities rise to 5-20 particles/cm^3 (Wolf and Harel, 1978). The plasma sheet has a planar geometry, stretching across the magnetotail from dawn to dusk, with a thickness of up to a few Re. The central region is surrounded by a more tenuous,

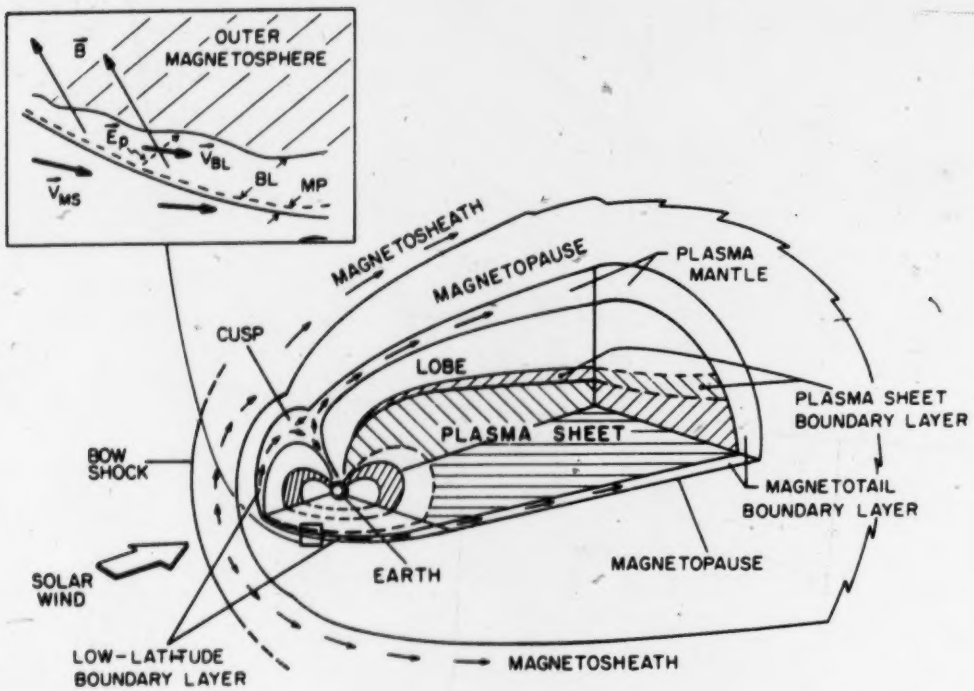

Figure 1.2 Cutaway view of the earth's magnetosphere showing the various plasma domains. Inset shows the detailed structure of the low latitude boundary layer (after Eastman et al, 1985).

turbulent plasma, the plasma sheet boundary layer (PSBL). A velocity shear and an electric field divergence exist across the PSBL,and the LLBL.

Equation 1.2 applied to typical tail $\underline{E}$ and $\underline{B}$ field conditions (Rostoker and Boström,1976) predicts Earthward drifting plasma in the CPS. As the particles drift Earthward they gain energy due to the increasing magnetic field strength; eventually the charge dependent curvature and gradient drifts dominate the convective drift. The resulting plasma flow is shown diagrammatically in figure 1.3. The hot ions and electrons drift in opposite directions causing a charge separation layer (the Alfvén layer) to be formed at the Earthward boundary of the drift paths of the CPS particles. Earthward of the inner edge of the plasma sheet layer is a boundary layer which separates the plasma sheet, which is dominated by the convection electric field, from the plasmasphere, which is dominated by the corotation electric field. This boundary, called the plasmapause, marks a sharp discontinuity in thermal plasma density, with the plasmasphere having a much higher density than regions outside the plasmapause.

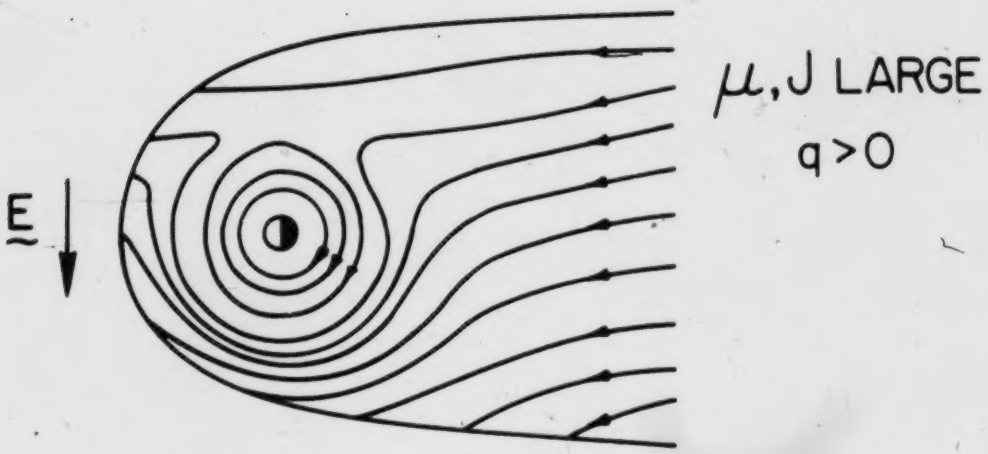

Figure 1.3 Proton drift paths for ions with finite kinetic energy, with the effects of the earth's rotation neglected. Electrons and protons with finite kinetic energy drift in opposite directions. The effect of the Earth's rotation is to cause both protons and electrons to drift eastwards, so that lower energy particles corotate with the Earth.(after Wolf, 1983).

B. Solar Wind-Magnetosphere Dynamics

The principal energy transport governing the dynamic processes in the magnetosphere is the plasma convection generated by interaction with the solar wind. The boundary layer plasmas flow tailward while the plasma of the inner central plasma sheet flows Earthward to complete the circulation. Two models have been used to describe the interaction between the solar wind and magnetosphere which results in this circulation pattern.

Axford and Hines (1961) proposed a model with a viscous interaction between the solar wind and interplanetary plasma, producing momentum transfer across the boundary. A viscous boundary layer would involve antisunward flowing plasma just inside the magnetopause. The circulation behind the obstacle (the dipole geomagnetic field) eventually leads to particles convecting Earthward as the population of the central plasma sheet. This is illustrated in figure 1.4a with the mapping of the velocity field to the ionosphere shown in figure 1.4b. This convection is consistent with an electric field $\underline{E}=-\underline{v}x\underline{B}$, having a dawn to dusk orientation in the central plasma sheet and polar cap ionosphere and a dusk to dawn orientation in the low latitude boundary layer and auroral oval. Although the correct convection velocities and electric fields are predicted, one difficulty with this model is that the plasmas are virtually collisionless so that the classic viscosity is several orders of magnitude too low. To correct this problem Axford and Hines suggested

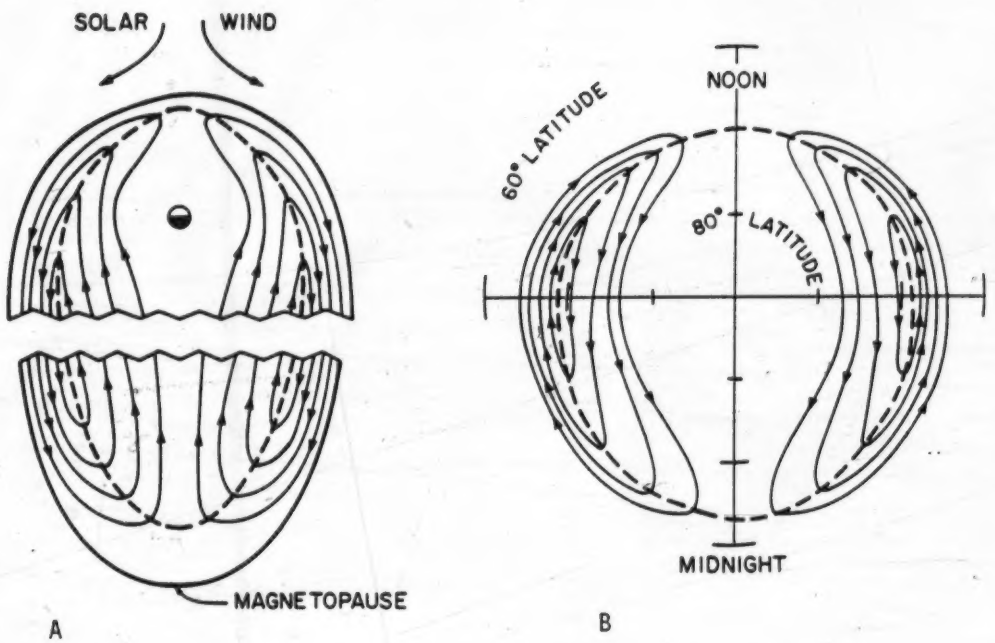

Figure 1.4 Velocity streamlines for the viscous interaction model (a)on the magnetospheric equatorial plane and (b)mapping to the polar-cap ionosphere. (after Hill,1983)

that solar wind-magnetosphere coupling, induced by plasma instabilities, might provide an "effective" viscosity which is sufficient to make the model viable.

In the Dungey reconnection model (Dungey,1961) momentum transfer occurs as a result of magnetic coupling between the solar and terrestrial fields. Interplanetary plasma, with frozen-in magnetic field, is swept up against the Earth's dipole field and in the process the IMF and geomagnetic field lines merge. These field lines are swept into the magnetotail where reconnection takes place, converting magnetic energy into kinetic energy of the plasma particles. In this way magnetic tension transfers solar wind momentum into the magnetosphere. The reader is referred to Petschek(1964) and Vasyliunas(1975) for details on field line reconnection.

As opposed to the Axford and Hines model in which all of the field lines are closed, in Dungey's model some high latitude geomagnetic lines extend into interplanetary space and thus connect the solar field directly to the polar regions of the Earth. The $-\underline{v}x\underline{B}$ interplanetary electric field penetrates along these field lines into the polar cap ionosphere creating a dawn to dusk electric field there. Figure 1.5 shows the results of this model for a southward interplanetary magnetic field(IMF). An attractive feature of this model is that it correctly predicts enhanced interaction for southward IMF as compared to conditions of northward IMF. Both models correctly account for the

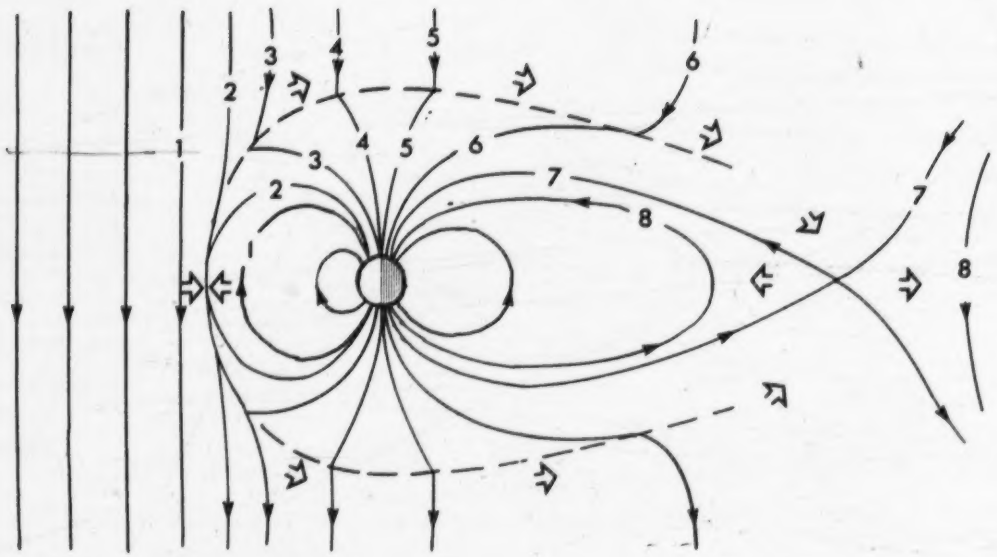

Figure 1.5 Dungey model of the interaction between the interplanetary and geomagnetic fields. The open arrows indicate the resulting motions of the plasma. The motion of the individual field lines is indicated by the numbers.

observed electric fields in the magnetosphere and ionosphere.

C. The Auroral Oval

The narrow belt of the ionosphere along which auroral arcs lie is termed the auroral oval. It encircles the geomagnetic pole, slightly offset toward the dark hemisphere due to the asymmetry of the magnetosphere. The dayside oval is a region of normally low luminosity auroral arcs caused by the magnetosheath plasma penetrating directly into the ionosphere through the polar cusp (Heikkila and Winningham, 1971). Intense auroral displays occur when energetic electrons are precipitated into the ionosphere at the midnight portion of the oval during the release of energy from the magnetotail. The average location of the auroral oval is indicated in figure 1.6. However, the position of the nightside oval varies considerably in latitude, from ≃75°N during periods of extreme quiet to ≃50°N during intense storms.

The average location of field-aligned currents is also indicated in figure 1.6. The region I field-aligned currents (Iijima and Potemra, 1976) flowing out of the poleward portion of the auroral oval in the evening sector and into the poleward portion of the oval on the morning side map along field lines to the interface between the CPS and LLBL (Rostoker et al, 1984). The field-aligned currents flowing into and out of the equatorward edge of the auroral oval

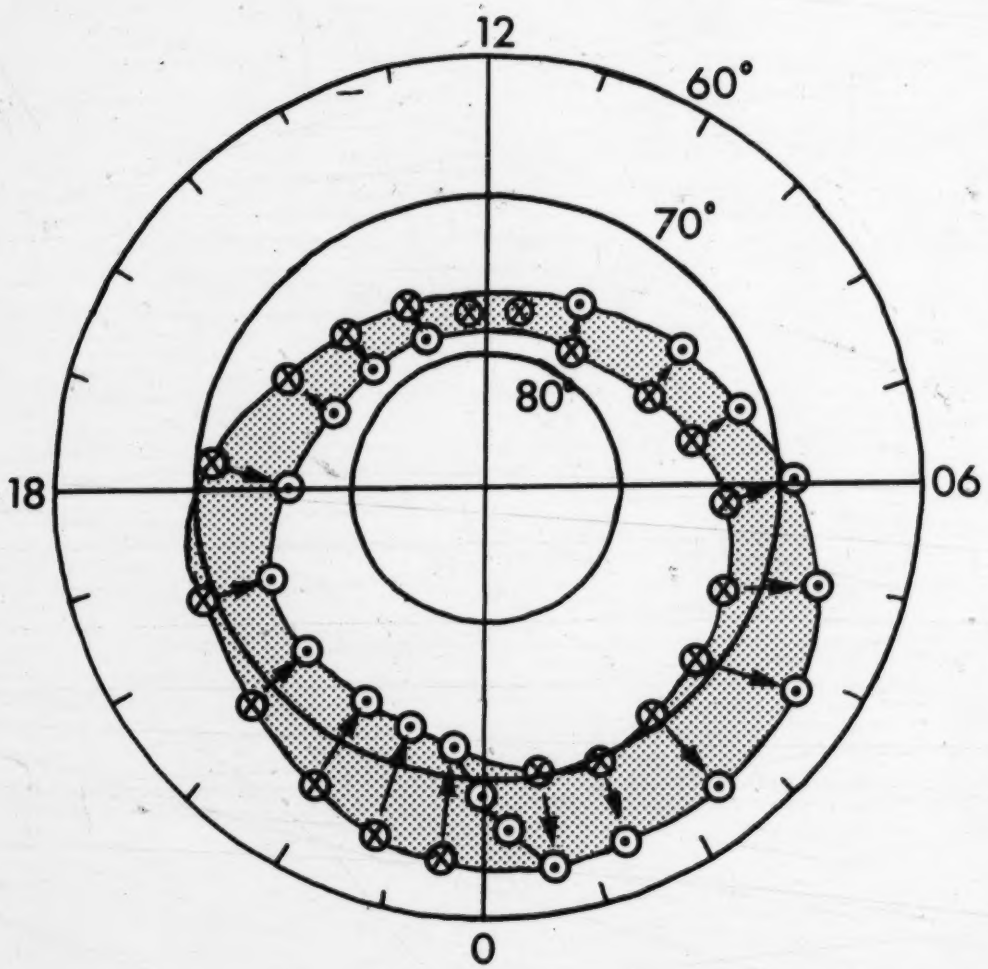

⊗ Flow into the auroral ionosphere

⊙ Flow out of the auroral ionosphere

Figure 1.6 Average positions of the auroral oval and locations of intense field-aligned currents. The arrows indicate the direction of Pederson current.

(the region 2 currents) connect to the CPS, extending as far Earthward as the inner edge of the plasma sheet (Rostoker et al, 1985); thus the particles precipitating into the auroral oval originate in the plasma sheet and LLBL. These field-aligned currents flow in response to the development of space charge as given by Maxwell's equation $\sigma=\epsilon_0 \nabla \cdot \underline{E}$. The electric field reversal and velocity shear zone of the LLBL also map down to a region near the poleward edge of the auroral oval ionosphere. The mapping of the electric fields to the auroral oval is indicated in figure 1.7. Note that the electric field, and therefore the convection velocity, change directions across a line of nearly constant latitude. This magnetospheric velocity shear zone is thought to be the site of electric currents associated with dynamic geomagnetic activity (Rostoker, 1983a).

Pederson current flows across the auroral oval in the E-region of the ionosphere, connecting downward field-aligned current to upward field-aligned current as shown in figure 1.6. The current system is closed in the plasma sheet; thus the Pederson current and associated field-aligned current configuration behaves as a solenoid and the magnetic field is not detected using ground-based magnetometers. Hall current in the ionosphere results from the differential velocity of ions and electrons in the ionosphere due to convective $\underline{E}x\underline{B}$ drift, the ions experiencing more collisions with neutrals than the electrons due to their larger cross sections. The Hall

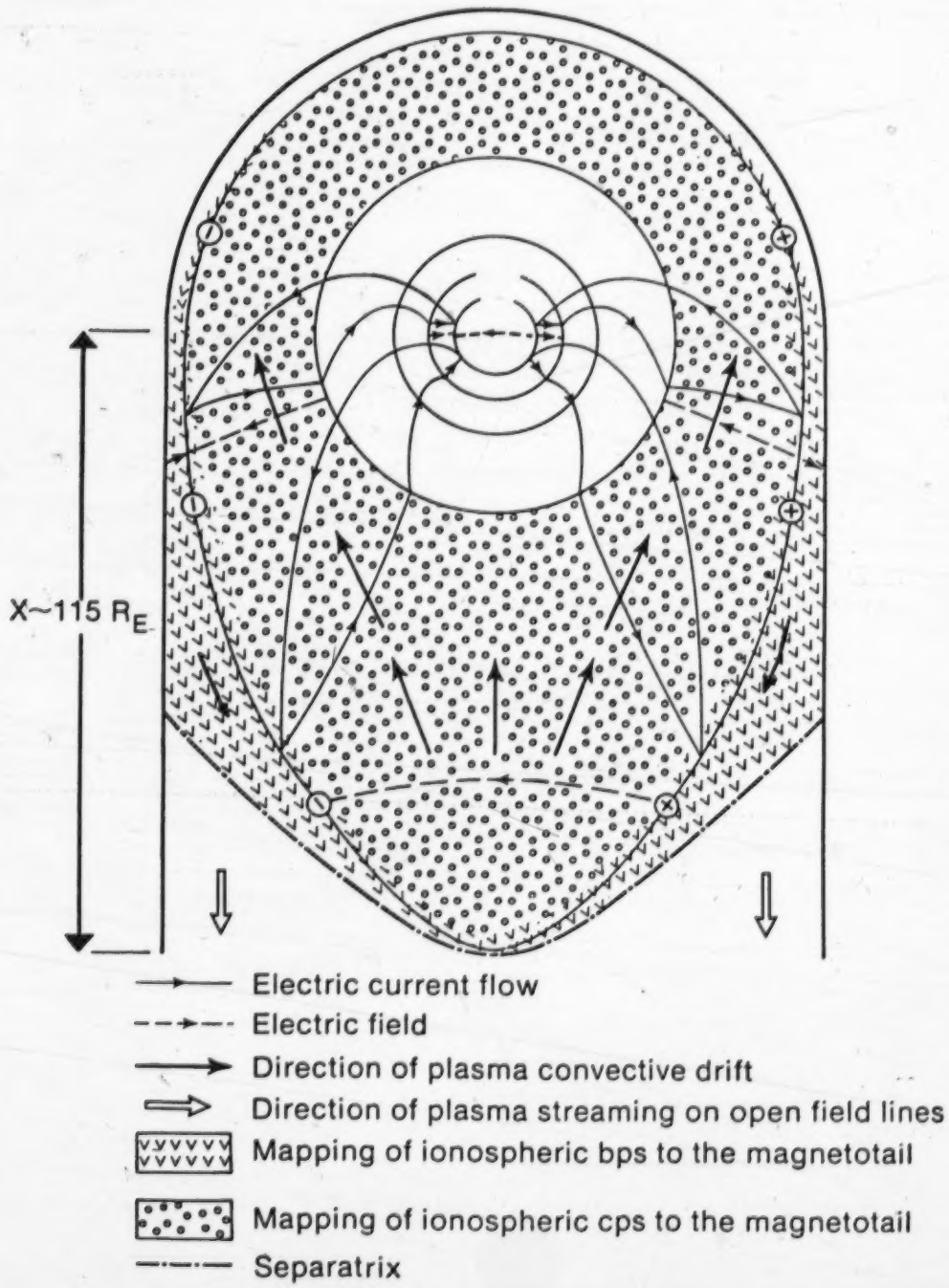
X~115 R_E
Electric current flow
Electric field
Direction of plasma convective drift
Direction of plasma streaming on open field lines
Mapping of ionospheric bps to the magnetotail
Mapping of ionospheric cps to the magnetotail
Separatrix

Figure 1.7 Mapping of electric fields and currents from the magnetotail to the auroral ionosphere (after Rostoker, 1986).

current flows in the direction $\underline{B}x\underline{E}$; thus it flows eastward in the evening sector and westward in the morning sector. These currents constitute the eastward and westward electrojets. Studies of the electrojets conducted using magnetometer data from meridian line and two-dimensional arrays (Kisabeth and Rostoker,1971,1974) have shown that a substorm expansive phase onset is characterized by a sudden intensification of the electrojets, and indicate that the eastward electrojet lies equatorward of the westward electrojet where they coexist at the same longitude in the evening sector. The typical electrojet configuration is shown in figure 1.8.

The region where the electrojets converge near midnight is called the Harang discontinuity. Intense electron precipitation occurs here during strong magnetospheric activity creating upward field-aligned current flow (Shawhan et al,1978).

D. Magnetospheric Substorms

The following definition of the magnetospheric substorm is taken from Rostoker et al (1980);

> "A magnetospheric substorm is a transient process initiated on the nightside of the Earth in which a significant amount of energy derived from the solar wind-magnetosphere interaction is deposited in the auroral oval and in the magnetosphere."

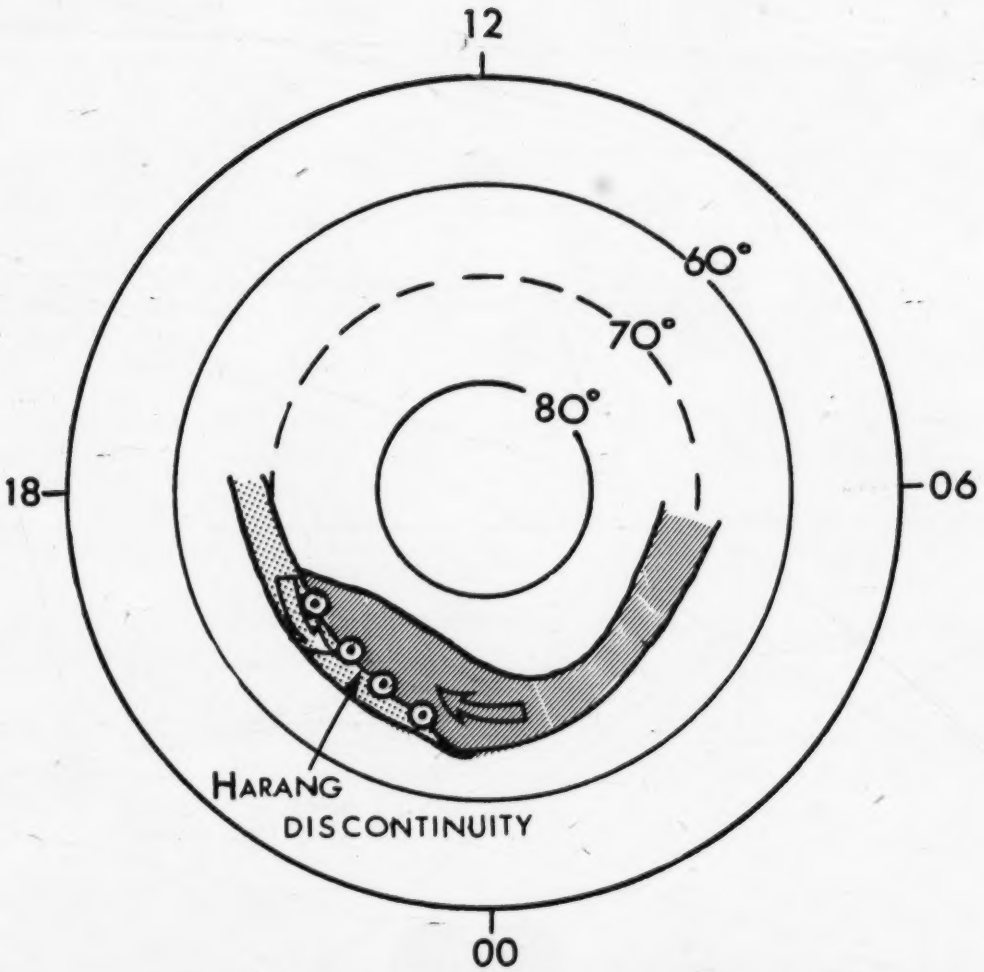

Figure 1.8 Schematic diagram of the auroral oval indicating the average positions of the eastward and westward electrojets and the Harang discontinuity. The Harang discontinuity is the site of upward field-aligned current as indicated by the arrowhead ⊙. Times indicated represent local time.

The interaction between the solar wind and the magnetosphere is enhanced during periods of southward IMF. This leads to increased geomagnetic activity as measured by the AE and Kp indices (Arnoldy, 1971; Rostoker et al, 1972). Thus substorm onset is defined as taking place at the time of the southward turning of the IMF.

Substorms are generally divided into a sequence of three phases in order to describe the physical processes occuring in an ideal, isolated substorm event. The growth phase (McPherron,1970), during which energy is stored in the magnetotail, is marked by a gradual increase of energy input to the ionosphere. The expansive phase is associated with the explosive increase in ionospheric energy dissipation and the recovery phase is a period during which activity returns to its pre-substorm level (Akasofu, 1968). For multiple substorm onsets, these phases can occur simultaneously.

The energy is dissipated through the production of ionospheric currents which cause magnetic substorms as well as through the production of aurorae. Figure 1.9 shows the growth and decay of a canonical auroral substorm event. During the growth phase the auroral arcs are diffuse but there may be an occasional appearance of rayed or folded structures. A fold is sometimes seen travelling rapidly westward along an arc. Expansive phase onset is characterized by a sudden brightening of a quiet arc along the equatorward edge of the region of discrete aurorae (Akasofu, 1977). The discrete arc activity then expands

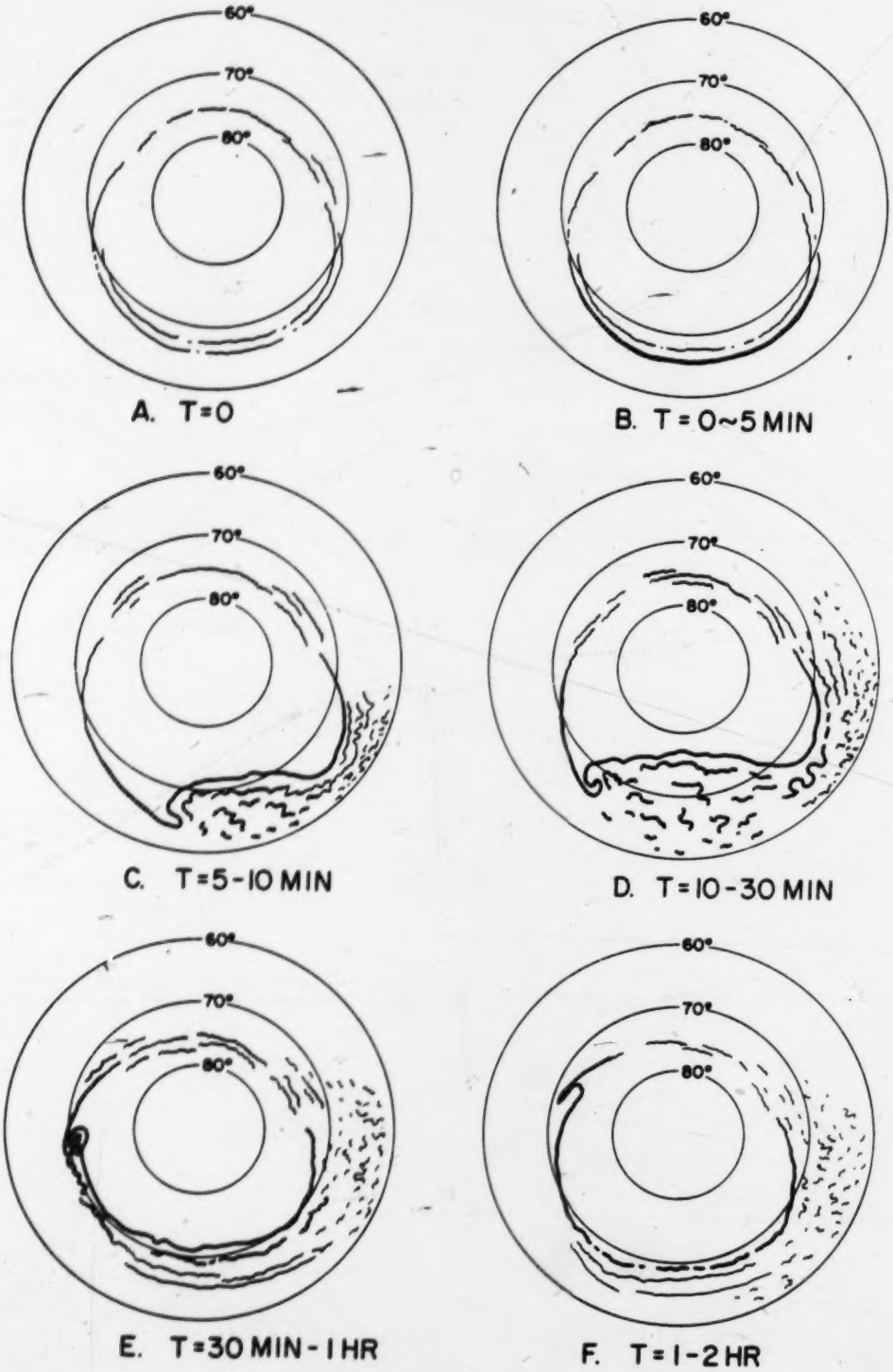

Figure 1.9 Development of a canonical auroral substorm (after Akasofu, 1968).

poleward rapidly, resulting in an auroral bulge (see figure 1.9c). This phase may consist of a series of discrete intensifications of the substorm, marked by the westward expansion of the disturbed region of the ionosphere. Each intensification has associated with it a large scale fold which develops on the evening side of the auroral bulge. The motion of these folds, which travel rapidly westward along an auroral arc, gives them the name "westward travelling surge". On the morning side of the disturbed region the arcs break up into smaller patches which drift eastward with a velocity of ≃300m/second. The auroral substorm ends with the recovery phase during which the auroral bulge contracts equatorward following the maximum poleward extension and activity returns to its presubstorm level.

Two processes are invoked to describe the manner in which substorm energy is dissipated in the ionosphere. These are the loading-unloading process and the directly driven process. The driven system involves a direct response of the magnetosphere to changes in the solar wind. In this case, energy input from the solar wind equals energy output in the form of geomagnetic activity and increased ring current strength with no intermediate storage of energy in the magnetotail. Perrault and Akasofu(1978) have developed a parameter which reflects the input energy flux from the solar wind; this is given by

$$\epsilon = vB^2 \sin^4(\theta/2) l_0^2 \qquad 1.6$$

where v is the solar wind velocity, B is the strength of the

IMF, θ is the polar angle of the IMF measured such that θ=0 for northward IMF, and $\bar{l}_o$ is the scale length over which the interaction takes place (≃7Re).

The loading-unloading process involves dayside reconnection, leading to the tearing away of field lines from the dayside magnetopause. The solar wind carries this magnetic flux to the magnetotail, causing the tail magnetic field magnitude to increase rapidly. Convection in the CPS increases, enhancing the convection electric field and resulting in plasma sheet thinning. Increased thinning of the plasma sheet results in the formation of a neutral line at which oppositely directed field lines meet, causing reconnection to take place. Reconnection transforms the magnetic field energy stored in the plasma sheet into kinetic energy of the plasma sheet particles. The resulting increase of vorticity in the plasma convective flow in the deep magnetotail results in a transient enhancement of positive (negative) space charge generated on the dawnside (eveningside) of the LLBL-CPS interface (Rostoker,1983a; cf figure 1.7). This causes field-aligned current to flow into the ionosphere on the dawnside and westward to the evening side where it flows out of the ionosphere into the tail region. This combination of the field-aligned and ionospheric currents constitute the substorm current wedge (see figure 1.10).

The major differences between the loading-unloading system and driven system are that, for the driven system,

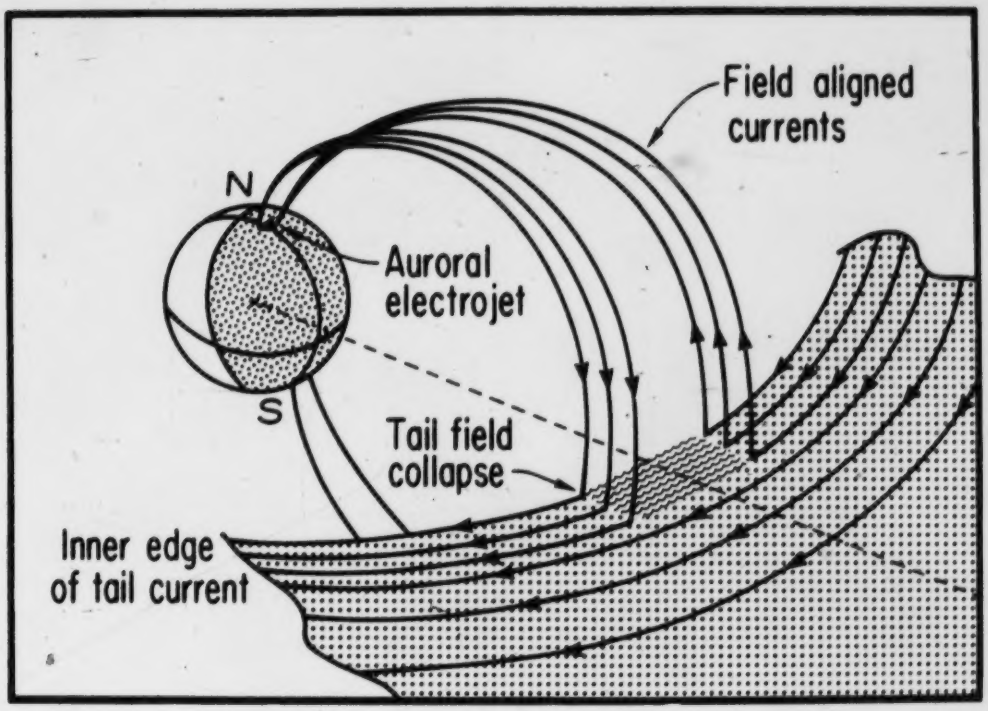

Figure 1.10 Sketch of the substorm current wedge showing the mapping of current from the magnetotail to the ionosphere (after McPherron et al, 1973).

the activity is not caused by conversion of stored energy at onset, but is simply a direct response to an input of energy from the solar wind. Thus no growth phase is involved in the driven system. A unified view of the morphology of substorm activity incorporates aspects of both models. That is, both the loading-unloading system and the driven system contribute to the overall substorm process. However, the amount of energy dissipation in the ionosphere that can be attributed to each process is not clear (Rostoker et al,1986). In either case, it is obvious that substorm phenomena must be discussed in terms of the solar wind-magnetosphere interaction.

E. Previous Studies into Substorm Precursors

Various geophysical methods have been used in conducting case studies into the growth of pre-substrom ionospheric systems. The results of Pellinen and Heikkila (1978), Opgenoorth et al (1980), and Baumjohann et al (1981) are summarized here.

It was found that, within minutes prior to expansive phase onset, the riometer readings show a decreased influx of precipitating electrons, indicating a decrease in field-aligned current. The lower influx of ionizing particles results in reduced conductivity in the auroral oval which in turn causes a reduction in ionospheric current. The reduction in current is detected by a decrease in magnetic field strength. The reduced conductivity is also

detected as a fading of auroral luminosity.

The auroral luminosity and the westward equivalent current intensify just before a fade. Increases in the H and D components of regional magnetometer records are correlated with times of increased auroral luminosity, returning to undisturbed values during each fade. This suggests that increases in auroral brightness are correlated with increases in field-aligned current. There may be a succession of auroral fadings and brightenings before expansive phase onset, occurring in a region as small as a few hundred kilometers in longitudinal length. The aurora may fade in place or the zone of fading may move either eastward or westward.

Just before onset the differential equivalent current vectors indicate the location of a counterclockwise, circular Hall current, indicative of upward field-aligned current which is carried by an influx of electrons. This is the locus of the auroral luminosity. With onset comes the sudden appearance of localized and intense upward field-aligned currents and more widespread and less intense downward field-aligned currents, to the west and east, respectively, of the enhanced westward equivalent current.

F. Purpose of Thesis

Observations provided by ground magnetometers indicate that the substorm expansive phase consists of a number of discrete episodes of enhanced energy release into the

vicinity of the Harang discontinuity. A study by Wiens and Rostoker (1975) illustrated that each episode involves a substorm current wedge intensification occurring to the northwest of the previous one. Each substorm current wedge involves an auroral surge. On the basis of the wavelike distortion of the auroral forms and their localization in the Harang discontinuity, which is characterized by a velocity shear, Rostoker and Samson (1984) suggested that each expansive phase intensification is a manifestation of the Kelvin-Helmholtz instability at the CPS/LLBL interface. This hypothesis is strengthened by the results outlined in the previous section, where it was shown that the substorm precursors appear as a series of impulsive intensifications of field-aligned current, suggesting a driving force, such as a plasma instability, in the magnetotail. Thus one might expect to see the signature of the growth of the Kelvin-Helmholtz instability in a sector which is about to be disturbed by the expansive phase onset. Since the growth time of the Kelvin-Helmholtz instability is on the order of 2-3 minutes (Rostoker, 1986), this signature should be detectable in the minutes before expansive phase onset.

In this thesis, an analysis of ground-based magnetograms taken from the midnight portion of the auroral oval will be presented in order to identify magnetic signatures that can be demonstrated to be precursors to the substorm expansive phase. Possible current configurations giving rise to the observed geomagnetic signatures will be

examined. Data from a number of magnetic observatories in western Canada, comprising two lines of constant geomagnetic longitude and one line of constant geomagnetic latitude, will provide adequate spatial coverage of the regions in which substorm expansive activity develops. These data will be examined with the object of finding physical mechanisms for generating these magnetic signatures. In particular, the Kelvin-Helmholtz instability arising from velocity shear at the CPS/LLBL interface will be examined as a potential triggering mechanism for the expansive phase.

II. DATA COLLECTION AND HANDLING

A. Sources of Data

Magnetic data from 23 observatories in western Canada and 1 in the northwest United States were used in this study of precursors to magnetic substorm expansive phases. The locations of the stations are shown in figure 2.1. As the figure indicates, the stations are arrayed along three lines, two of constant geomagnetic longitude (the Churchill line to the east and the Alberta line to the west) and one of constant geomagnetic latitude, the East-West line. The geographic and geomagnetic (centred dipole) coordinates of each of the observatories are listed in table 2.1.

The stations operated by the University of Alberta are marked by an asterisk in table 2.1. Triaxial fluxgate magnetometers, yielding digital recordings of the magnetic disturbances, were in place at each station. These magnetometers were aligned such that the disturbances were recorded in the local magnetic coordinate system (H,D,Z). H is defined as positive northward, D is positive eastward, and Z is positive downward. The sampling rate for these records was 1 point per 2.56 sec to an accuracy of at least ∓.1 sec. The dynamic range of each magnetometer was ∓1000nT with a sensitivity of better than ∓1nT. The recording system included a 12 bit analogue to digital conversion system with the least significant bit representing approximately 1 nT. Each magnetometer sensor was buried in the ground to reduce

TABLE 2.1

Geographic and Geomagnetic Coordinates of Magnetometer Stations

Station Name	Code Name	Geomagnetic Coordinates		Geographic Coordinates	
		Latitude(°N)	Longitude(°E)	Latitude(°N)	Longitude(°E)
Resolute Bay	RESO	83.1	291.6	74.7	265.1
Pelly Bay	PEB#	78.6	321.7	68.5	270.5
Baker Lake	BAKE	73.8	317.0	64.3	264.0
Rankin Inlet	RIT#	72.8	324.0	62.8	267.7
Eskimo Point	EKP#	71.0	322.7	61.1	265.9
Fort Churchill	CHUR	68.7	324.3	58.8	265.9
Back	BKC#	67.6	324.8	57.7	265.8
Gillam	GIM#	66.4	325.2	56.4	265.6
Island Lake	ISL#	63.9	326.4	53.9	265.6
Whiteshell	WHIT	59.8	326.9	49.8	264.8
Norman Wells	NOW#	69.3	279.2	64.9	234.5
Fort Simpson	FSP#	67.3	287.5	61.8	238.8
Fort Providence	PROV*	67.5	292.1	61.3	242.4
Hay River	HAYR*	67.3	294.6	60.8	244.1
Fort Smith	SMIT*	67.3	300.0	60.0	248.0
Fort Chipewyan	FTCH*	66.1	301.0	58.8	248.0
Uranium City	URAN*	67.5	304.7	59.6	251.5
Lynn Lake	LYN#	66.0	316.1	56.9	258.9
Cambridge Bay	CAMB	76.8	296.5	69.1	255.0
Yellowknife	YELL	69.2	294.5	62.5	245.5
Fort McMurray	MCMU*	64.3	303.5	56.7	248.8
Meanook	MENK	61.9	302.4	54.6	246.7
Leduc	LEDU*	60.7	302.9	53.3	246.5
Newport	NEWP	55.2	301.3	48.3	242.9

Figure 2.1 Map of Canada showing magnetic observatories.

fluctuations in the readings that would be caused by temperature variations.

Riometers (relative ionospheric opacity meters) were also in place at each Alberta station. The riometer measures the ionosphere's absorption of cosmic radio noise at 30 MHz. The absorption is dependent upon the electron energy flux, thus the riometer measures energetic electron precipitation events. Unfortunately, many of the riometers were no longer in operation for the events presented in this study. For details on the Alberta stations and the instrumentation used, see Kisabeth (1972).

The nine observatories of the International Magnetospheric Study (IMS), denoted by # in table 2.1, also recorded digitally, but with a sampling interval of 10 sec. One minute averaged values were calculated for each of the three magnetic field components and saved on magnetic tapes. The one minute averaged data were used for this study. Unfortunately, a few of these stations were plagued by transmitter interference, resulting in data anomalies occurring once every 12 minutes. Another difficulty encountered was that of a recurring disturbance with a wavelike nature superimposed upon the magnetic record. Since the disturbance had a frequency of approximately one minute, approximately equal to the sampling rate, it could not be filtered out due to aliasing problems.

Analogue recordings of the magnetic field were made at the remaining stations. Before further use, these recordings

had to be digitized, resulting in timing errors of up to 30 seconds.

B. Data Presentation

The two primary modes of data presentation used for this study are the component magnetogram format and the profile format.

In the stacked magnetogram format, the H, D, and Z components are plotted as a function of time. The size of the perturbations in the the H and Z components gives an indication of the strength of the substorm electrojets while the D component indicates the position of the station with respect to the western edge of the surge which marks the onset of the substorm expansive phase. For this study, this mode of presentation is used mainly to locate the position of the magnetic observatories with respect to the head of the surge.

In analyzing precursory activity, the exact onset time of the substorm expansive phase must be determined. In order to do this, the magnetogram data are high-pass filtered in order to display the Pi2 pulsations associated with the expansive phase onset. The rapid rise time of the Pi2 pulsations in the source region gives accurate timing of the onset (to within one minute). The filtered data are presented in the same format as the normal magnetogram data.

In a latitude profile, the perturbations at a given instant of time for stations arrayed along a common geomagnetic meridian are plotted as a function of the latitude of the stations. Similarly, in a longitude profile the perturbations at a given instant of time for stations along a common line of geomagnetic latitude are plotted as a function of longitude. In a background profile, all perturbations are taken with respect to a quiet time. With the excellent station coverage that was available for this study, the longitude profile permitted a greater resolution than has been possible in previous studies.

Profiles are useful for inferring the instantaneous configuration of the three-dimensional current systems which give rise to the observed magnetic perturbations. The spatial and temporal development of the current systems can be followed by plotting successive profiles, separated by short intervals of time.

In order to more carefully analyze the changes in the current systems before onset, differential profiles are used. In this profiling technique, the perturbations are zeroed at a time t_o shortly before the interval of interest. For the purpose of this study, the time t_o was chosen during a time of relative quiet occurring within 10 minutes of onset. This was determined by examining the background profiles. The assumption made in using this method is that the pre-existing current systems at time t_o remain constant while a secondary current system is superimposed upon the

first. (This assumption may break down, however, resulting in an ambiguity in interpretation.) Any change in the differential profile may be interpreted as the result of a growth of a secondary current system or the breakdown of the pre-existing one. As well, perturbations may arise on a differential profile as a result of movement of the background current system.

C. Method of Analysis

A number of theoretical profiles are presented in this section to serve as aids in analyzing profiles that will be encountered later on. In calculating the profiles, an elementary current loop is constructed in which the ionospheric currents are connected to the magnetosphere by means of field-aligned currents at each end. The loop may be closed in the magnetospheric equatorial plane, but is often left open for the purpose of calculations because at this distance an equatorial current of 4×10^4A, 75° in longitudinal extent, gives a maximum perturbation of less than 1 nT as detected at the surface of the Earth. Figure 2.2a shows the configuration of this current loop involving a westward ionospheric current; figure 2.2b shows the configuration for a southward ionospheric current. Of course the direction of the current may be reversed for the given circuit geometry. Any three-dimensional current system may

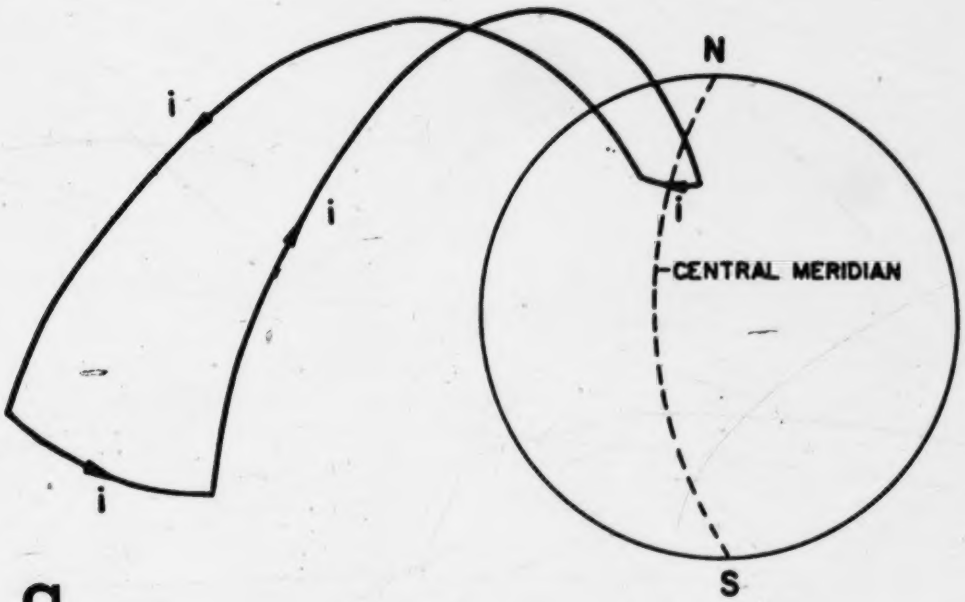

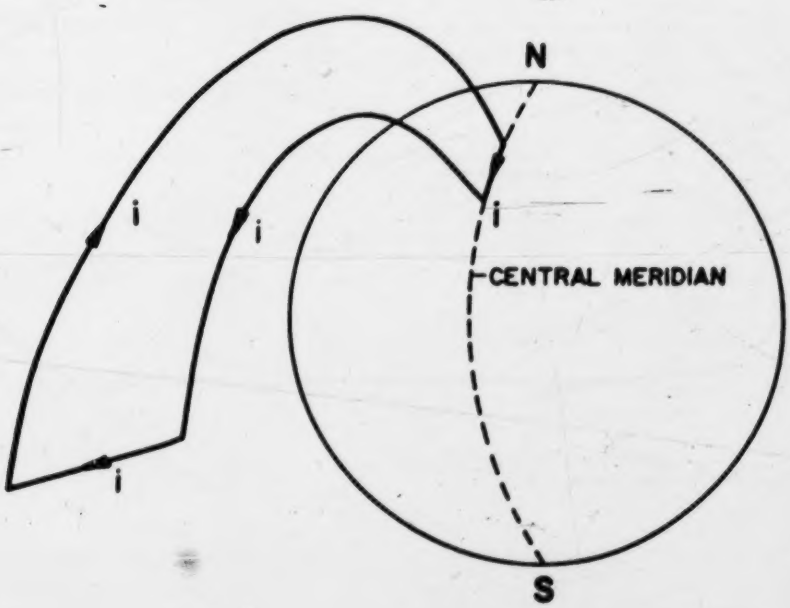

Figure 2.2 Elementary current loop associated with (a) a westward ionospheric current and (b) a southward ionospheric current (after Kisabeth, 1972).

be modelled as a superposition of the two types of current loops shown in figure 2.2. To calculate the components of the perturbation magnetic field associated with the current system the magnetic effects of the individual current loops are calculated using the Biot-Savart law, and summed. For a more detailed account of this method see Kisabeth (1972).

Figure 2.3 illustrates a number of latitude profiles for station lines at various positions at the Earth's surface for a three-dimensional current system involving a westward ionospheric electrojet. The total current is 1.0×10^4 A distributed uniformly over 20° in longitude and 5° in width (from 65° to 70°N). At the central meridian the H component reaches a negative maximum and Z undergoes a transition from negative to positive. The further the station line lies from the central meridian, the greater is the asymmetry of the Z component and the width of the Z and H peaks. For a station line to the west of the central meridian (see figure 2.3f) the sign of the D profile perturbation is reversed relative to a station line to the east of the central meridian.

Profiles may be constructed for many other hypothetical situations. In particular, uniform current densities were assumed for the profiles of figure 2.3 but the current may have some other functional form. Also, a current may flow along a path that is tilted with respect to a line of constant geomagnetic latitude. In this case the H component perturbation decreases and the D component perturbation

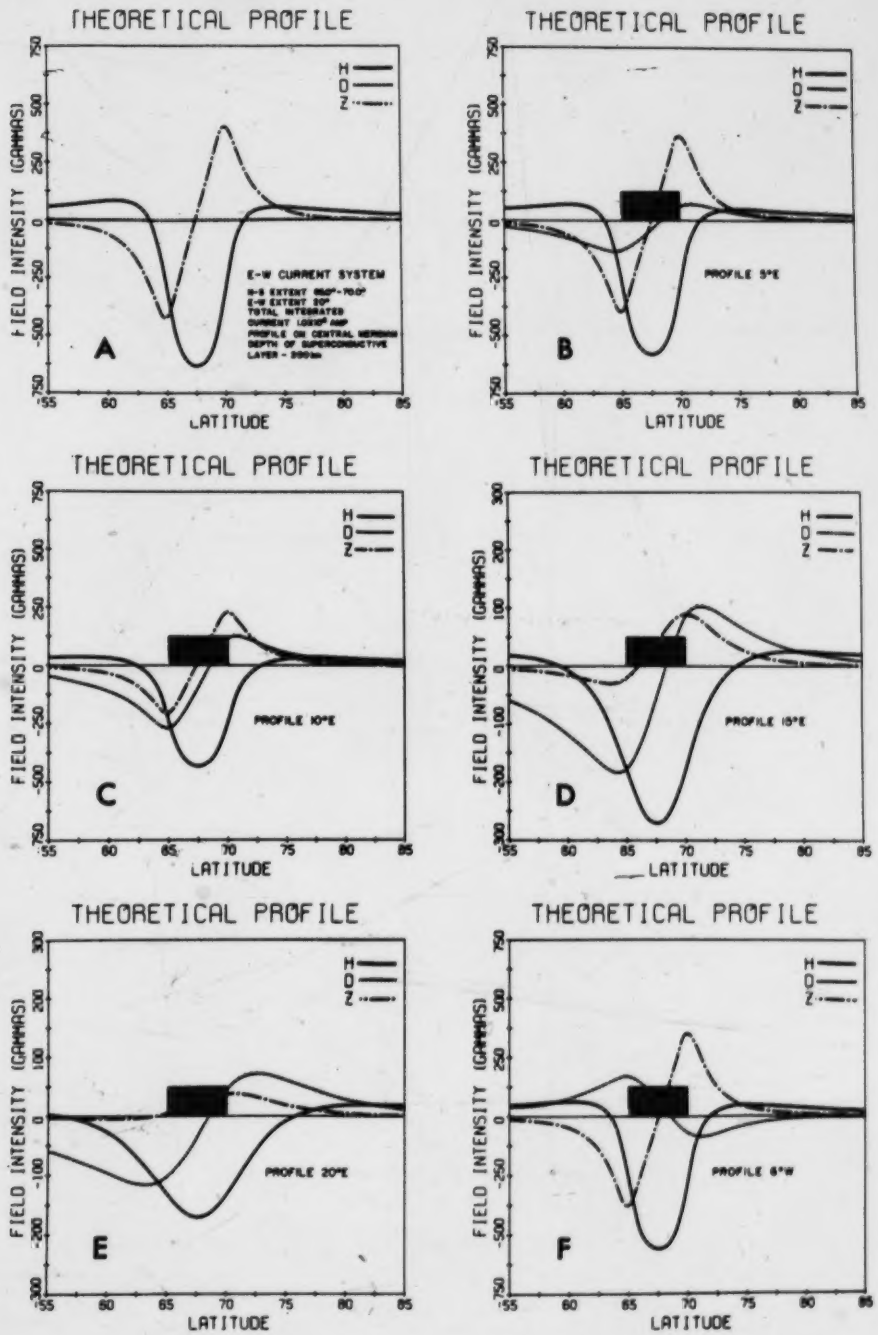

Figure 2.3 Theoretical profiles for a westward electrojet. Profiles are shown for various longitudes east and west of the central meridian (after Kisabeth, 1972).

increases in such a way that H^2+D^2 is a constant. A profile in which the shape and polarity of the D component follows that of the H component is indicative of a current system which is tilted from northwest to southeast with respect to a line of constant geomagnetic latitude.

Another important parameter to be included is the effect of induced currents in a conducting Earth. To simplify its complex conductivity structure the Earth is assumed to have an outer layer of zero conductivity, underlain by a core of infinite conductivity (Kisabeth, 1972). Had a finite value of conductivity been assumed for the core, time varying magnetic fields associated with the induced currents would have had to be included, making the mathematics intractable. Thus the assumption of infinite conductivity was made for simplicity. The thickness of the zero conductivity layer can be varied. As well, the height of the ionospheric currents may be varied, resulting in broader peaks in H and D as the height increases. An average height range is 105 to 125 km (Boström, 1964). The depth to the Earth's core of infinite conductivity is taken as 250 km and the height of the ionosphere is taken as 115 km for the models used in this study. In analyzing any profile it must be kept in mind that various current configurations may give rise to similar profiles, that is, the model systems are non-unique.

D. Selection of Events

Two main criteria were used in selecting events for this study. The first criterion was the presence on at least one of the Alberta magnetograms of a sharp positive D spike accompanied by the signature of substorm activity in the H and Z components. The D spike indicates the north-south and upward field-aligned currents associated with the presence of a surge structure overhead and, when not preceded by a slowly developing H bay, indicates that the substorm expansive phase is being initiated in or near our sector.

Secondly, since the magnetic precursors to the substorm expansive phase are expected to be of a low intensity in comparison level of substorm activity, events were chosen such that the level of magnetic activity in the two hours preceding onset was low in comparison that of the expansive phase onset itself. Thus it was hoped it would be possible to separate the expansive phase precursors from the signatures of other processes.

In order to provide good coverage of the precursory events, the events had to be chosen such that both the U of A and the IMS lines were in operation. This limited us to the interval from October,1977 to October,1979. The difficulty of finding isolated substorms is evidenced by the fact that only 8 events were found in this interval which satisfied the criteria given above. Of these, two were rejected due to the absence of data for key stations and two were rejected due to timing errors. Three of the remaining

four were selected as being representative, and are presented in the next chapter.

III. DATA INTERPRETATION AND MODELLING OF CURRENT SYSTEMS

A. Event Analysis-Day 231

Development of the Event

The expansive phase of the substorm of August 19, 1978 was triggered in response to a sudden northward turning of the IMF after a 1 hour period of southward IMF (Rostoker, 1983b). The stacked magnetograms for the Alberta stations are illustrated in figure 3.1. All times indicated represent universal time.

The start of our event, as defined by the southward turning of the IMF, occurred at approximately 0700. Satellite data from the IMP 8 magnetometer experiment was used to determine the timing of the southward turning. The magnetograms show that the geomagnetic activity is exceptionally low in the interval from the substorm onset up until the time of the northward turning over one hour later. A small positive deflection in H appears at a number of the stations during the growth phase, indicative of the growth of driven system eastward current.

From the associated Pi2 pulsations, shown in figure 3.2, the expansive phase onset is determined to occur at 0817. Thus this is a morning sector event, since local midnight at the Alberta is approximately 0700. Small negative deflections in D, occurring precisely at the time of the expansive phase onset, are recorded at each station.

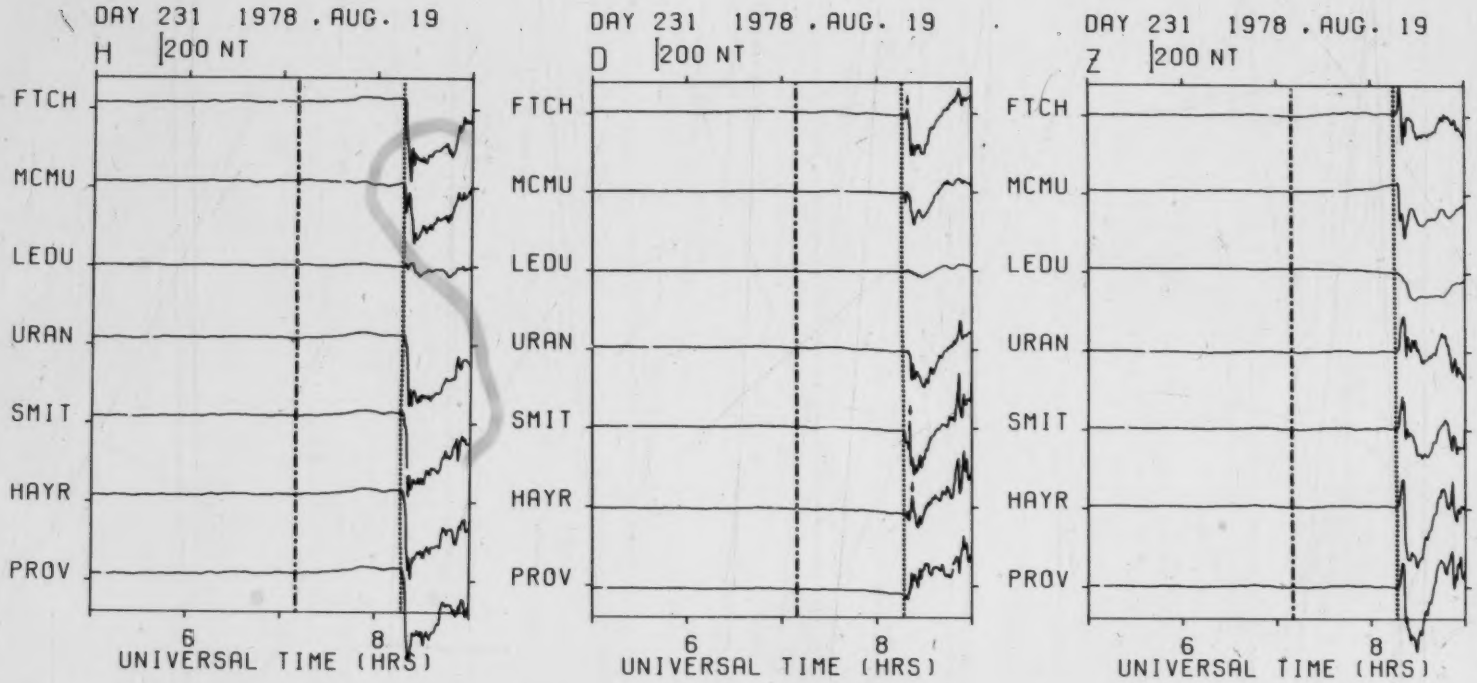

Figure 3.1 Stacked magnetograms for the Alberta array stations. The dashed line indicates the beginning of the growth of the driven system, marked by a southward turning of the IMF, while the dotted line shows the time of the expansive phase onset. The arrows in figure (b) indicate regions of interest referred to in the text.

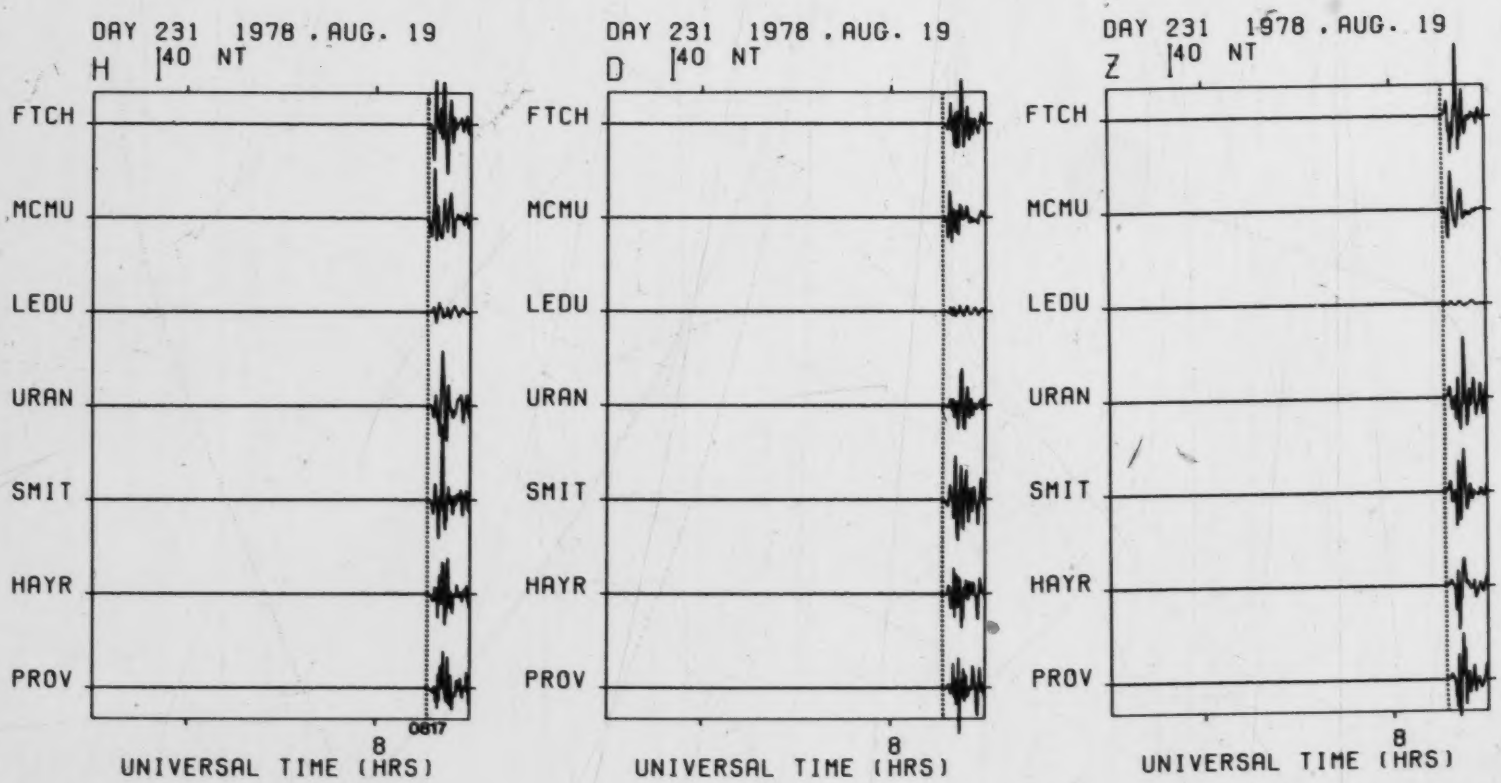

Figure 3.2 Pi2 pulsations for day 231, 1978 indicating expansive phase onset at 0817.

Sharp positive spikes in D occurring at FTCH, SMIT, and HAYR very shortly thereafter signify that a westward travelling surge has moved in overhead. This indicates that the expansive phase onset is initiated to the east of the station array and rapidly moves in over our stations. The surge appears over the array first at FTCH at 0818, then moves westward to appear at SMIT 3 minutes later, and at HAYR yet one minute later. The lack of any significant activity prior to 0817 indicates that this is an isolated substorm event. All stations, with the exception of LEDU, show large negative values in H during the expansive phase, indicating that they lie in the region of the substorm-enhanced westward current.

Riometer data were obtained for the PROV, SMIT and MCMU stations. Figure 3.3 indicates a sudden influx of energetic electrons occurring at 0817 at MCMU. This is followed by precipitation events at PROV and SMIT and a second precipitation event at MCMU, occurring approximately 8 minutes later, indicative of a second surge event. This is an example of a multiple onset event. However, only the precursors to the first onset were studied since the precursors to the following onsets could not be separated from the signatures of nearby surges. A smaller influx, more broadly distributed in time, appears at MCMU beginning at approximately 0755 and probably reflects the slow growth of the driven system.

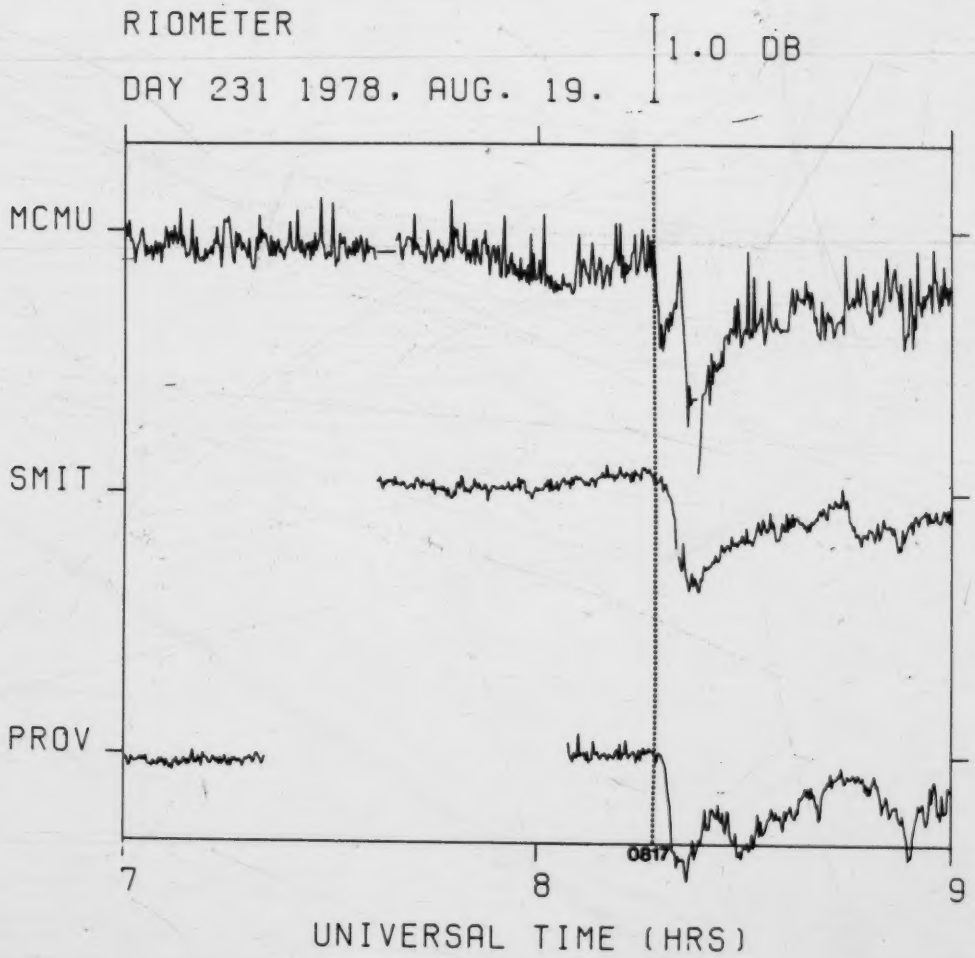

Figure 3.3 Riometer data for the day 231, 1978 event. The dotted line shows the time of the expansive phase onset.

The baseline for the profiles was chosen at 0700, August 19, prior to the onset of the driven system activity. In the interval from 0700 to the time of the expansive phase onset the slow development of an electrojet current system can be traced. The latitude profiles along the Alberta array (figure 3.4) indicate a westward electrojet lying to south of a broad eastward current sheet with an enhanced southern edge. A smaller eastward electrojet lies to the south of the westward electrojet. The D component becomes increasingly negative going from south to north across the westward electrojet indicating the presence of net upward field-aligned current across it. A slow equatorward motion of the entire electrojet system is evident until 0810 (cf. the profiles from 0745 to 0810). The westward electrojet grows slowly in intensity throughout this time. The latitude profiles for the Churchill line are similar to those of the Alberta line (see figure 3.5).

During the interval preceding the expansive phase onset the stations of the east-west line lie in the region of the high latitude eastward current sheet (see the east-west profiles of figure 3.6). The FTCH station lies slightly to the south of the east-west station line; thus the poor agreement between the FTCH station and the other stations in the 0745 longitude profile exhibits the high degree of latitudinal localization of the current structures. In the following profiles, as the current moves southward, the agreement is better.

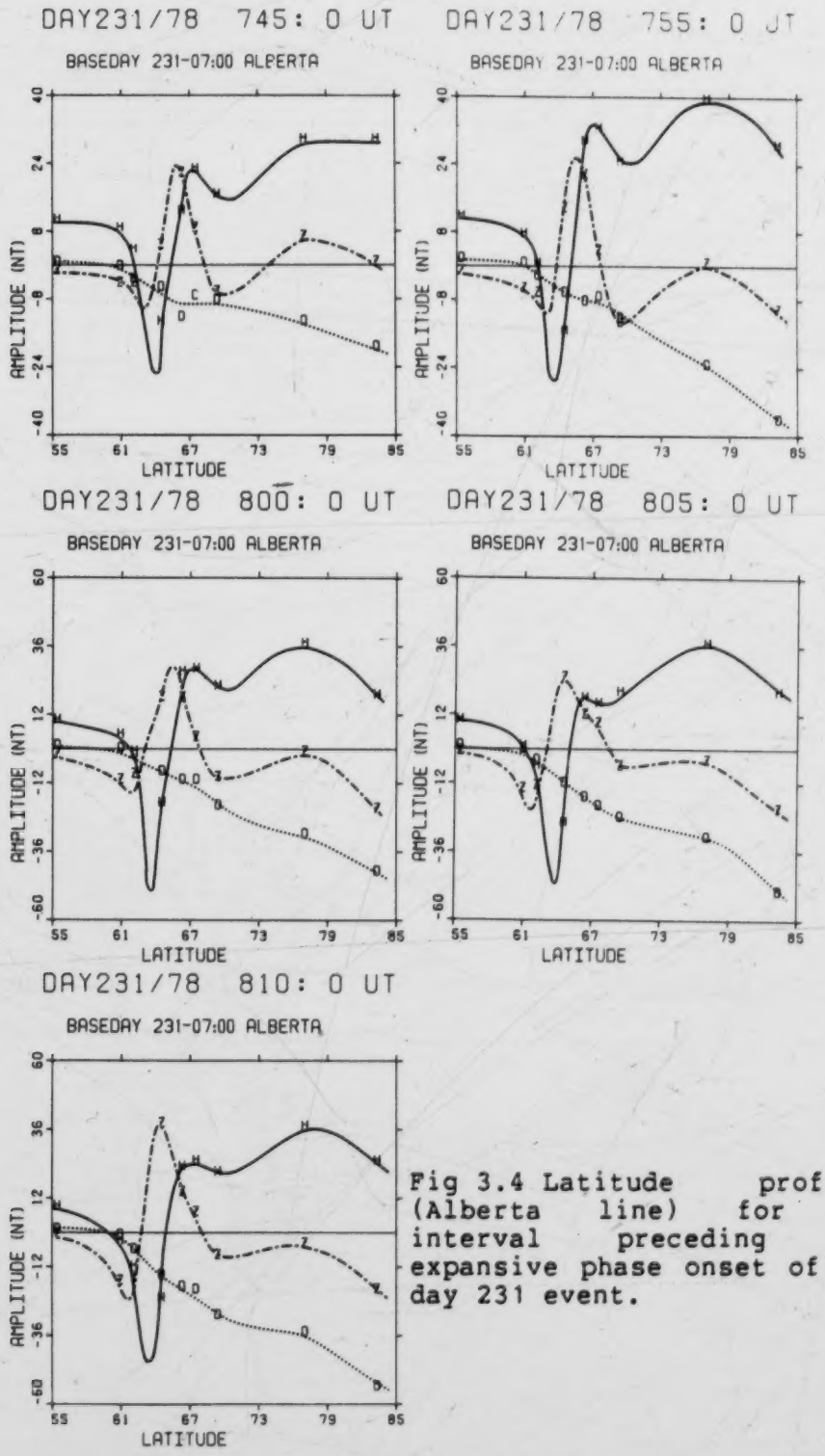

Fig 3.4 Latitude profiles (Alberta line) for the interval preceding the expansive phase onset of the day 231 event.

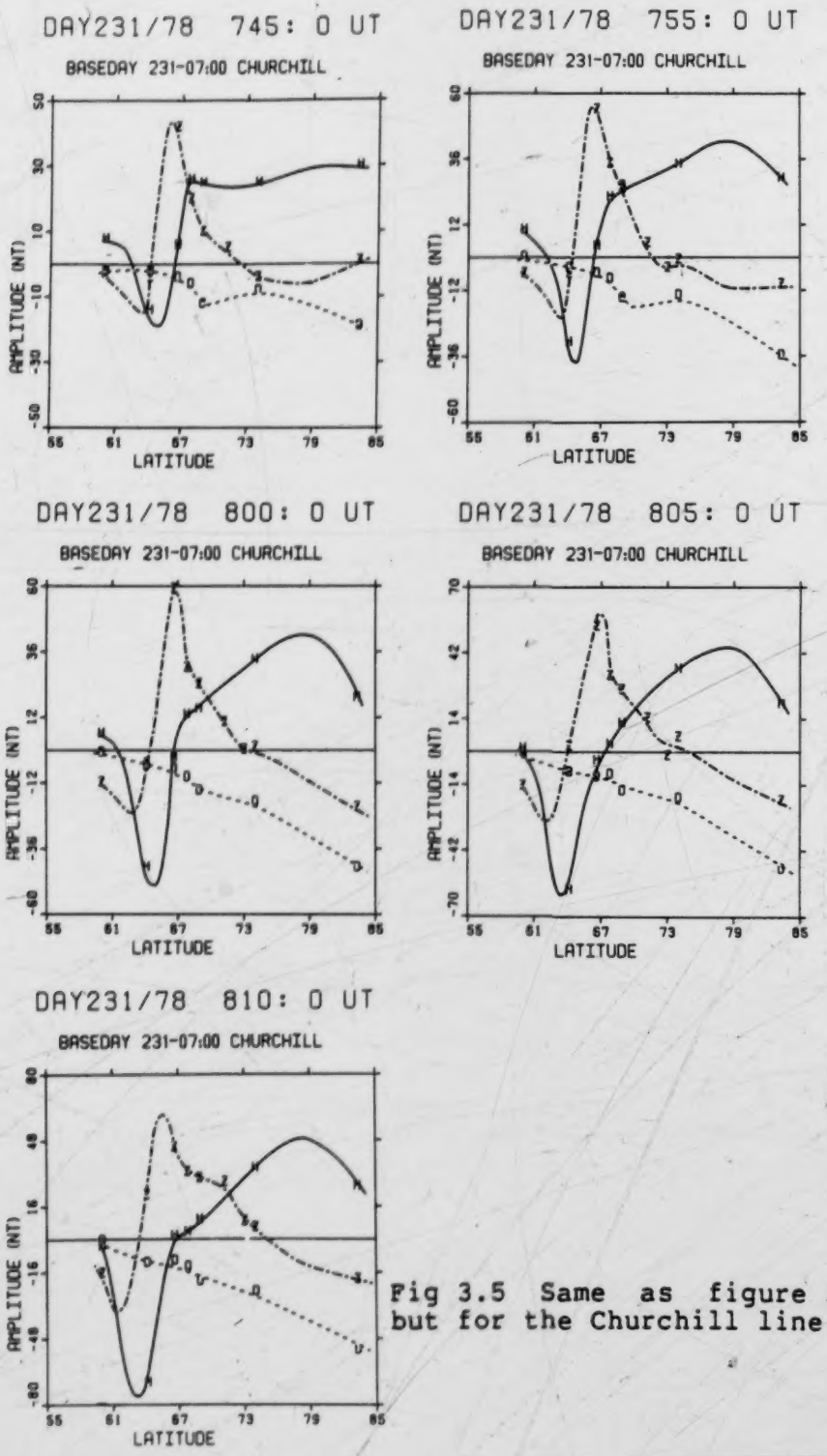

Fig 3.5 Same as figure 3.4 but for the Churchill line.

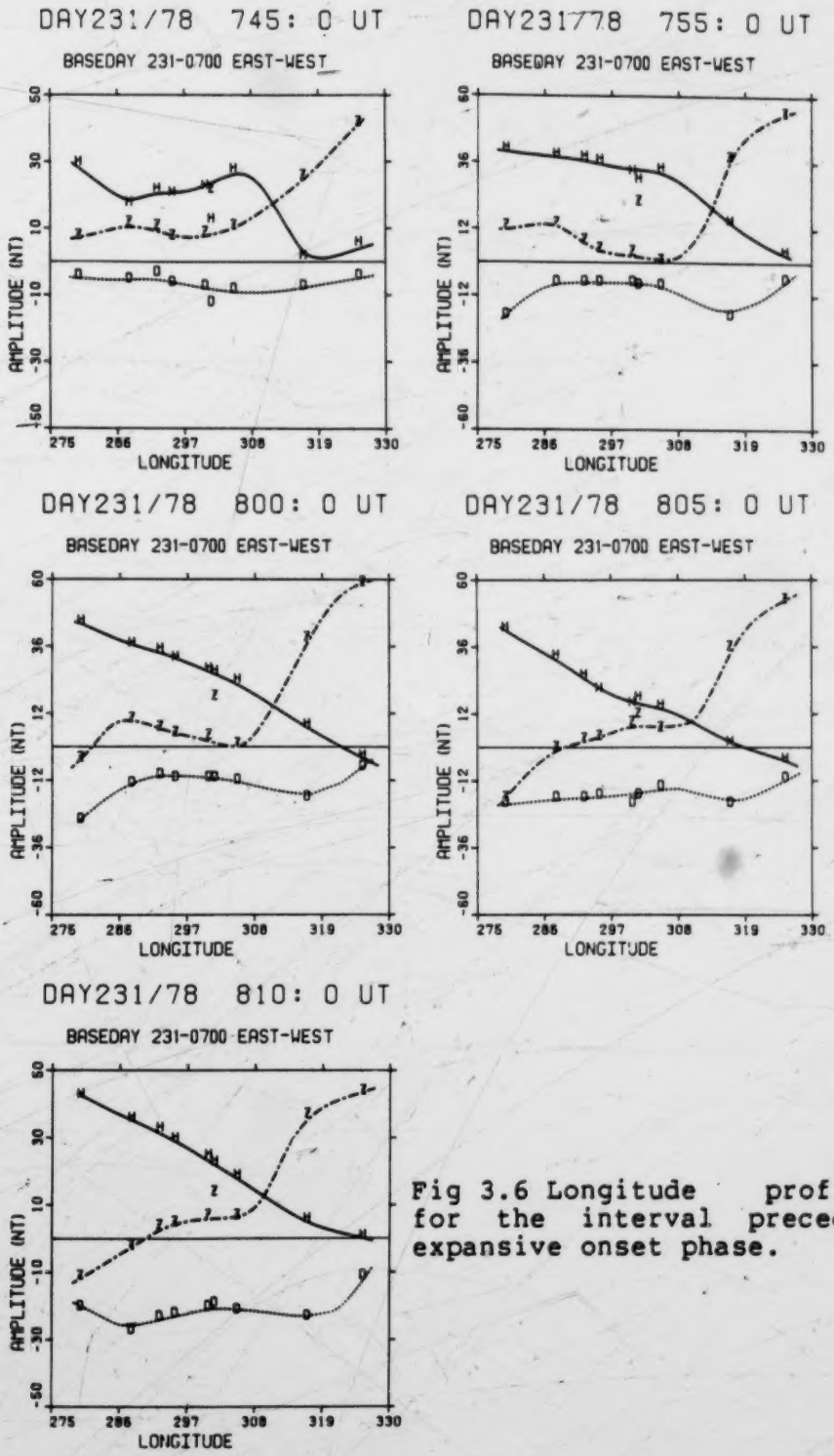

Fig 3.6 Longitude profiles for the interval preceding expansive onset phase.

The profiles at 0818 (figure 3.7) indicate the localization of the substorm enhanced activity. The longitude profile indicates that the region of substorm enhanced activity is located over the Alberta line at this time, while the Alberta profile shows that a substorm enhanced electrojet is centred near MCMU.

Modelling the Current Systems

The basetime for the differential profiles was chosen at 0812. Fig 3.8 shows the profiles for the background current system at this time. This current system is modelled as a narrow westward electrojet positioned between a broad eastward current sheet to the north and an eastward electrojet to the south. The westward electrojet narrows slightly from east to west. The entire system is tilted from southwest to northeast, consistent with the tilt of the morningside auroral oval. The background model system is shown in figure 3.9a; the model parameters are given in table 3.1. The profiles based on this system are shown in figure 3.10; these are to be compared with those of figure 3.8. Note that for the purpose of modelling the profiles, extra points were added to fill in the gaps between stations.

The only unusual feature of this model is the strong eastward current just poleward of the westward electrojet. The boundary plasma sheet electrons precipitated into this region usually have low energies, causing weak Hall

TABLE 3.1

CURRENT SYSTEM PARAMETERS FOR DAY 231, 1978

Eastward/Westward ionospheric current	Downward Current Flow S.edge-N.edge (°E) (°N)		current density (mA/m)	Upward Current Flow S.edge-N.edge (°E) (°N)		current density (mA/m)
A)Background profile						
East	275 63	275 84	63	350 68	350 89	63
West	350 64.8	350 68	98	275 60.8	275 63	140
East	275 53.3	275 60.8	20	350 57.3	350 64.8	20
B)Differential profile						
East	275 63.5	275 84.5	63	350 68.5	350 89.5	63
West	350 65.3	350 68.5	98	275 61.3	275 63.5	140
East	275 53.8	275 61.3	20	350 57.8	350 65.3	20
West	306 65.5	306 66	360	296 64.9	296 65.4	360

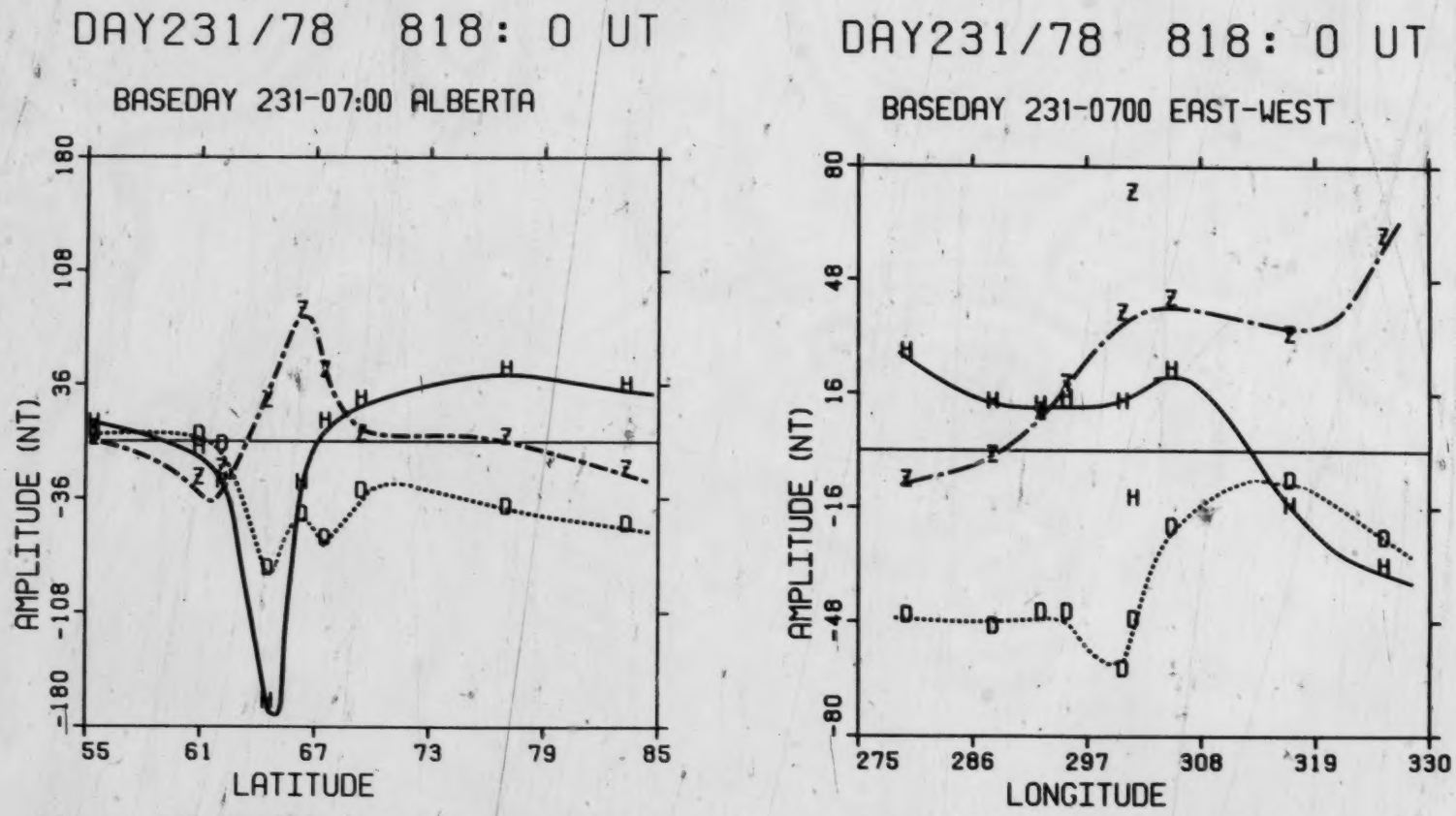

Figure 3.7 Profiles taken one minute after onset indicating the region of the substorm enhanced activity. Note the latitudinal localization of the westward electrojet.

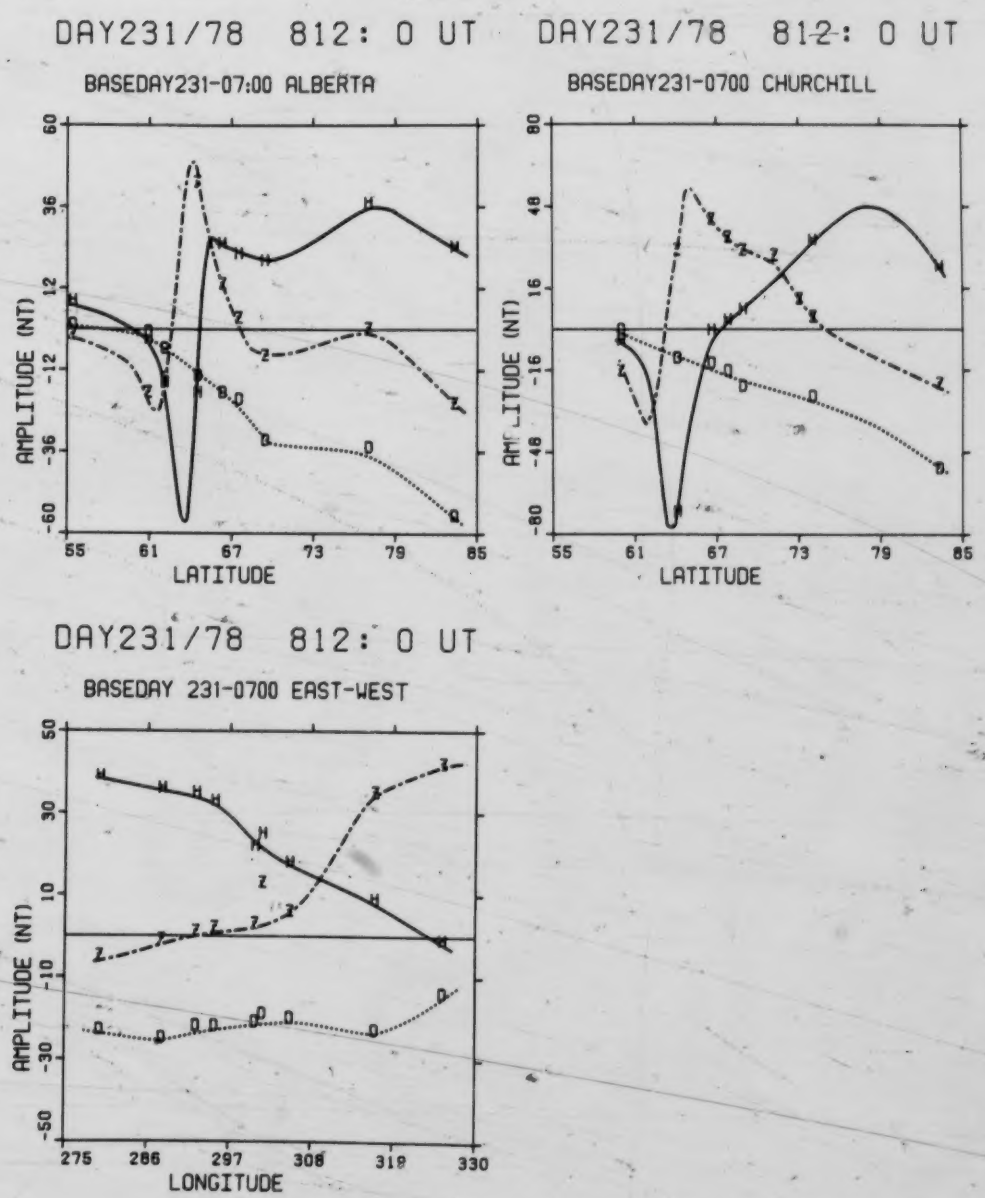

Figure 3.8 Observed profiles for the current system at 0812, day 231.

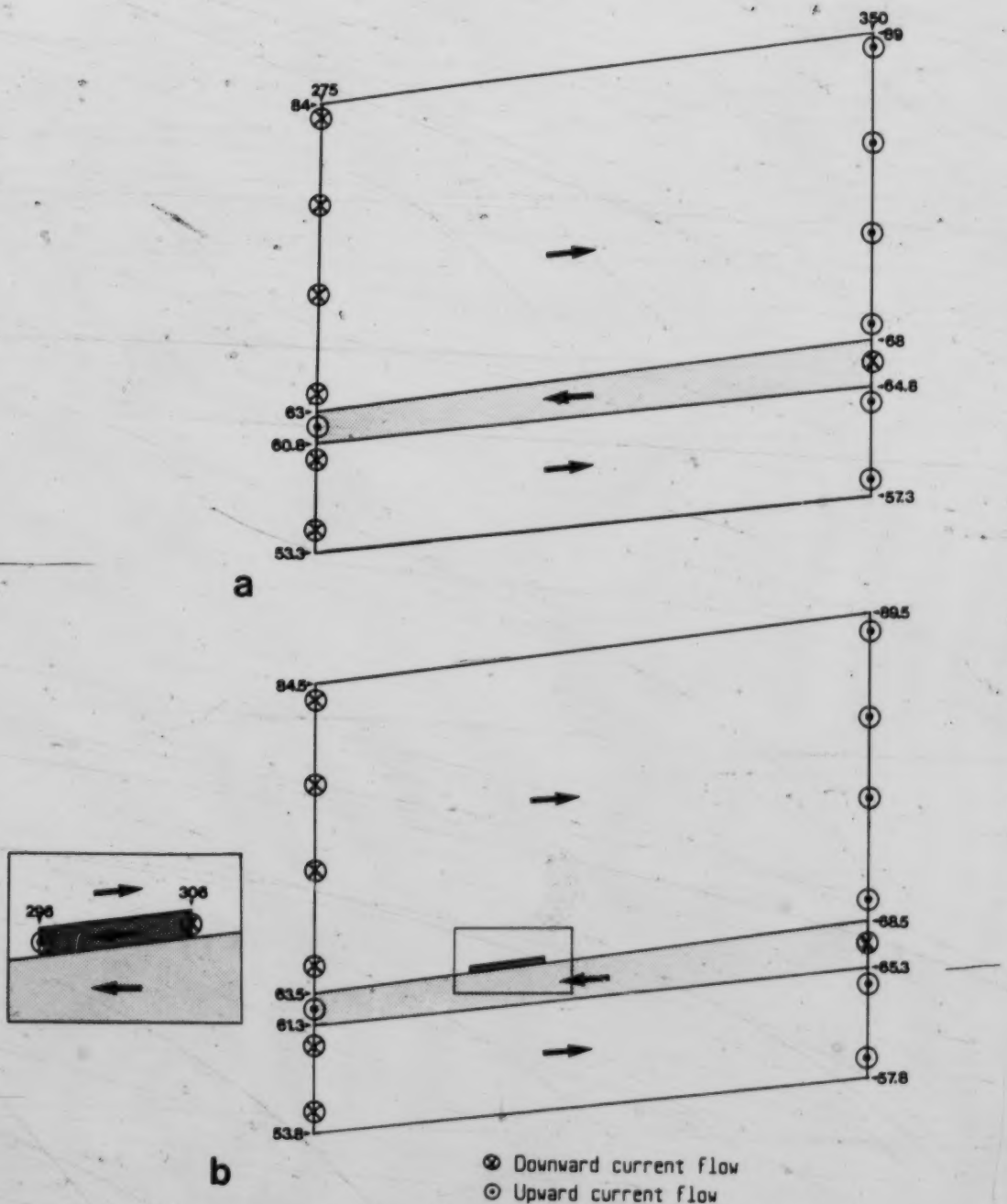

Figure 3.9 Models of the current systems for day 231, a) the background profiles and b) the differential profiles. The enlargement shows the filamentary westward electrojet.

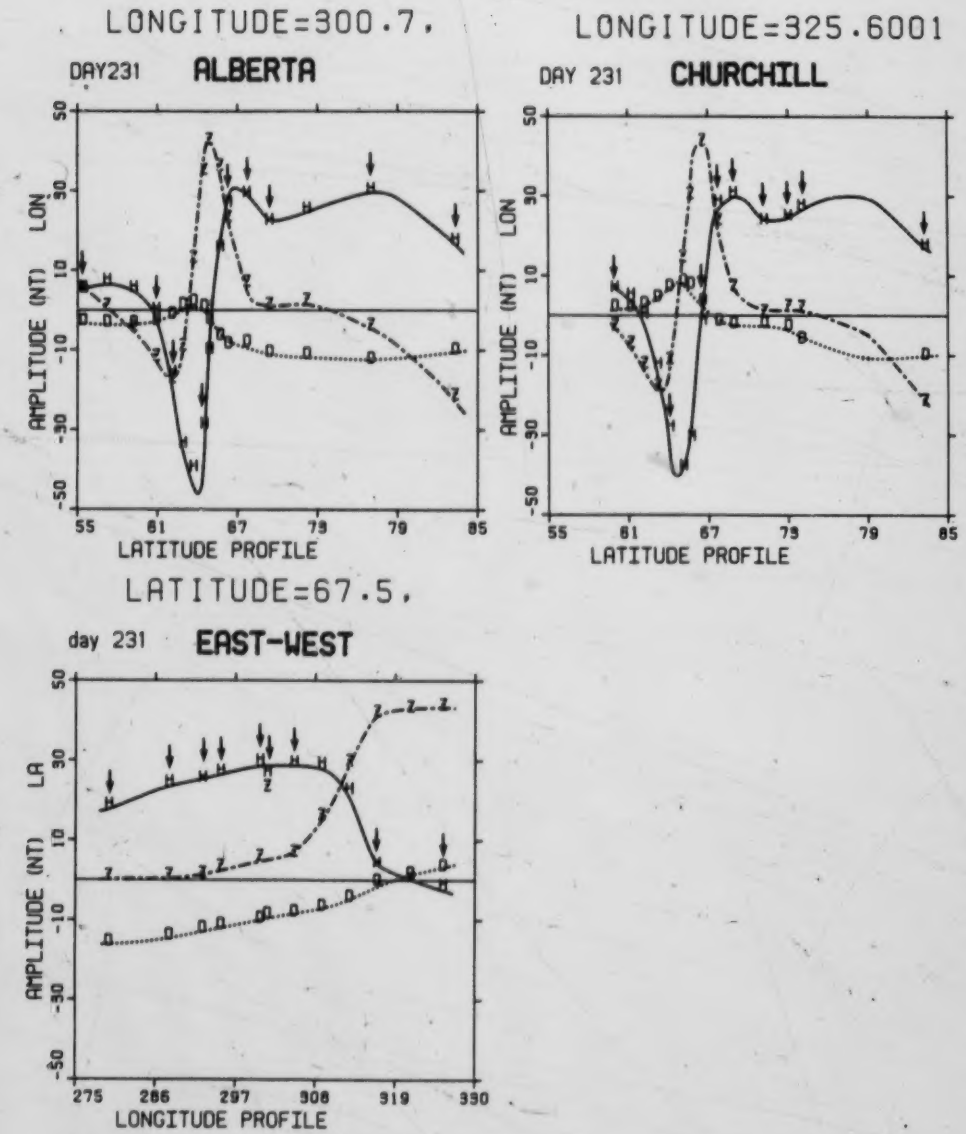

Figure 3.10 Theoretical profiles corresponding to the model shown in figure 3.10a. The arrows indicate the locations of the magnetometer stations.

conductivity and hence negligible current. However in the case of a strong magnetic substorm, the electrons are energized sufficiently so that they can create significant conductivity leading to a detectable electrojet current (Rostoker et al, 1985). Since an electric field transition exists at the poleward border of the westward electrojet, the particle $\underline{E}x\underline{B}$ velocity poleward of the transition is in the opposite direction to that in the region of the westward electrojet. Thus the currents are oppositely directed in these two regions. This band of high conductivity generally has variable width and is taken to be on the order of 3° for this event. A uniform distribution of current is used for the eastward and westward electrojets.

Comparison of figures 3.8 and 3.10 indicates that the data have a negative bias in D with respect to the model system. This is the result of a DP2 current system which was not included in the model. The DP2 current system involves poleward current flow in the local midnight sector and equatorward current flow in the pre-noon quadrant. The condition for DP2 current flow is IMF Bz<0 (Braithwaite and Rostoker,1981). The DP2 current will be enhanced if the polar cap conductivity is high. Both conditions are met for this event; the ionosphere was continually sunlit at and beyond the geographic latitude of 66.5°N. This corresponds to a magnetic latitude of approximately 72°N. Thus the polar cap conductivity would be high due to photo-ionization, so that a portion of the DP2 current could flow from midnight

to noon across the polar cap. This results in a negative bias in the D component near local midnight.

A discrepancy exists between the model and data results for the Churchill line, especially between the latitudes 66°N to 70°N. This is a result of the fact that the model includes a sharp discontinuity between the westward electrojet and the eastward current sheet. This sharp gradient appears to exist further to the west, as shown by the good agreement between data and model results on the Alberta profiles. However, at 325°E the sharpness of the border between the two oppositely directed currents appears to have lessened somewhat. This variation in the gradient could not be modelled because although there are fluctuations and irregularities in the ionospheric currents, the modelling program, in its present state of development, only allows variations in a direction perpendicular to the current flow. Thus the discrepancy must be attributed to limitations of the current modelling program.

Note that the point corresponding to the FTCH station on the east-west line indicates a high degree of latitudinal localization of the current structures, as does the corresponding point in the longitude profile of figure 3.10.

The differential profiles at 0816, one minute before onset, are shown in figure 3.11. The feature of particular interest is the reversal in polarity in D observed in the longitude profile near 300°E. This suggests the presence of antiparallel field-aligned currents which are confined in a

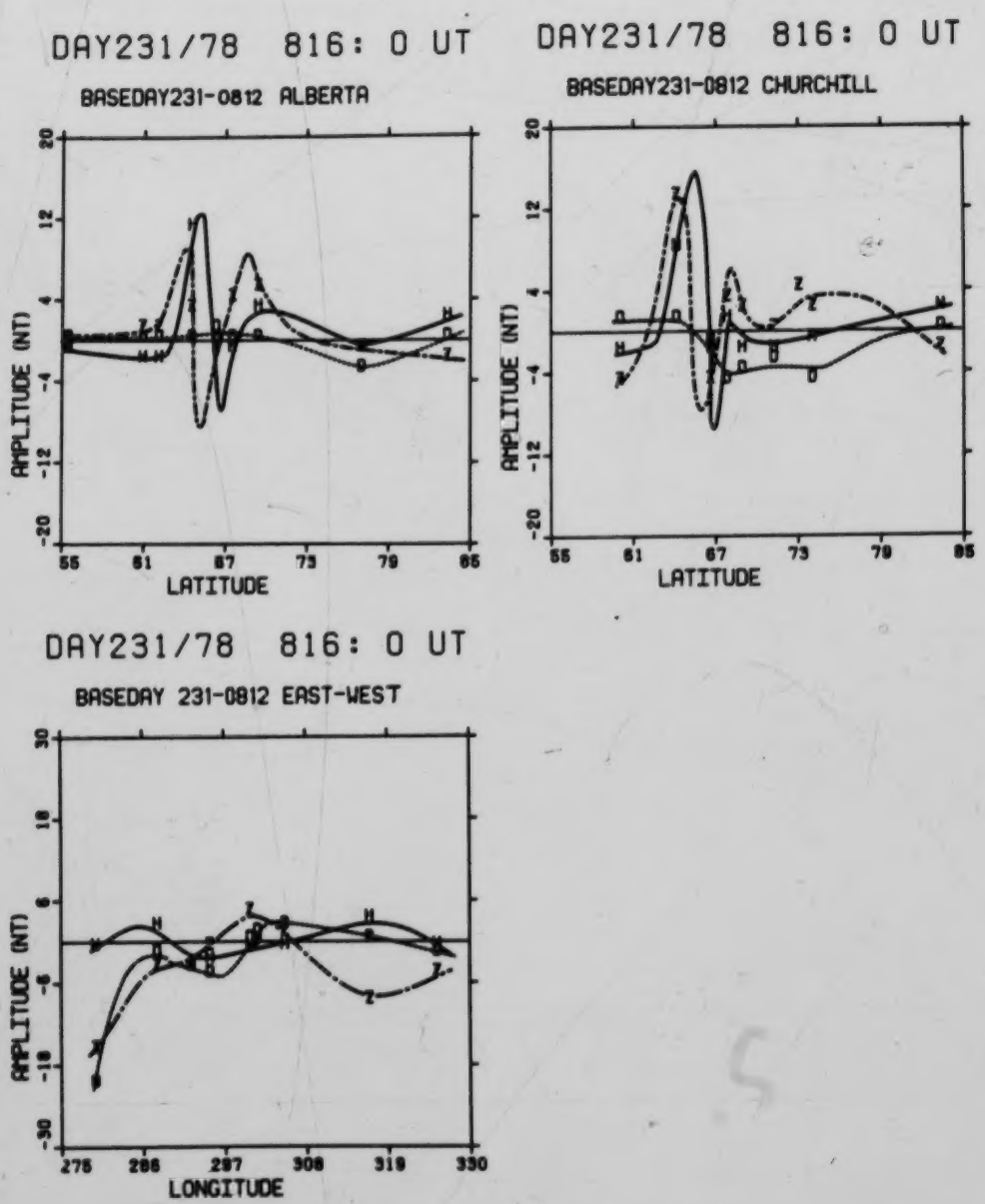

Figure 3.11 Observed differential profiles for day 231, 1978 taken one minute before expansive phase onset.

longitudinal sense. The latitude profiles indicate that the current system has moved northward in the interval since 0812. The differential current system is modelled as shown in figure 3.9b. To create the differential current system, the background current system of figure 3.9a is moved northward by 1/2°. A filamentary westward electrojet, 10° in length (1/2° in width),with downward current at the eastern edge and upward field-aligned current at its westward edge is superimposed upon the system, just to the north of the westward electrojet. The field-aligned current links this filamentary electrojet to the magnetotail. The differential profiles corresponding to this model are shown in figure 3.12.

The positive and negative peaks in H for the latitude profiles are slightly displaced from those indicated by the data. This effect is accounted for by variations in the current densities. In the ionosphere, the current densities can be irregular on a small spatial scale, while the model can only incorporate grosser effects.

The agreement in D and H in the source region is good for the longitude profile. The Z component of the longitude profile in figure 3.12 has a positive bias with respect to that of figure 3.11. Note that the NOW station, at the western edge of the longitude profile, is closer to the region of the Harang discontinuity. The currents in this region are expected to be larger and to bleed up the field lines. This effect is not incorporated in to the model and

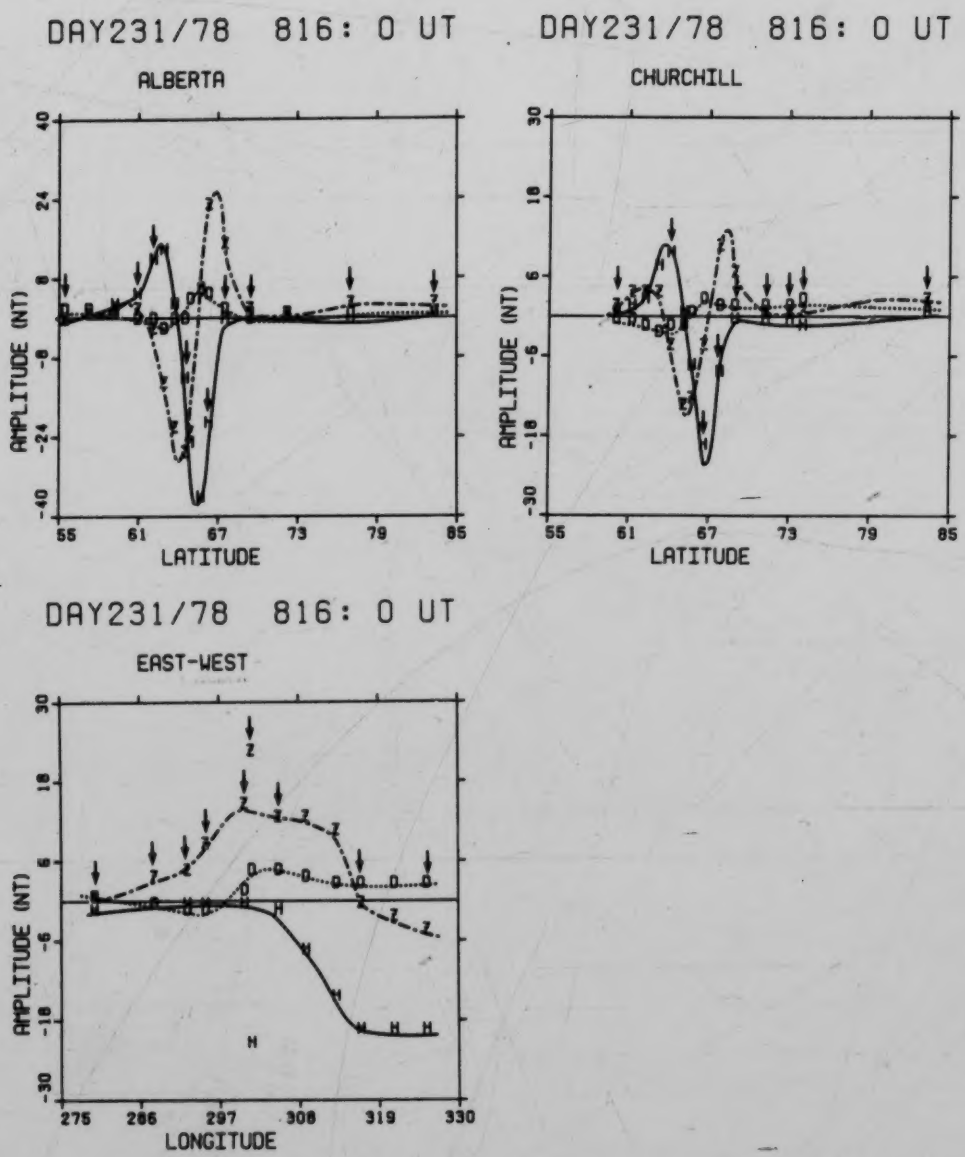

Figure 3.12 Theoretical differential profiles depicting the magnetic perturbations due to northward motion of the current system and the intrusion of a weak current wedge. The arrows indicate the positions of the magnetometer stations.

hence the disagreement between data and model results at NOW.

Summary of Day 231

The important features of the day 231 event are the northward motion of the entire current system and the introduction at the northern border of the westward electrojet of a filamentary westward current linked to the magnetotail by upward and downward field-aligned current at the western and eastern edges, respectively. The field-aligned currents associated with the filamentary westward current have a magnitude of 360 mA/m.

The interface between the eastward and westward electrojets maps to the CPS/LLBL interface (cf. 1.7) so that the northward motion of this interface implies the intrusion of CPS plasma into a region of space previously occupied by the LLBL plasma.

The filamentary westward electrojet, with its associated field-aligned currents, which was added in constructing the differential profile, is in effect a weak substorm current wedge. This is significant in that we are observing the wedge before the onset of the expansive phase.

B. Event Analysis-Day 59, 1979

Development of the Growth Phase

The substorm of February 28, 1979 is presented in detail in this section. The H, D, and Z component magnetograms are shown in figure 3.13. The associated Pi2's are shown in figure 3.14.

On the basis of the Pi2 pulsation activity, the expansive phase onset was determined to occur at approximately 0809 so that, like day 231, this is a morning sector event. The activity occuring at several stations between 0700 and 0730 suggests that the substorm is not entirely isolated, however the distinctness of the substorm onset at 0809 indicates that it is not connected to the previous activity. Also, the magnetic disturbances return to almost zero level after the initial activity, so that this event may be considered to be separated from the earlier disturbance. The riometer data appear to support this conclusion (see figure 3.15). An electron precipitation event is evident at the time of onset with no suggestion of electron influx at an earlier time.

Surge features appear overhead at HAYR and PROV, then later at SMIT and URAN as evidenced by the positive D spikes at those stations(figure 3.13). Because the initial deflections at HAYR and PROV are positive we may conclude that the expansive phase was triggered directly over our station array. This is in contrast to the day 231 event, in

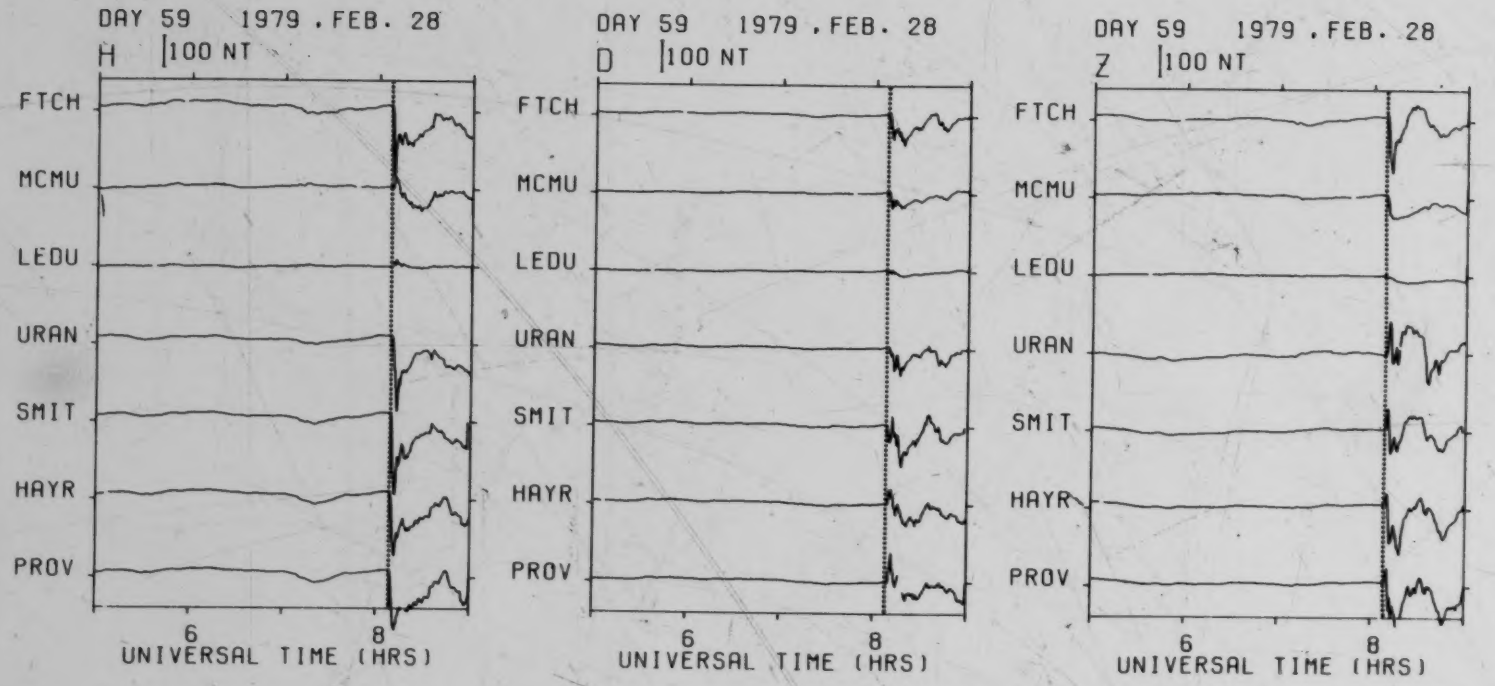

Figure 3.13 Stacked magnetograms for the Alberta stations. The dotted line indicates the time of the expansive phase onset.

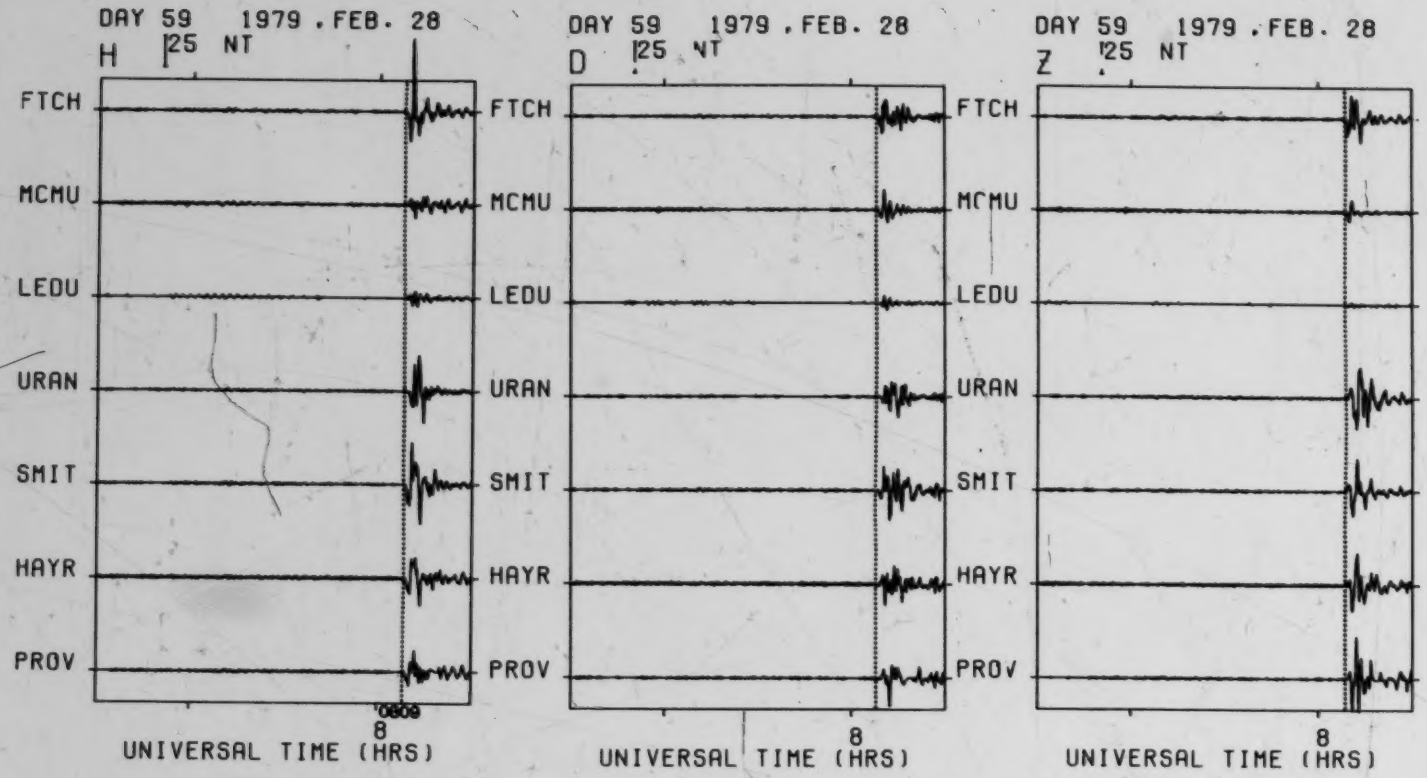

Figure 3.14 Pi2 pulsations for day 59, 1979 indicating expansive phase onset at 0809.

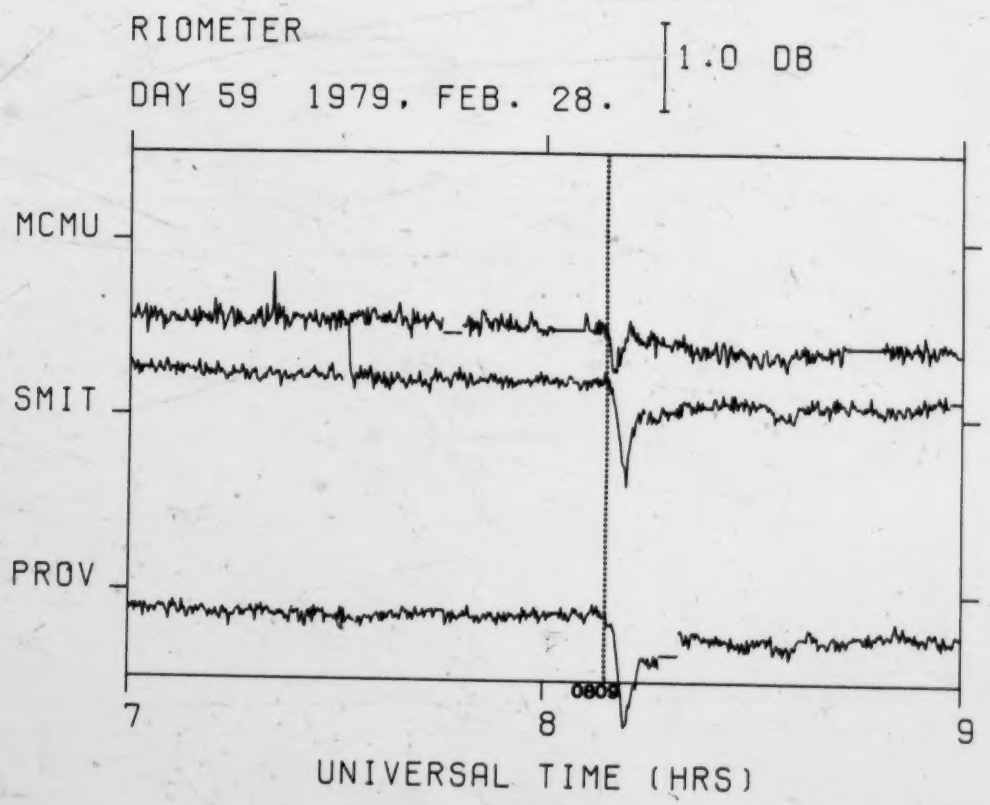

Figure 3.15 Riometer data for the day 59, 1979 event. The dotted line shows the time of the expansive phase onset.

which the surge appeared initially to the east of the Alberta stations and then moved westward over the array. The positive D spikes at SMIT and URAN are indications of a secondary onset occurring to the east of the first one. Negative H bays occuring after onset at the FTCH, URAN, SMIT, HAYR, and PROV stations, indicate that they lie in the region of substorm enhanced westward electrojet. The two southernmost stations, MCMU and LEDU, initially show small positive H, indicative of eastward electrojet.

The quiet time baseline for the profiles is taken at 0630. Latitude profiles from the Alberta line at 0740 indicate the presence of a westward electrojet sandwiched between an eastward electrojet to the south and a broad eastward current sheet to the north. (figure 3.16). The westward electrojet has a thickness of approximately 3°, centred at 67° N. As in the previous event, there appears to be a southward motion of the current system prior to substorm onset. By 0755, a narrow band of intense eastward current has appeared to the north of the westward electrojet superimposed upon the broad sheet current. Net upward field-aligned current is indicated by the polarity reversal in D at the border between the eastward and westward electrojets.

A similar current configuration is indicated to the east by the latitude profiles of the Churchill line (see figure 3.17), except that the westward electrojet is much wider in this sector. Due to the station spacing it is

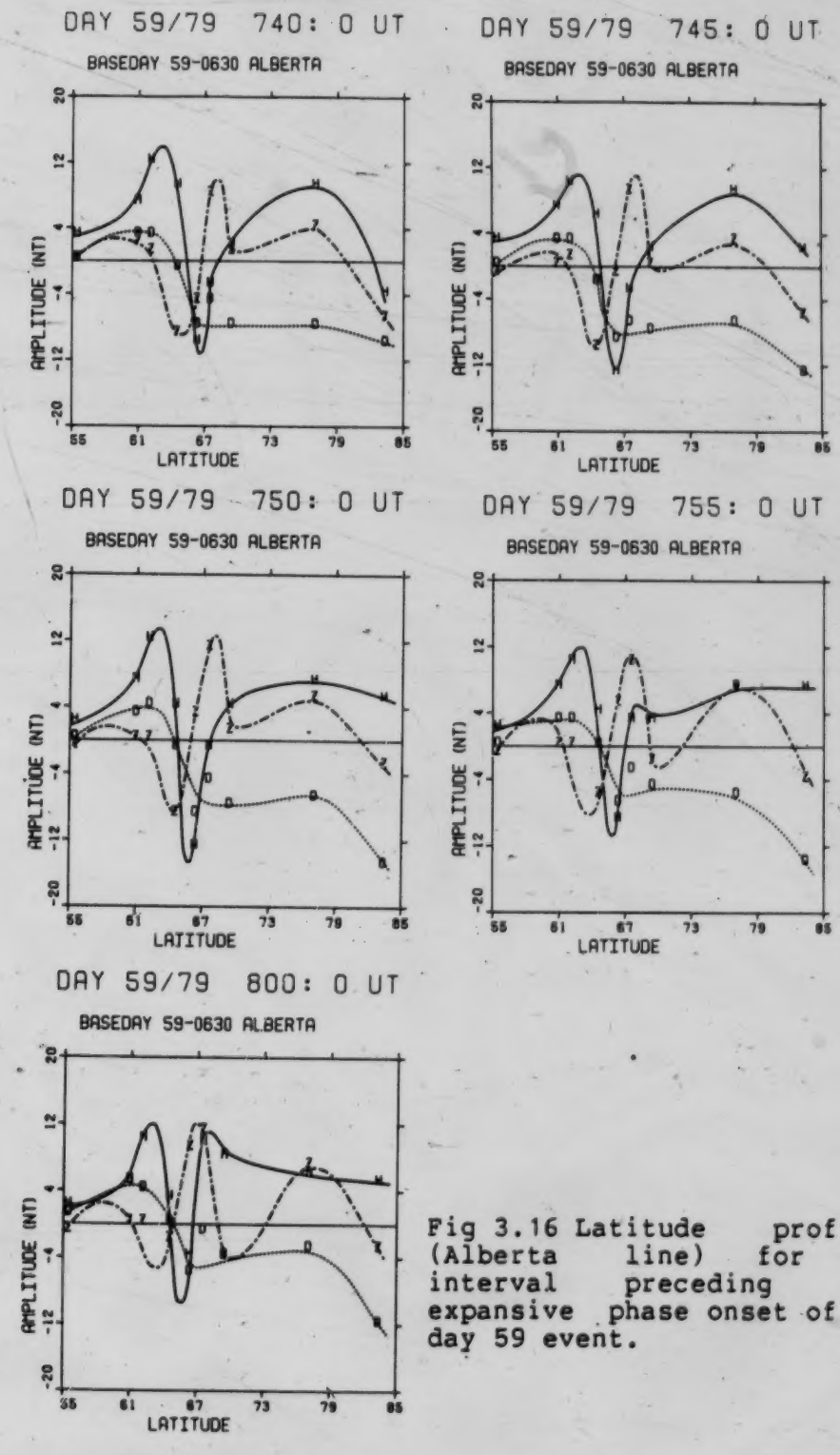

Fig 3.16 Latitude profiles (Alberta line) for the interval preceding the expansive phase onset of the day 59 event.

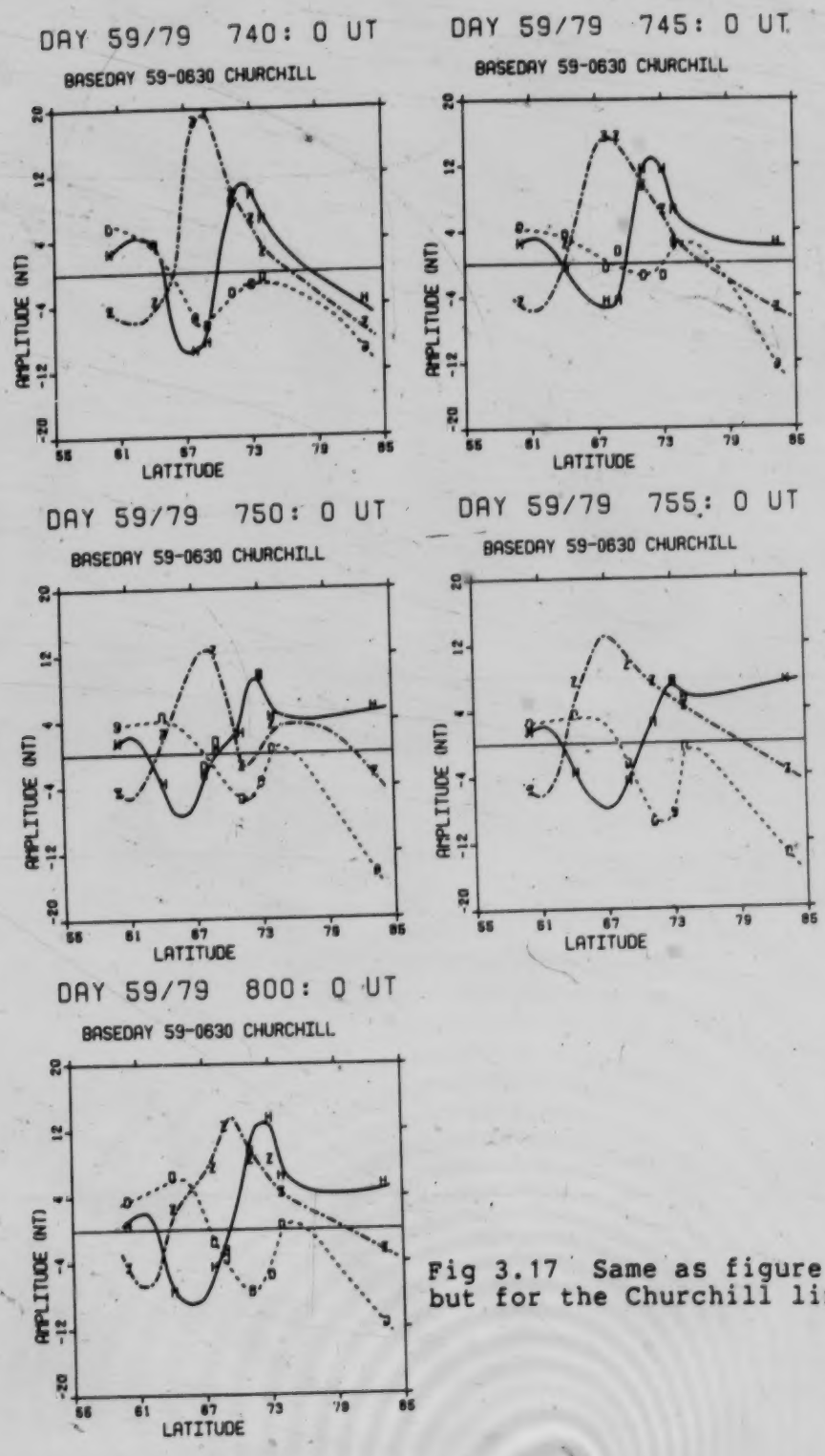

Fig 3.17 Same as figure 3.16 but for the Churchill line.

difficult to ascertain whether or not there is any latitudinal motion of the current system.

The negative H component of the longitude profiles (figure 3.18) shows that the stations lie in the region of overhead westward electrojet at 0740. As the system evolves the H component becomes increasingly positive indicating that the eastward current sheet is moving into this sector. Thus the longitude profiles confirm that there is a southward motion of the current configuration during this interval. The disagreement between the FTCH station and the rest of the line gives an indication of the latitudinal localization of the electrojets.

At 0809, expansive phase onset takes place at 301°±2°E and 65°±1/2°N (Samson and Rostoker, 1983). That is, it takes place over the Alberta line, between MCMU and FTCH.

Modelling the Current Systems

The baseline for the differential profiles is taken at 0800, about nine minutes before the onset. The profiles for the background current system at this time are illustrated in figure 3.19. The westward electrojet appears to widen considerably going from west to east. The polarity reversal in D suggests the presence of upward field-aligned current at the border between the eastward and westward electrojets.

The background current system is modelled as shown in figure 3.20a; the model system parameters are given in table 3.2. The model consists of a broad eastward current sheet to

TABLE 3.2

CURRENT SYSTEM PARAMETERS FOR DAY 59, 1979

Eastward/Westward ionospheric current	Downward Current Flow S.edge-N.edge (°E) (°N)		current density (mA/m)	Upward Current Flow S.edge-N.edge (°E) (°N)		current density (mA/m)
A)Background profile						
East	275 65.7	275 84.7	11	350 70	350 89	11
West	350 62	350 70	19	275 65.6	275 65.7	1500
West	350 62	350 70	7	350 62	275 65.6	1.6
East	275 60.5	275 65.6	61	350 62	275 65.6	10
B)Differential profile						
East	275 65.7	275 84.7	8	350 70	350 89	8
West	350 62	350 70	17	275 65.6	275 65.7	1300
West	350 62	350 70	7	350 62	275 65.6	1.6
East	275 60.5	275 65.6	61	350 62	275 65.6	10
West	306.5 68.5	306.5 69	125	296.5 67.9	296.5 68.4	125

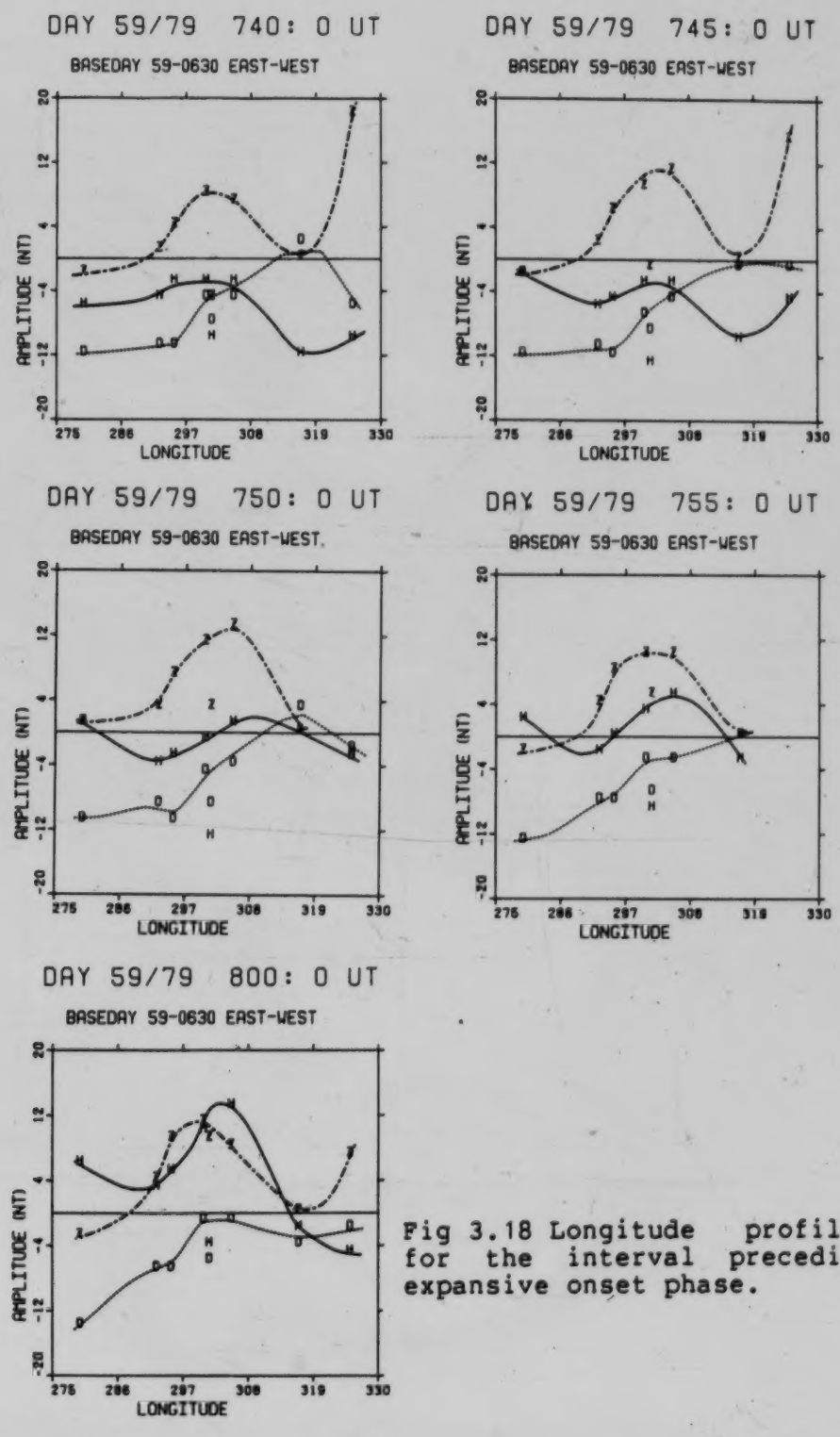

Fig 3.18 Longitude profiles for the interval preceding expansive onset phase.

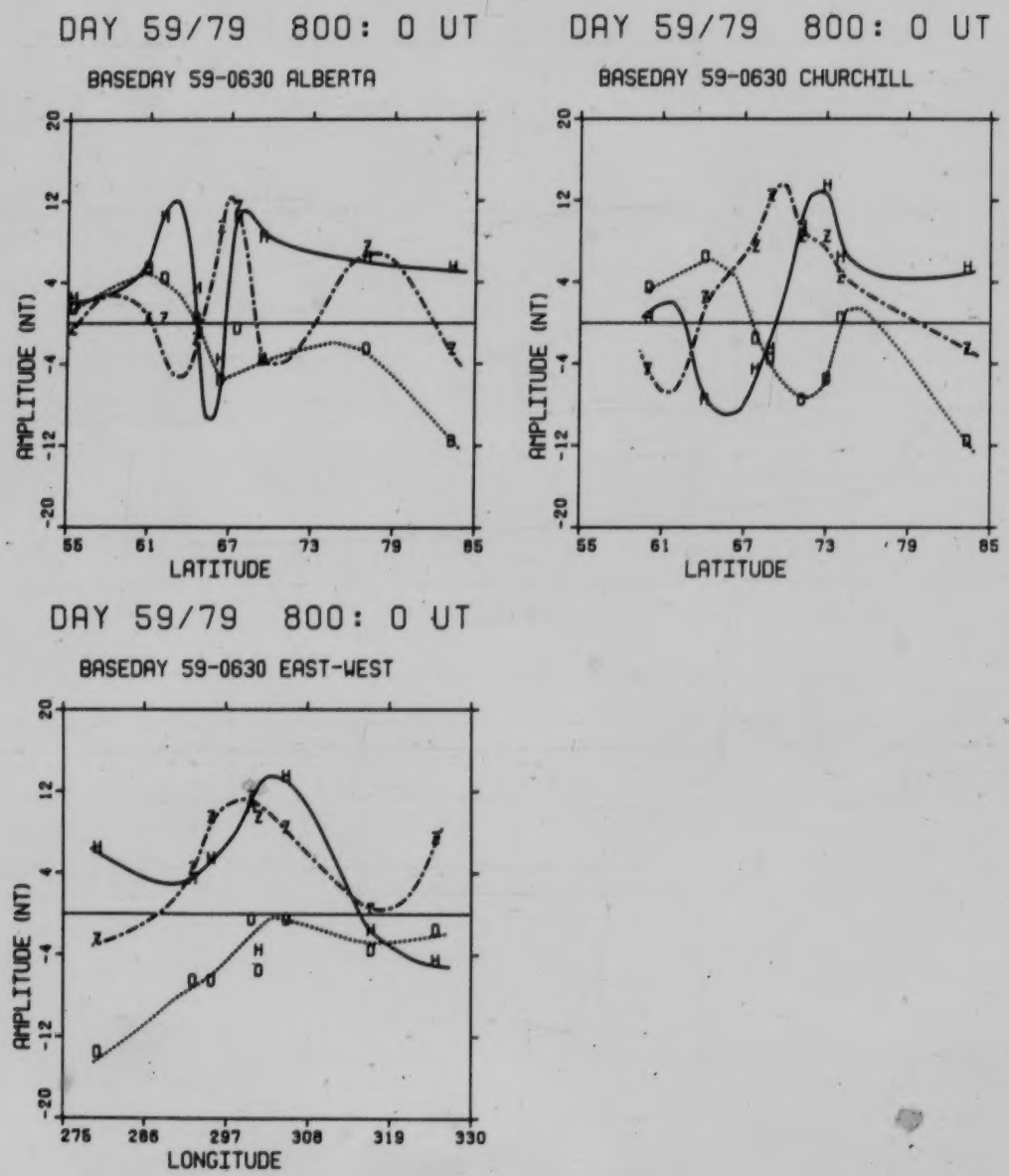

Figure 3.19 Observed profiles for the current system at 0800, day 59.

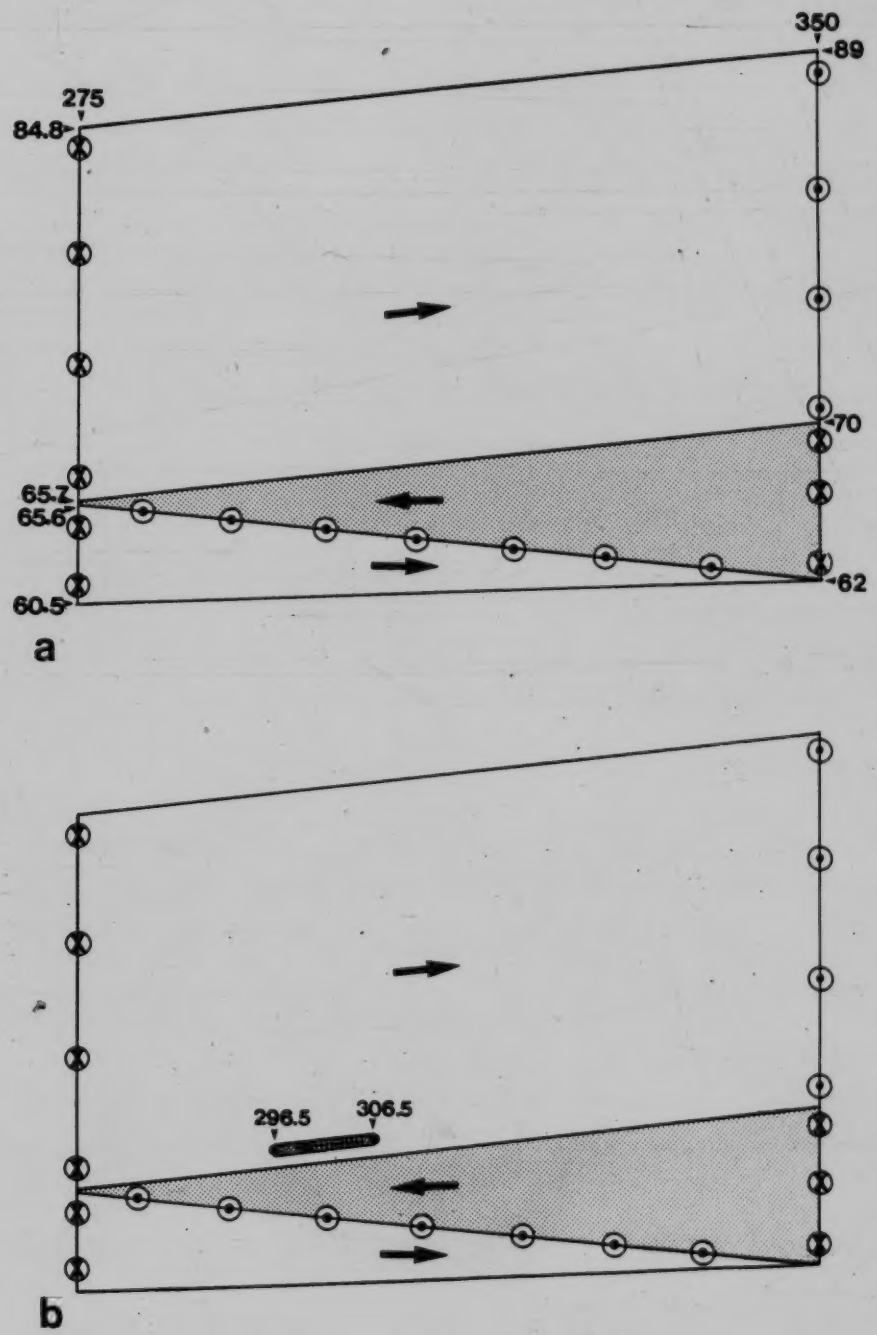

Figure 3.20 Models of the current system for day 59, a) the background profiles and b) the differential profiles.

the north of a westward electrojet which narrows from east to west. Approximately 1/4 of the westward current diverges upward along its lower border. A narrow eastward electrojet appears to the south of the westward electrojet. The entire eastward current is drawn upward along the upper border. This interface between the westward and eastward electrojets along which current is drawn upward models the effects of the Harang discontinuity. The field-aligned current at the interface has a total current density of approximately 12 mA/m.

As in the case of the day 231 event, the eastward current sheet is profiled in such a way as to reproduce the effect of the high conductivity channel just to the north of the westward electrojet. Again, this is due to energetic boundary plasma sheet electrons precipitating to the north of the electric field transition. The model results are shown in figure 3.21; these are to be compared with the profiles of figure 3.19.

Discrepancies exist between the data and the model results, particularly at high latitudes along the Churchill line. As was the case for the day 231 event, this can be attributed to the fact that the discontinuity between eastward and westward flowing currents is less sharp at the Churchill line than it is further to the west at the Alberta line. Again, this variation in the gradient cannot be modelled with the modelling program at its present state of development. Since the surge form is ultimately activated in

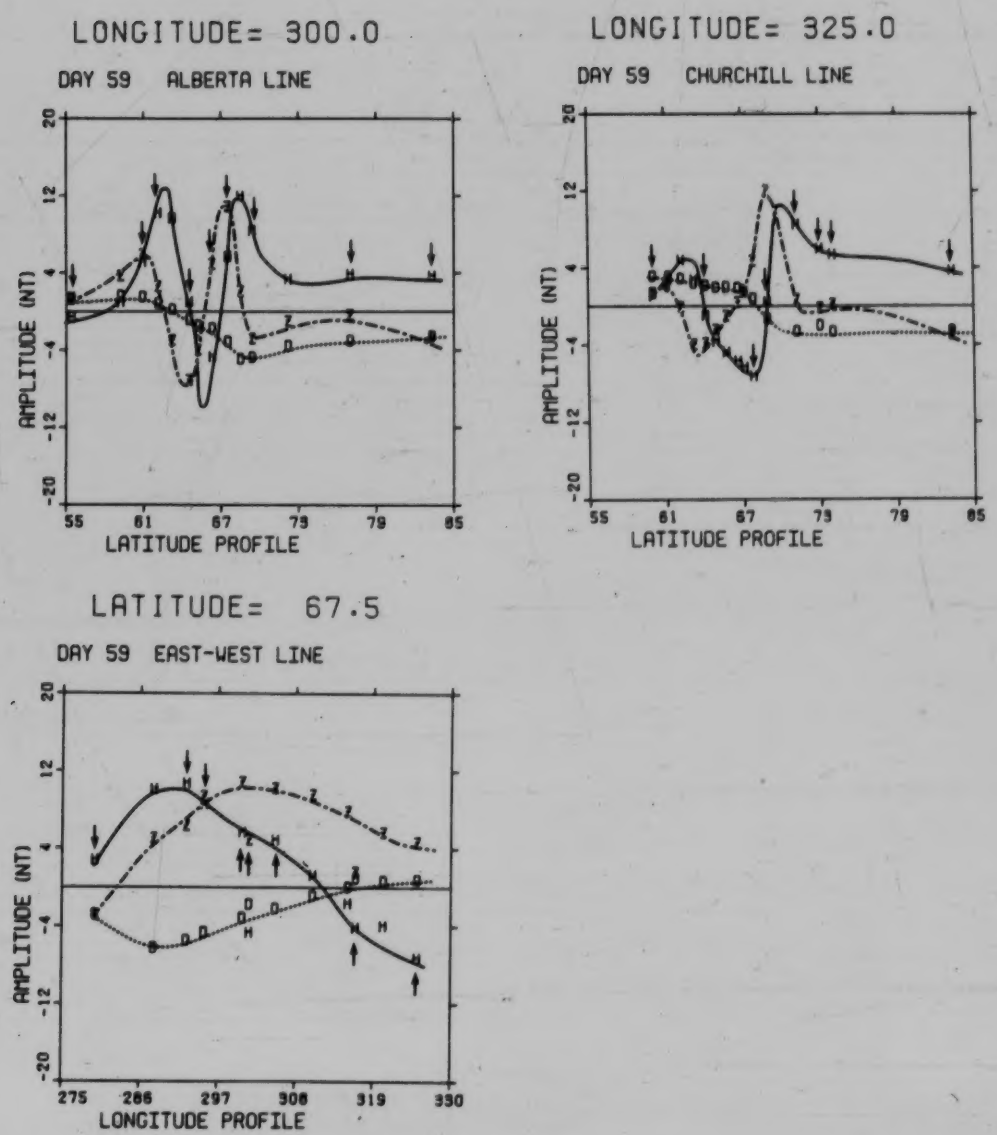

Figure 3.21 Theoretical profiles corresponding to the model shown in figure 3.20a. The arrows indicate the locations of the magnetometer stations.

the Alberta sector, the model was constructed to agree with the Alberta line. The Resolute station also shows an anomalously high field magnitude at this time. Since this is a polar cap effect which is not pertinent to this study, this effect was not reproduced in the model. Note that in the east-west profile, the agreement in the Z profile is excellent, although the curve was drawn through the the points corresponding to stations at a constant latitude of 67.5°N rather than the point corresponding to LYN.

The differential profiles at 0808, within one minute of onset, are illustrated in figure 3.22. The Alberta differential profile suggests the presence of a narrow region of westward current flowing to the north of a thin band of eastward current. The negative H component on the Churchill line occurs in the region in which eastward current appeared on the background profile (cf. figure 3.19); this indicates a decrease in the background eastward current to the north of the westward electrojet. The perturbation in the D component on the longitude profile suggests the presence of field-aligned current in the Alberta sector. These observations suggest the model differential profile of figure 3.20b. A filamentary westward electrojet of width 1/2° and length 10° appears to the north of the background westward electrojet. The westward electrojet is connected to the magnetotail by upward and downward field-aligned currents at the western and eastern edges, respectively. Furthermore, the magnitudes of the

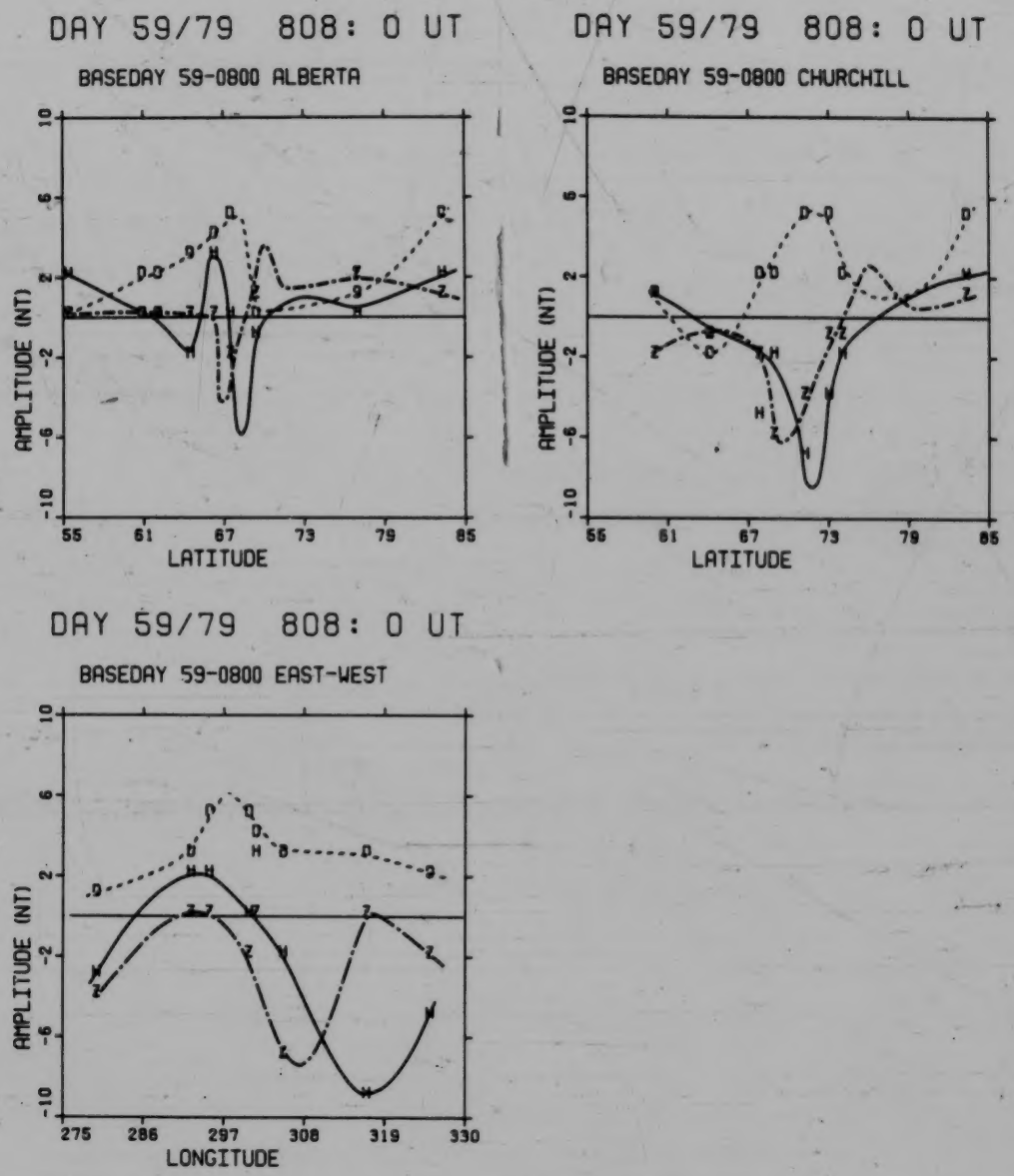

Figure 3.22 Observed differential profiles for day 59, 1979, taken one minute before the expansive phase onset.

background eastward current sheet and westward electrojet are reduced by 25% and 10% respectively in going from the background current system of figure 3.20a to the differential current system of figure 3.20b. These decreases in the westward and eastward currents give the apparent eastward and westward currents, respectively, as seen on the differential latitude profiles.

The differential profiles based on this current model are shown in figure 3.23. Discrepancies between the observations and model predictions exist due to the fact that east-west variations in the current structures could not be modelled. As an example, note the apparent eastward electrojet which appears at the southern end of the model Churchill profile. This feature does not appear on the observed Churchill profile. It results from a decrease in the background westward electrojet, a step which was necessary in modelling the Alberta latitude profile.

Summary of Day 59

The precursors to the day 59 event were the decrease in the eastward current sheet and the westward electrojet and the introduction to the north of the background westward electrojet of a filamentary electrojet linked to the magnetotail by field-aligned currents, with current densities of 125mA/m.

The substorm current wedge is modelled as a westward electrojet with field-aligned currents feeding it at its

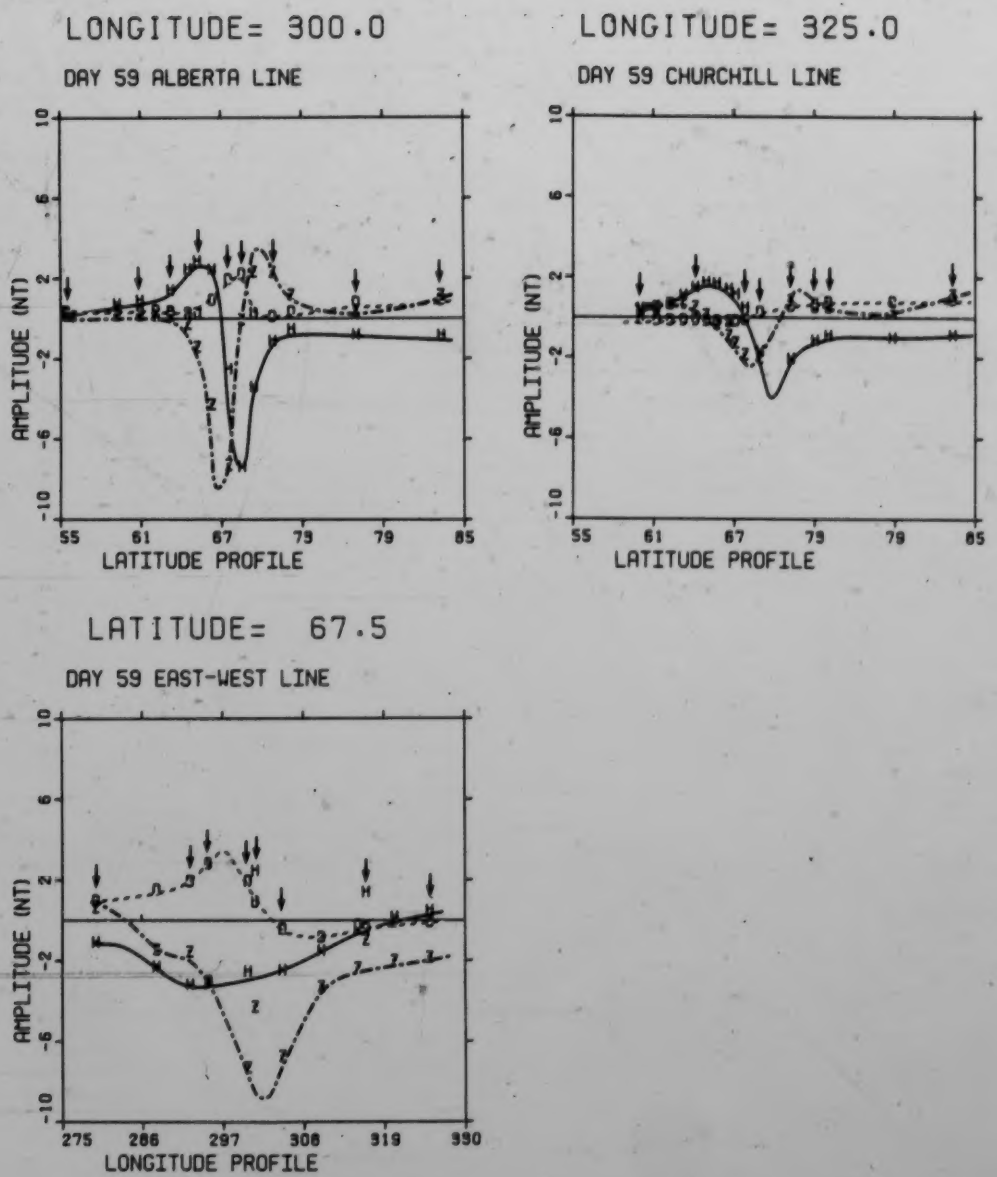

Figure 3.23 Theoretical differential profiles for day 59, 1979 based in the current model of fig 3.20b. The arrows indicate the positions of the magnetometer stations used for this event.

east edge and draining it at its west edge. This resembles the filamentary westward electrojet observed as a precursor to this event. Note that it occurs at approximately the same longitude and slightly to the north of the eventual location of the substorm enhanced westward electrojet.

C. Event Analysis-Day 20,1978

Development of the Event

The third substorm presented occurred on January 20, 1978. This event is another clear example of the activation of an expansive phase due to the northward turning of the IMF (Rostoker, 1983b). The IMF was directed southward for over 2 hours preceding this event. The stacked magnetograms are shown in figure 3.24. On the basis of the associated Pi2 pulsations, illustrated in figure 3.25, the expansion phase onset can be pinpointed at 0607, making this an evening sector event, unlike the previous two events that were analyzed.

A period of southward IMF commenced shortly before 0400, marking the start of the substorm event. The growth of the driven system eastward electrojet during the period of southward IMF is clearly indicated by positive deflections in H at most of the Alberta stations. This is accompanied by a negative deflection in Z at a number of the stations, evidence that these stations are in the northward portion of an eastward electrojet. The D component does not respond

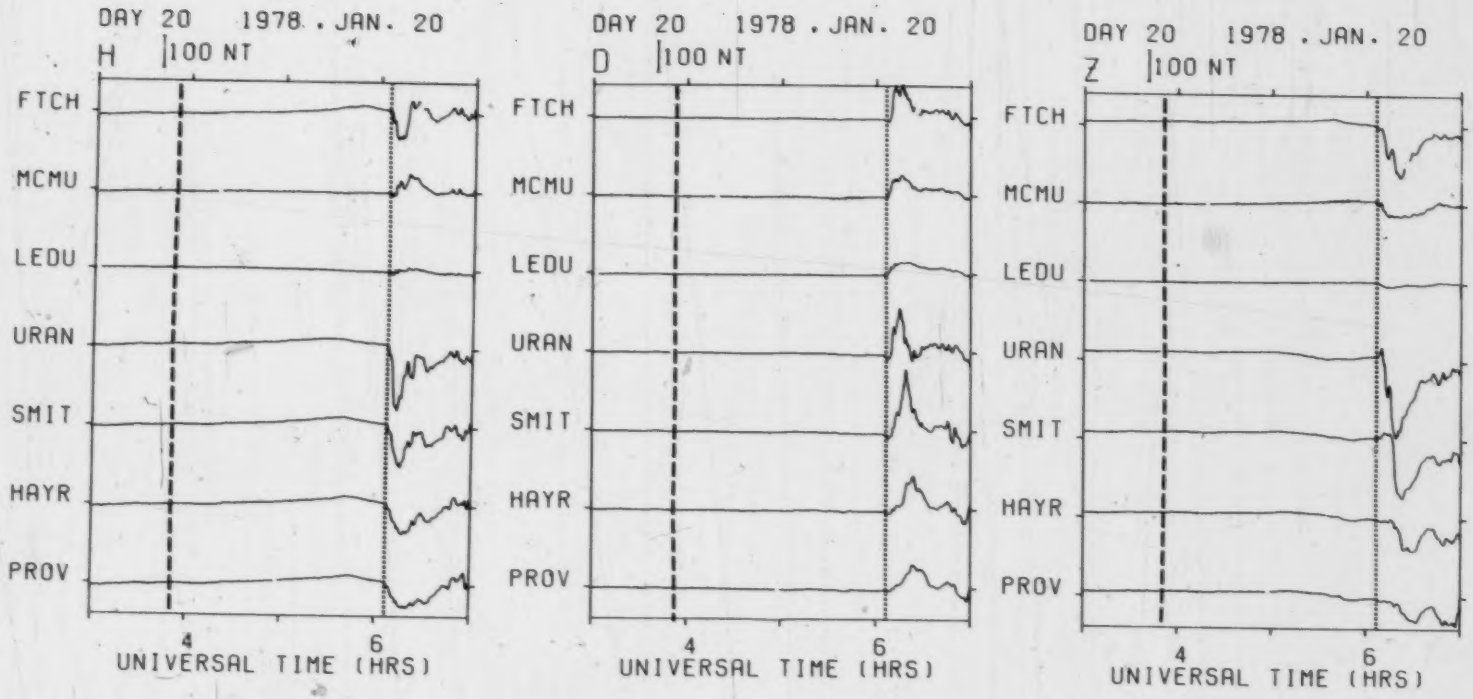

Figure 3.24 Stacked magnetograms for the Alberta stations. The dashed line indicates the beginning of the growth phase while the dotted line shows the time of the expansive phase onset.

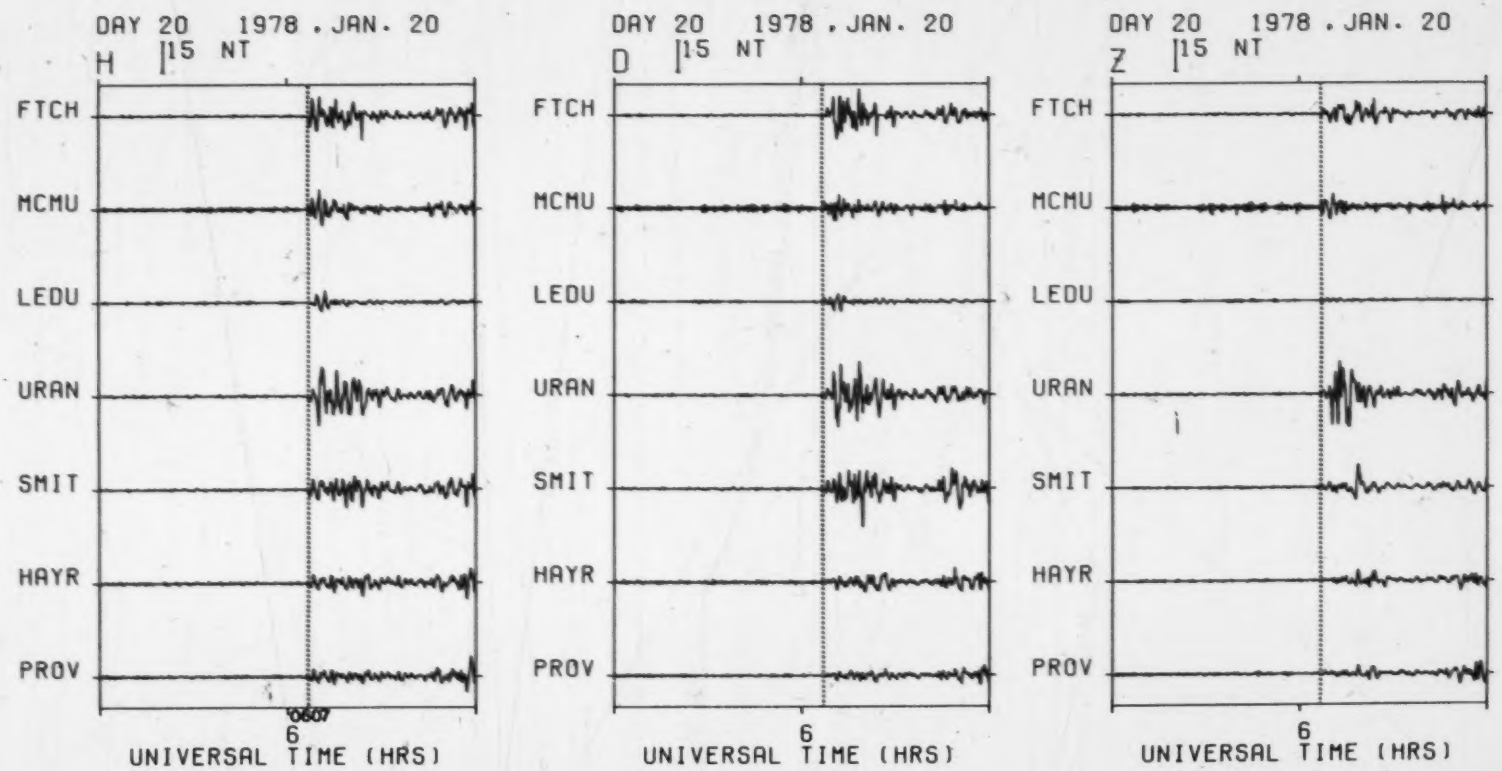

Figure 3.25 Pi2 pulsations for day 20, 1978 indicating expansive phase onset at 0607.

immediately at 0607, which means that the surge is initiated to the east, then moves westward over these stations.

The riometer data for this event are illustrated in figure 3.26. The URAN station indicates sudden electron precipitation at 0609, indicating that a surge is activated in this region two minutes after the onset of the expansive phase to the east. The riometer response at SMIT occurs 8 minutes later, indicating either a westward movement of the surge or a second surge appearing to the west of the first one. A very small precipitation event occurs further west at HAYR at approximately 0623, however, the magnitude indicates that the surge feature has decayed considerably by this time. The lack of change in the MCMU and PROV stations indicates that the surge event is a highly localized event.

On the basis of comparison with quiet days the baseline was chosen at 0340, before any significant driven system activity. The latitude profiles of the Alberta line are shown in figure 3.27. The profile at 0530 shows the signature of a thin eastward electrojet, centred at approximately 67° N. The D component becomes increasingly negative from south to north with a small enhancement in D superimposed under the region of the eastward electrojet. The positive enhancement may indicate that the current system is tilted with respect to a line of constant geomagnetic latitude while the slope in D suggests the effects of a distant field-aligned current. By 0555 the slope in D has steepened into a sharp "step" at

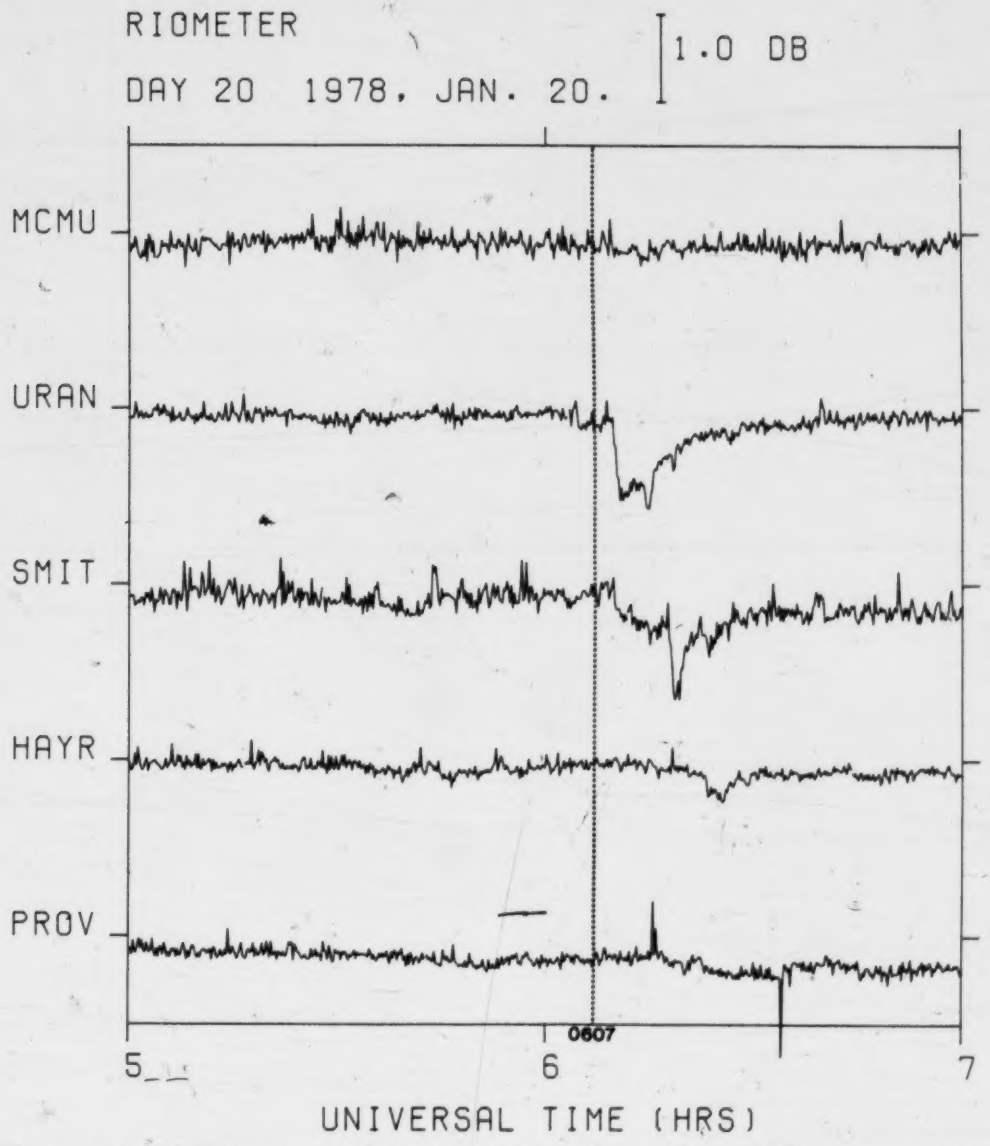

Figure 3.26 Riometer data for the day 20, 1978 event. The dotted line shows the time of the expansive phase onset.

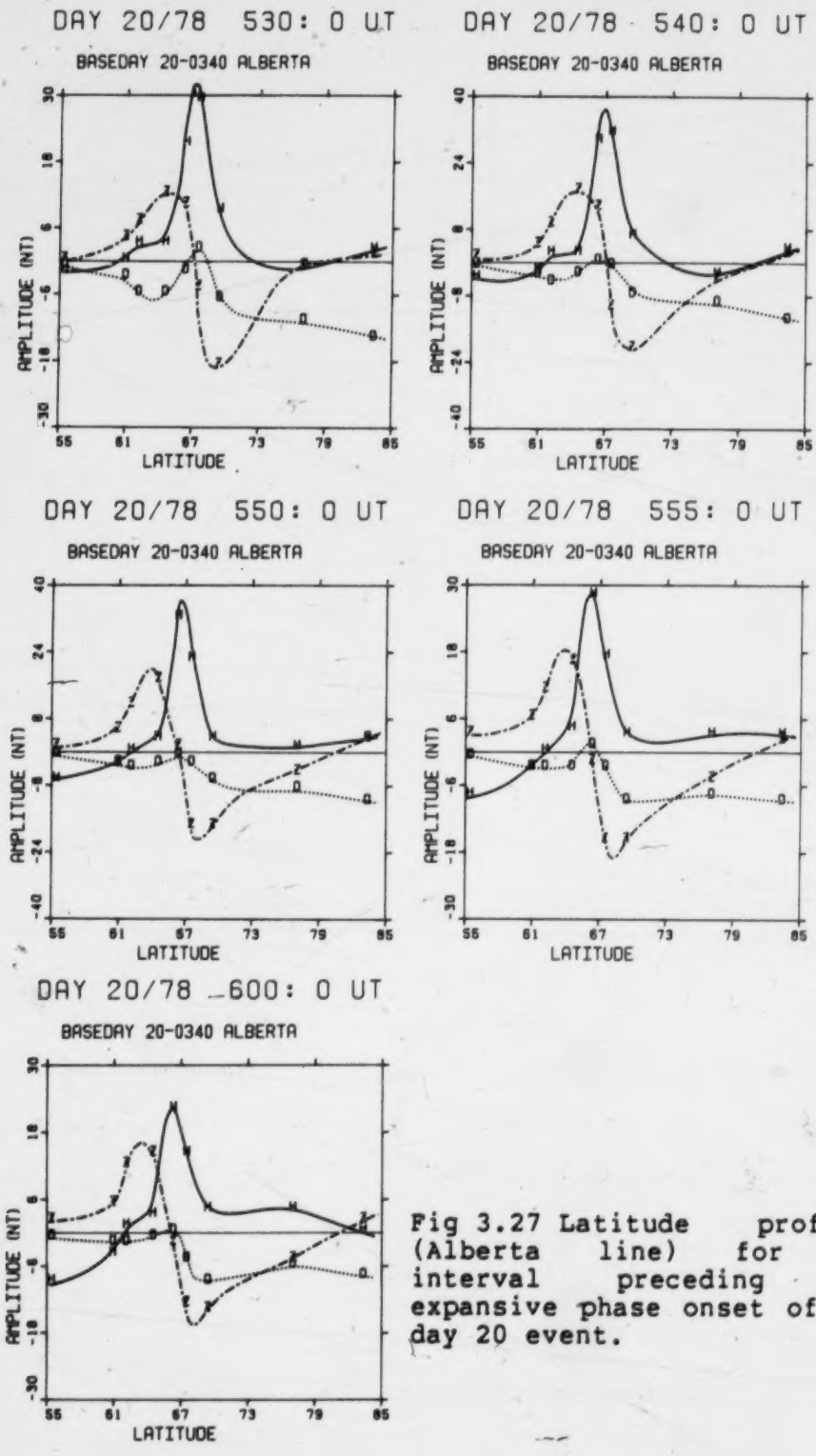

Fig 3.27 Latitude profiles (Alberta line) for the interval preceding the expansive phase onset of the day 20 event.

approximately 67°N, indicating that the region of upward field-aligned current has moved into this sector.

Values of ΔH values (as measured from 0340 to 0600) on the order of -5 to -10nT at the Tucson, Fredricksburg, and Victoria stations (not illustrated) suggest that the negative values in H for the southernmost stations are not the result of a westward electrojet. Nearly constant values of DST rule out the ring current as the source of the negative H values as well. Coleman and Cummings (1971) found that the H component values decreased during substorm activity and attributed it to an increase in tail current. Thus the anomalous H values must be a result of increased tail current. A southward motion of the electrojet can be detected between 0530 and 0555. This is most noticeable in the shift in the H component peak from SMIT at 0530 to FTCH at 0555.

The latitude profiles of the Churchill line to the east resemble those of the Alberta line. Again, a narrow eastward electrojet appears, centred at approximately 66° N. The sharp "step" in D, indicative of upward field-aligned current, appears earlier in this sector, at approximately 0540. This is as expected, since the easternmost stations move into the region of the Harang discontinuity, which is characterized by upward field-aligned current, before those to the west. Due to the station spacing on this line it is impossible to determine whether or not there is any southward motion of the current system in this sector.

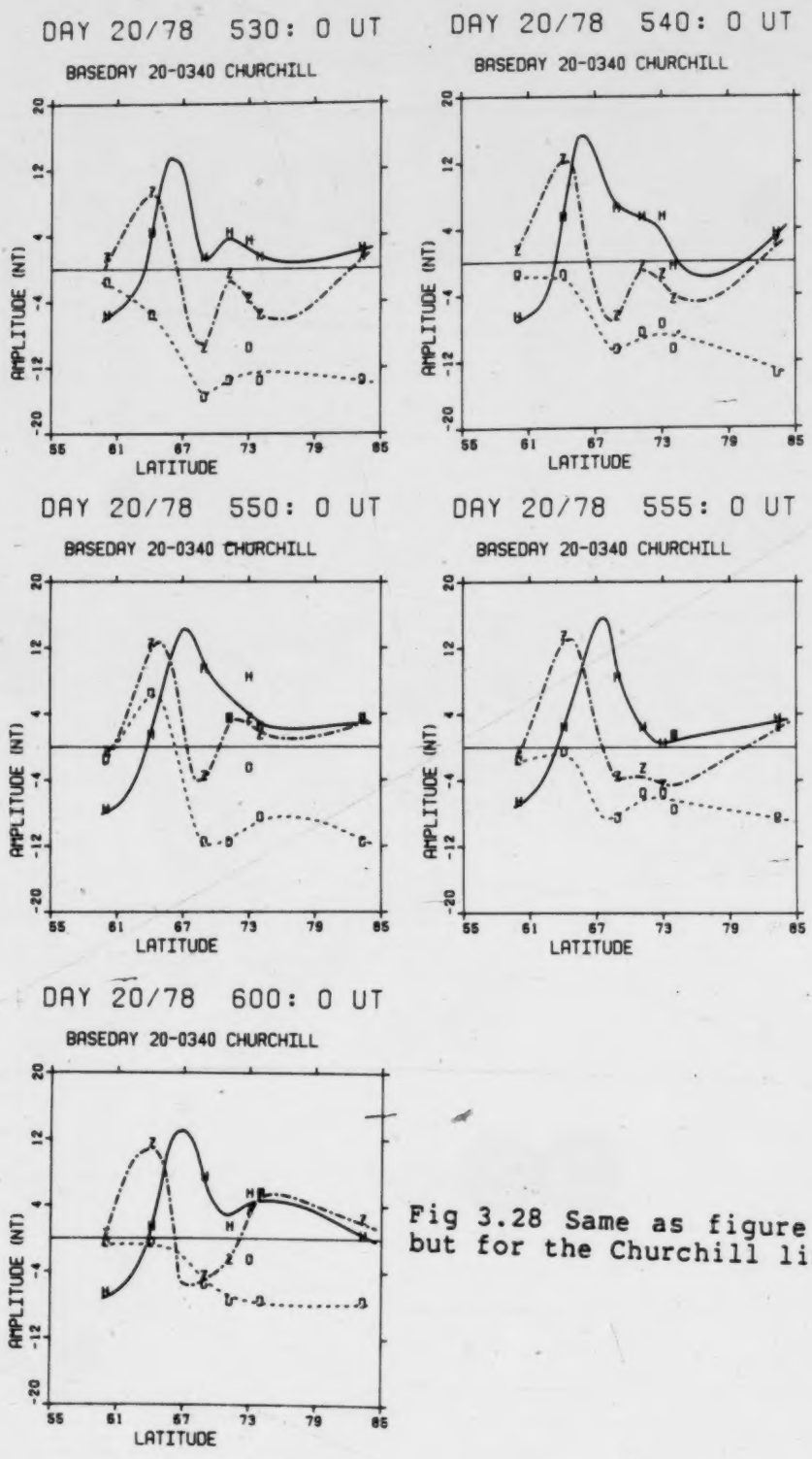

Fig 3.28 Same as figure 3.28 but for the Churchill line.

The east-west station line is located approximately along the middle of the eastward electrojet at 0530 (cf. figure 3.29). The southward motion of the current system from 0530 to 0555 is evident in the Z component; the increasingly negative Z component indicates that the eastward electrojet is moving southward over the station line. The latitudinal localization is again indicated by the FTCH station.

The location of the surge formation is more difficult to pinpoint for this event since the substorm expansive phase is triggered to the east, then moves westward into the morning sector. The Alberta profiles from 0610 to 0620 (not shown) indicate a narrow substorm-enhanced westward electrojet, the centre of which moves northward from 67°N to 69°N in that interval. The east-west profiles indicate movement of the surge into the Alberta sector.

Modelling the Current Systems

The basetime for the differential profiles is taken at 0600, 7 minutes before the expansive phase onset. The background profiles are shown in figure 3.30.

The model of the current system at 0600 consists of a broad eastward current sheet to the north of a filamentary eastward electrojet. The electrojet is drawn up the field lines along its length (cf. figure 3.31a). The entire system is tilted from northwest to southeast, consistent with the shape of the evening side auroral oval. No westward

TABLE 3.3

CURRENT SYSTEM PARAMETERS FOR DAY 20, 1978

Eastward/Westward ionospheric current	Downward Current Flow S.edge-N.edge (°E) (°N)		current density (mA/m)	Upward Current Flow S.edge-N.edge (°E) (°N)		current density (mA/m)
A)Background profile						
East	275 66	275 81	8.9	340 67.7	340 81	10
East	275 66	275 66	2.1x10⁶A (total current)	340 64.7	295 65.6	10
B)Differential profile						
East	275 66	275 81	8.9	340 67.7	340 81	10
East	275 66	275 66	2.1x10⁶A (total current)	340 64.7	295 65.6	10
West	301 67.5	301 68	125	286 67.5	286 68	125

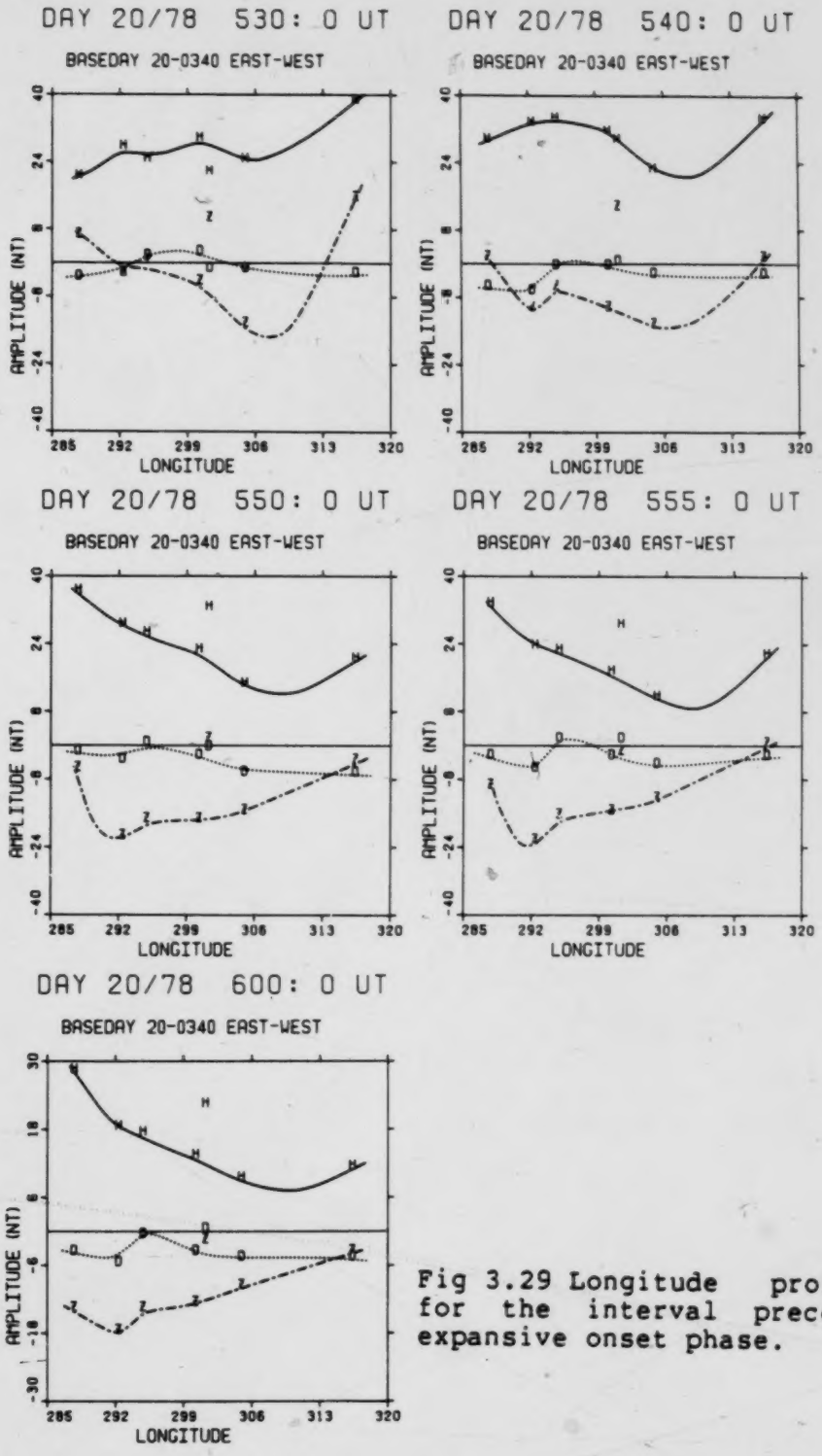

Fig 3.29 Longitude profiles for the interval preceding expansive onset phase.

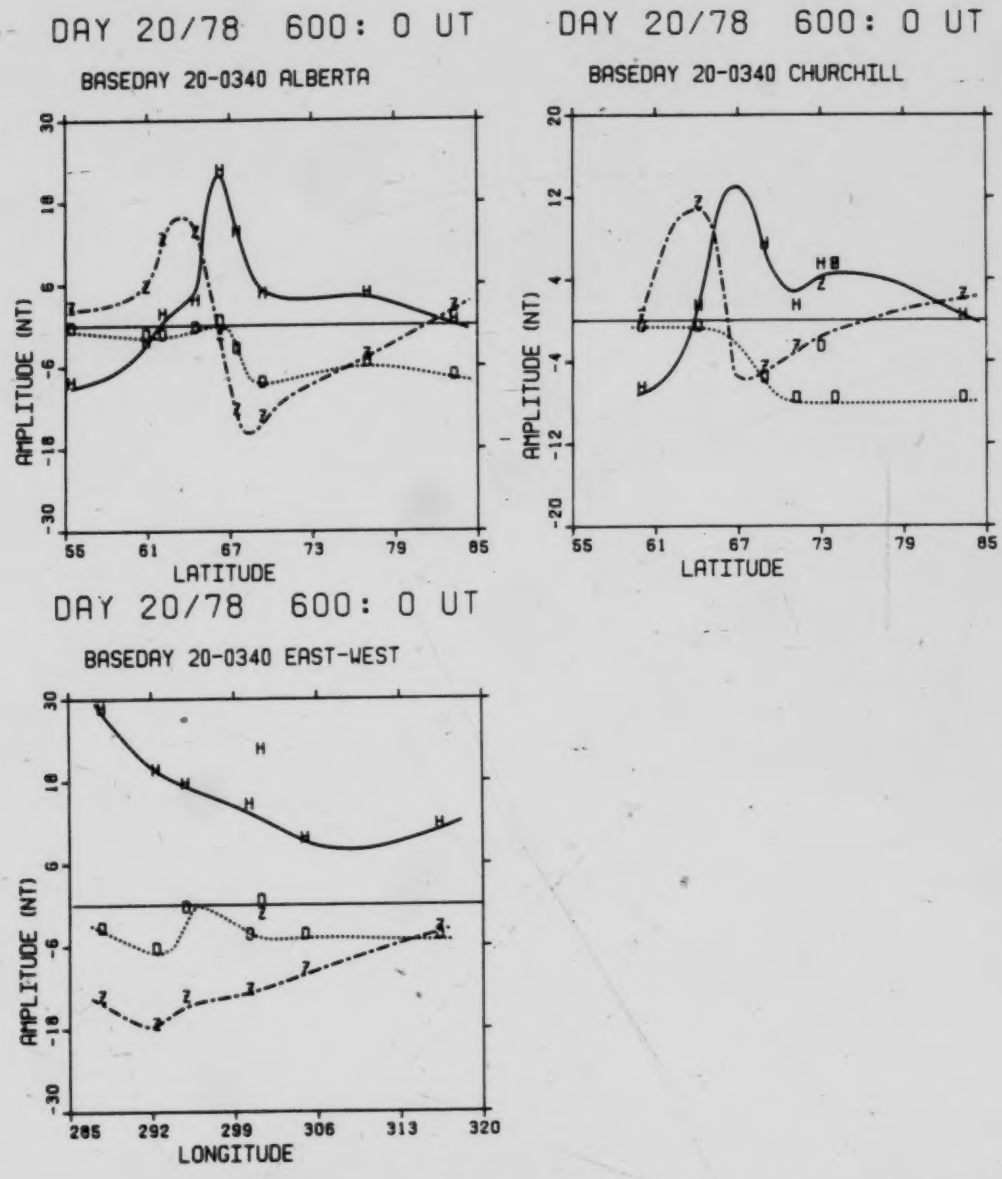

Figure 3.30 Observed profiles for the current system at 0600, day 20.

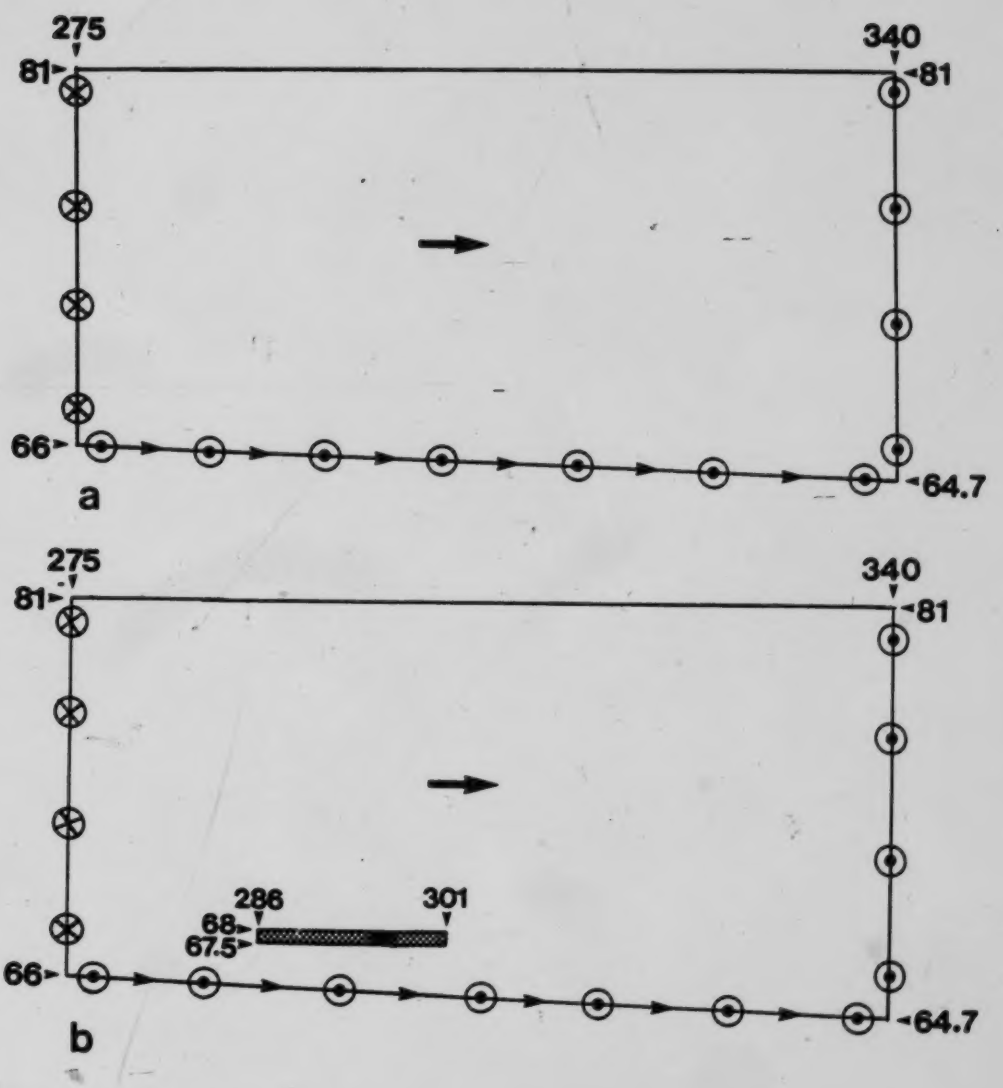

Figure 3.31 Models of the current system for day 20, 1978. The background system is shown in figure a) and the differential system in figure b).

electrojet is seen since in this sector the westward electrojet would be too narrow and weak to be detectable on the ground. This model resembles the current configuration at the western end of the Harang discontinuity. The model parameters are given in table 3.3. The profiles resulting from this model are shown in figure 3.32; these are to be compared to those of figure 3.30.

Comparison of figures 3.32 and 3.30 reveals several small discrepancies between corresponding profiles. The first is that the data have a negative bias in both H and D with respect to the model profiles. The bias in H has already been explained in terms of enhanced tail current. The negative bias in D may be explained in terms of the DP2 current system. The IMF is directed southward at this time and although the polar cap conductivity is low, it may be sufficient to allow a small DP2 current system to be set up.

The FTCH station on the east-west line indicates the high degree of latitudinal localization of the model current system; this agrees with the results shown in the longitude profile of figure 3.30. Local fluctuations in the current densities may explain the larger current magnitudes seen in the data at FSP than are seen in the model results. Discrepancies between model predictions and data results would likely have been reduced had the current modelling program been designed to allow for variable curvature in the electrojets. In its present state of development, the program is set up such that only currents flowing along

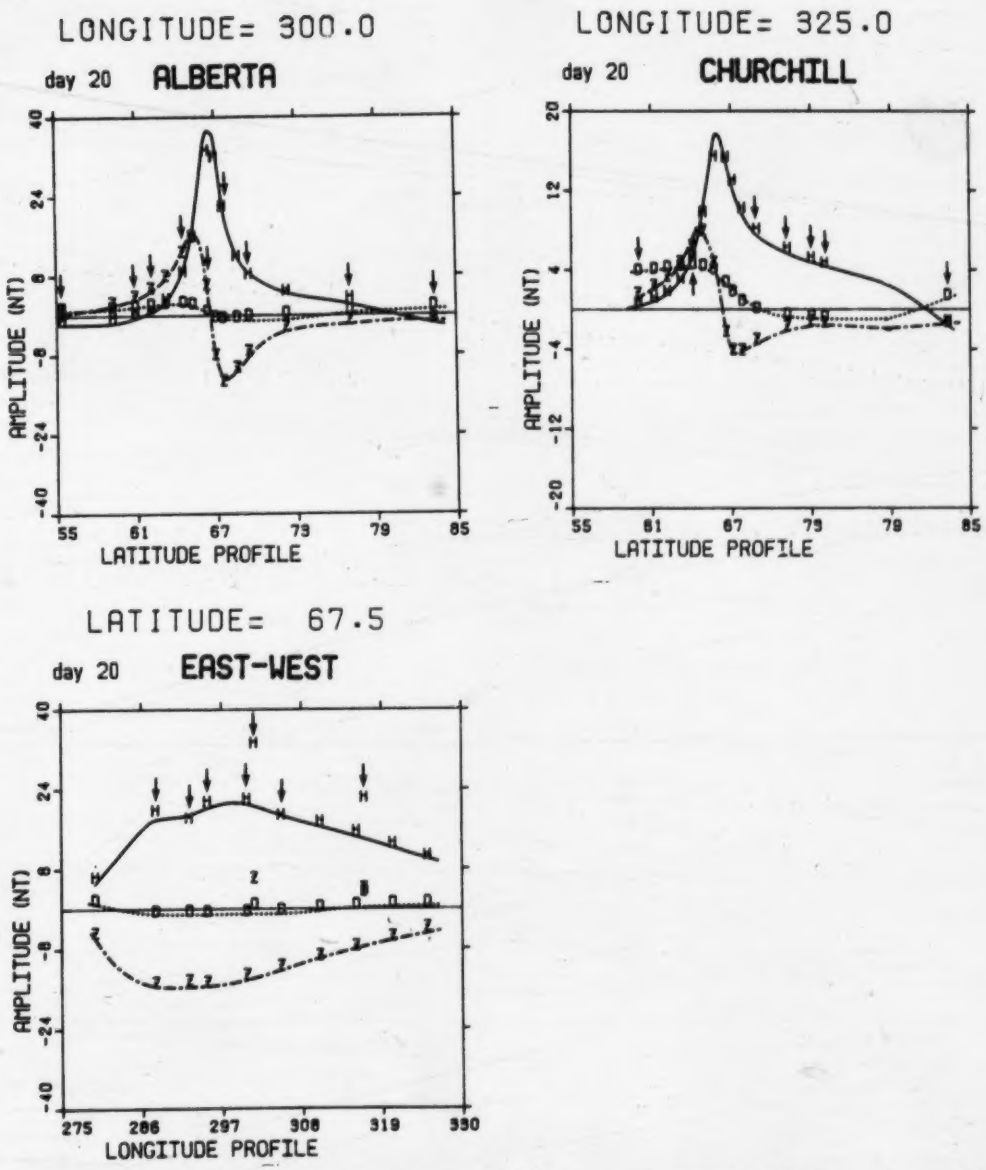

Figure 3.32 Theoretical profiles corresponding to the current model of figure 3.31a. The arrows indicate the positions of the magnetometer stations.

great circle paths, or along lines of constant derivative of longitude with respect to latitude, can be easily calculated.

Figure 3.33 shows the differential profiles at 0606, at one minute before the expansive phase onset in the Alberta sector. The development of a westward electrojet in the Churchill profile indicates that the surge has already been initiated to the east. Note that the LYN station has been omitted in the longitude profile. This was done because the surge was already evident in that sector, so that the perturbations there were on a scale that drowned out the variations being studied at the west end of the line. A reversal in polarity in the D component has developed on this line, however the reversal is in the opposite direction to the case for day 231. The Alberta station indicates the presence of a small westward electrojet centred at a latitude of approximately 67°N.

The perturbations were modelled as shown in figure 3.31b. A filamentary westward electrojet of length 15° and width 1/2° is superimposed upon the background current system just to the north of the east-west line stations. This produces the correct polarity reversal as seen on this line (cf. the model results shown in figure 3.34). No attempt was made to include in the model the effects of the expansive phase to the east of the line, hence the disagreement between model and data results at the Churchill line.

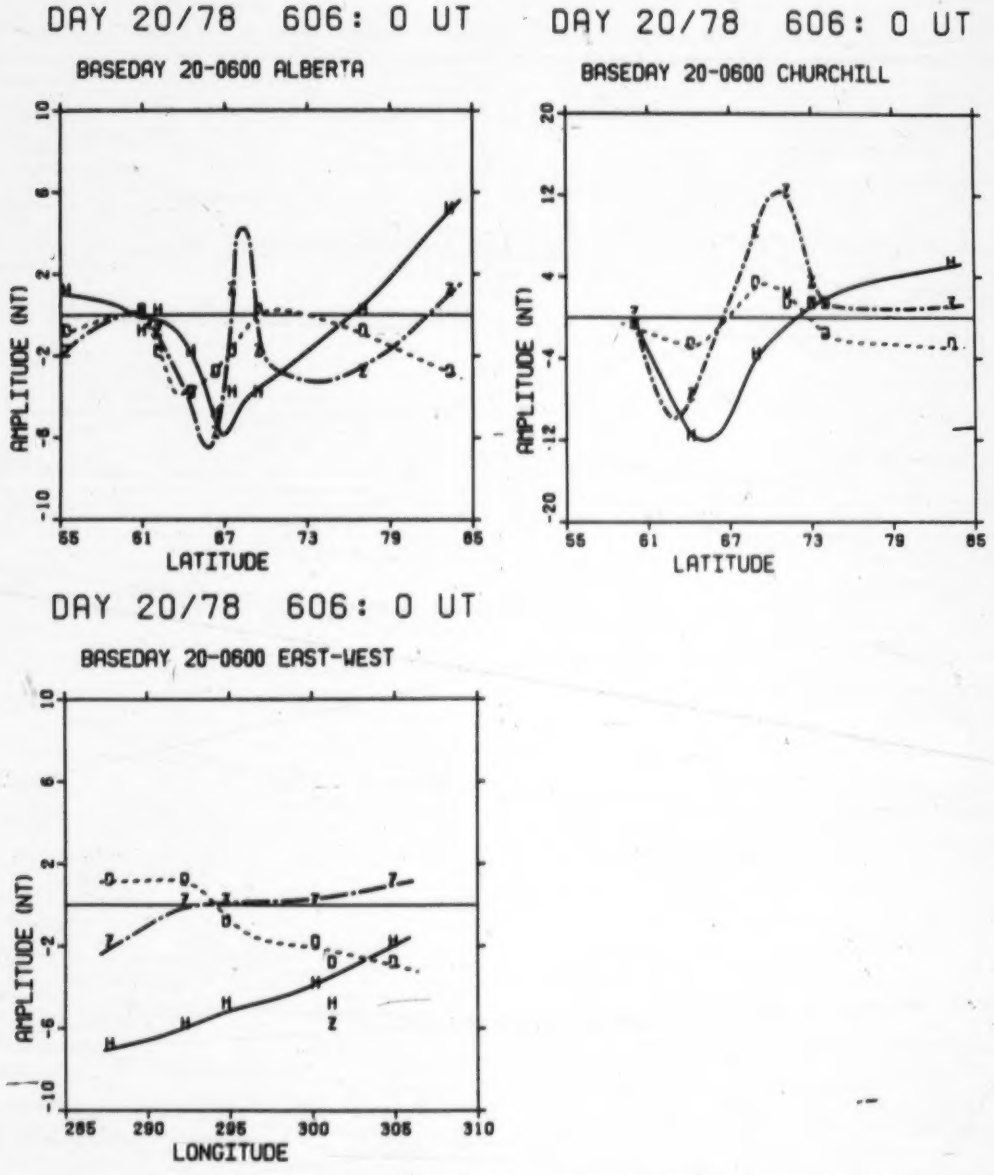

Figure 3.33 Observed differential profiles for day 20, 1978 taken one minute before expansive phase onset.

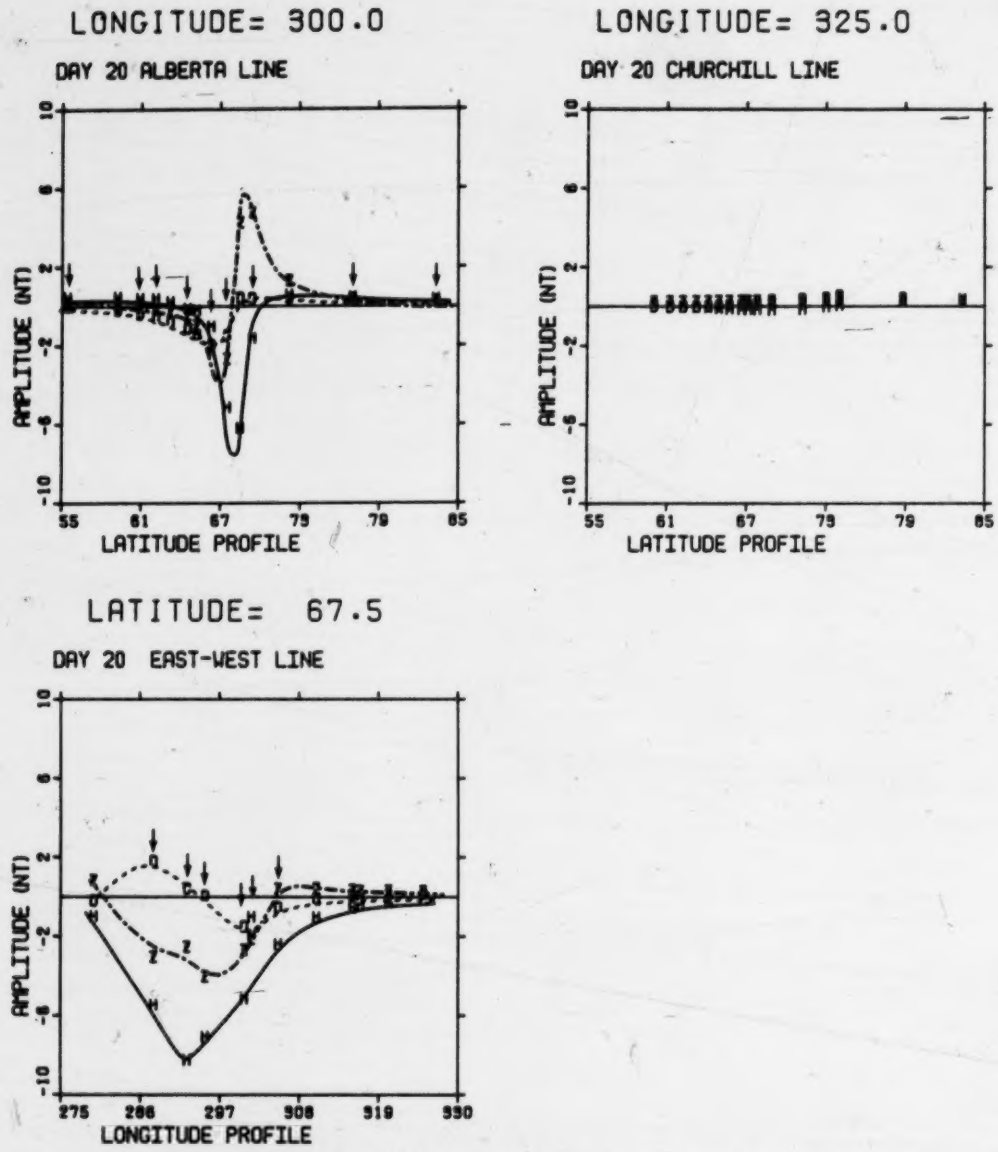

Figure 3.34 Theoretical differential profiles for day 20, 1978 based in the current model of fig 3.31b. The arrows indicate the positions of the magnetometer stations used for this event.

Summary for day 20

The most important feature of the day 20 event is the appearance of two antiparallel field-aligned currents connected by a filamentary westward current just prior to the expansive phase onset. This feature is identified with the substorm current wedge. It appears slightly north of the latitude at which the substorm-enhanced westward electrojet is observed just after the onset.

As was the case with the previous two events, the current configuration identified with the substorm current wedge appears to the north of the region of Harang discontinuity.

IV. DISCUSSION AND CONCLUSIONS

A. Summary of Results

This research was initiated for the purpose of finding geomagnetic signatures which could be identified as precursors to the expansive phase onset and to establish the nature of the current systems responsible for these perturbations. It was hoped that the examination of these signatures would lead to an understanding of the cause of the expansive phase onset.

In the previous chapter, a detailed analysis was presented for each of three events. While the features of the base model were highly dependent upon the longitude of the event with respect to the Harang discontinuity, it was found that the substorm precursors were fairly similar in each case.

For the case of day 231, it was found that, in the few minutes before expansive phase onset, the base current system moved northward. A decrease in the intensity of the westward electrojet and the eastward current sheet was found to occur in the few minutes before the expansive phase onset of day 59.

A common feature in the modelling of each differential profile was the introduction of a filamentary westward electrojet of length 10-15° with upward (downward) field-aligned current at its western (eastern) edge. This electrojet appeared to the north of the region of the Harang

discontinuity, where the Harang is defined as the border between the eastward and westward electrojets. For the day 20 event, the Harang discontinuity is defined as being along the line of upward field-aligned current.

This filamentary westward electrojet is part of a weak substorm current wedge. As outlined in chapter 1, the expansive phase starts with the sudden brightening of a quiet arc at the southern-most edge of the region of discrete arcs. This is south of where we observe the precursory substorm current wedge. For each of the three events examined, it was also noted that the precursory wedge develops to the north of the location at which the substorm enhanced westward electrojet is observed after onset. This result is significant in that it indicates the presence of the substorm current wedge before the onset of the expansive phase can be identified, and occurring to the north of the location of eventual expansive phase onset.

B. Limitations of the Modelling Program

A current model is a summation of elementary current loops similar to the type shown in figure 2.2. Each current loop is two dimensional in that it has width but no thickness, but three dimensional in the sense that it spans three dimensional space. For each current element to be included, the height to the ionosphere and the depth to the superconducting core must be specified. In addition, two sets of geomagnetic coordinates must be given to specify the

southward and northward limits for each of the upward and downward field-aligned current sheets. Current flows in the ionosphere from the downward to the upward field-aligned currents. The current densities need not be uniform, but may vary in a direction perpendicular to the direction of current flow.

This leads to two major difficulties in the current modelling. The first is that variable curvature of the current systems cannot be incorporated into the models. This was found to cause some difficulties in the modelling of day 20.

The second, and major, limitation of the modelling program is that currents cannot vary in a direction parallel to the current flow. That is, since field-aligned currents are constrained to flow into or out of the ionosphere along sheets, rather than along some finite volume, the ionospheric current magnitudes must be constant in order to maintain current continuity.

Despite the limitations of the modelling program, fairly good agreement was obtained between model and data results, even for small geomagnetic perturbations. This suggests that, as a first approximation, the ionospheric currents, and associated field-aligned currents, can be modelled adequately using this program.

Since the purpose of this study was to find physically meaningful current systems related to expansive phase onset, and since, even for an ideal modelling program the current

systems are non-unique, the modelling program was considered adequate for this study.

C. Kelvin-Helmholtz Instability

The sudden appearance of a substorm current wedge prior to the expansive phase onset suggests the presence of an impulsive driving force, which could be provided through the action of a plasma instability in the magnetotail. Kelvin-Helmholtz waves in the magnetotail are believed to be the driving mechanism for a variety of waves and pulsations observed in the high latitude ionosphere. These include ULF pulsations in the Pc3 to Pc5 range, as well as Ps6 waves. It has been proposed (Rostoker and Samson, 1984) that auroral arcs and surge features are driven by the same instability. The field line mapping of the velocity shear region of the LLBL/CPS interface to the disturbed regions of the auroral oval (see figure 1.7) has led to the suggestion that the Kelvin-Helmholtz instability is the driving mechanism behind these surface waves. The resemblance of the auroral arc forms and omega bands (Ps6 waves) to rippled fluid patterns created by the Kelvin-Helmholtz instability reinforce this interpretation.

Knowledge of the structures of the LLBL and CPS in which the Kelvin-Helmholtz oscillations are excited is necessary for the construction of appropriate models to describe the growth of this instability. An electric field transition occurs across the boundary betweenthe CPS and the

LLBL. In the central plasma sheet the electric field is directed from dawn to dusk, while in the LLBL the direction is from dusk to dawn. The plasma β (the ratio of the thermal to magnetic pressure) in both the LLBL and the CPS are on the order of one. Thus the plasmas of both regions are compressible. Plasma flow in the LLBL is directed tailward, while in the CPS the flow is in the sunward direction, so that a velocity shear exists across the boundary separating them. The thickness of the LLBL increases tailward of the subsolar region (Paschmann, 1979) but is pinched off by the separator line in the deep magnetotail (cf. figure 1.7) so that its thickness there may be negligible. The separator line divides the region of open field lines, where the plasma streams parallel to the field direction, from that of the closed field lines, where plasma convects perpendicular to $\underline{B}$. The magnetic field is approximately perpendicular to the direction of the flow in both the LLBL and the CPS.

The above characteristics suggest that an appropriate model would be one that incorporates a boundary layer of finite thickness, composed of compressible plasma. However, MHD models incorporating these features must be dealt with numerically; thus a simpler model will be presented here and the necessary modifications for finite boundary thickness and compressibility will be given. The simpler model is one which assumes an incompressible plasma ($\beta>>1$) and a tangential discontinuity. The tangential discontinuity divides the coordinate system into two regions, denoted by 1

(x>0) and 2(x<0). In a system with a change in plasma velocity v_o across the interface between regions 1 and 2, unperturbed plasma densities ρ_1 and ρ_2 and Alfvén velocities $\underline{v}_{a1}$ and $\underline{v}_{a2}$, this model yields the following condition for instability:

$$(\underline{k}\cdot\underline{v}_o)^2>(\frac{1}{\rho_1}+\frac{1}{\rho_2})[\rho_1(\underline{k}\cdot\underline{v}_{a1})^2+\rho_2(\underline{k}\cdot\underline{v}_{a2})^2] \qquad 4.1$$

where $\underline{k}$ is the wave number for the Kelvin-Helmholtz wave. This equation is derived in the Appendix. This condition reveals a few of the properties of the Kelvin-Helmholtz instability. From the right hand side it is obvious that the wave is destabilized most quickly for values of $\underline{v}_o$ parallel to the direction of wave propagation. The left side of the equation indicates that the instability will grow most quickly for $\underline{k}\cdot\underline{v}_{a1}\simeq 0$ and $\underline{k}\cdot\underline{v}_{a2}\simeq 0$, that is, for waves growing with wave vectors perpendicular to the Alfvén velocity, i.e. parallel to the direction of the unperturbed magnetic field. Thus the instability will grow most quickly in a region in which the magnetic field is perpendicular to the bulk plasma flow. This condition exists in the LLBL and CPS regions. However, if the thickness of the LLBL is negligible, the open field lines in the region beyond the separatrix provide a finite $(\underline{k}\cdot\underline{v}_a)$ term which will act to damp the instability.

When compressibility and the finite width of the boundary layer are taken into account, the instability condition becomes more complicated. At high velocities a velocity shear in compressible plasma will involve the conversion of unstable surface waves into stable

magnetosonic waves (Pu and Kivelson, 1983).

For any tangential discontinuity, linear theory predicts the growth rate of the instability to be proportional to the tangential component of the wave number $\underline{k}$, with no upper limit on $\underline{k}$. This would imply that the waves grow without bound for very short wavelengths; thus the tangential discontinuity model must fail when the wavelengths are on the order of the boundary layer thickness. Using a model incorporating smooth variations across a finite boundary, Walker (1981), found that the growth rate is maximized for $kd \simeq 0.6$, where d is the boundary layer thickness.

D. Generation of Field-aligned Current

Kelvin-Helmholtz waves at the CPS/LLBL interface are coupled to the auroral region by means of field-aligned currents which are driven by the the Kelvin-Helmholtz instability. These field-aligned currents are created by local accumulations or depletions of space charge. Space charge (σ) is generated when a component of the magnetic field ($\underline{B}$) lies parallel to the vorticity generated by two plasmas with relative flow velocity $\underline{v}_o$. This follows from the equations $\sigma=\epsilon_o \nabla \cdot \underline{E}$ and $\underline{E}=-\underline{v}\times\underline{B}$. This leads to the expression for space charge

$$\sigma=-\epsilon_o \underline{B}\cdot\nabla\times\underline{v} \; + \; \epsilon_o \underline{v}\cdot\nabla\times\underline{B}$$

where $\nabla\times\underline{v}$ is the vorticity and ϵ_o is the permittivity of free space. Using the relations $\mu_o\underline{J}=\nabla\times\underline{B}$ and $\mu_o\epsilon_o=1/c^2$, the

second term becomes $\underline{J}\cdot\underline{v}/c^2$. Since only a small component of the current flows in a direction parallel to the plasma velocity, this second term is negligible. Thus the expression for the space charge can be simplified to

$$\sigma=-\epsilon_0\underline{B}\cdot\nabla\underline{v} \qquad 4.2$$

The space charge leads to field-aligned currents which can be expressed mathematically as

$$J_{\parallel}=B\int\left[\frac{\rho}{B}\frac{d}{dt}\left[\frac{\Omega}{B}\right] + \frac{2J_{\perp}}{B^2}\cdot\nabla B + \frac{1}{B^3}\left[\frac{d\underline{v}x\underline{B}}{dt}\right]\cdot\nabla\rho\right]dl \qquad 4.3$$

(from Hasegawa and Sato,1978), where ρ is the mass density, $J_{\parallel}$ and $\underline{J}_{\perp}$ are the currents parallel and perpendicular to the magnetic field, respectively, Ω is the projection of the vorticity in the direction of the magnetic field, and l is the length of the field line from the CPS/LLBL interface in the magnetospheric equatorial plane to the ionosphere.

To solve for the space charge and field-aligned current generated by the Kelvin-Helmholtz instability we use the hydrodynamic analogy to solve for the vorticity in a shear layer between two oppositely directed fluid flows and use equations 4.2 and 4.3 to solve for the space charge and resulting field-aligned currents in the MHD case. A shear layer, with velocity given by $v=1+\tanh(x)$, has been examined by Hama (1962). This model simulates the case of a boundary of finite thickness. A small sinusoidal perturbation is applied to the boundary between two fluids, and the instantaneous locations of the individual particles are computed and streaklines thus derived. Twenty particles are

released at x=y=0 at regular intervals of time and their subsequent motion tracked. In this way the time evolution of the system can be traced. The resulting streaklines (lines connecting the locations of the particles at any given moment) obtained by connecting five sets of twenty particles, are shown in figure 4.1. Note that the streakline at the critical layer appears to be amplified and rolls up into spirals. The particles tend to accumulate at the spirals, creating particle depletions at the ligaments.

In a subsequent study, Michalke (1965) found that, for a velocity shear of the same form and with the same initial perturbation, after a while the vorticity is concentrated near the centres of the spirals. Comparing this result to those shown in figure 4.1 it is obvious that the Kelvin-Helmholtz instability causes the particles to be redistributed such that they tend to accumulate and be depleted in alternating regions of greater and lesser vorticity.

Extending these results to the plasma shear at the evening sector CPS/LLBL boundary layer, we can see from equation 4.2 that the vorticity there is consistent with negative space charge (cf. figure 1.7). When a perturbation disturbs this boundary the space charge would be redistributed in a fashion as shown in figure 4.1. Excess negative charge at the spirals would alternate with depletions of negative space charge at the ligaments.

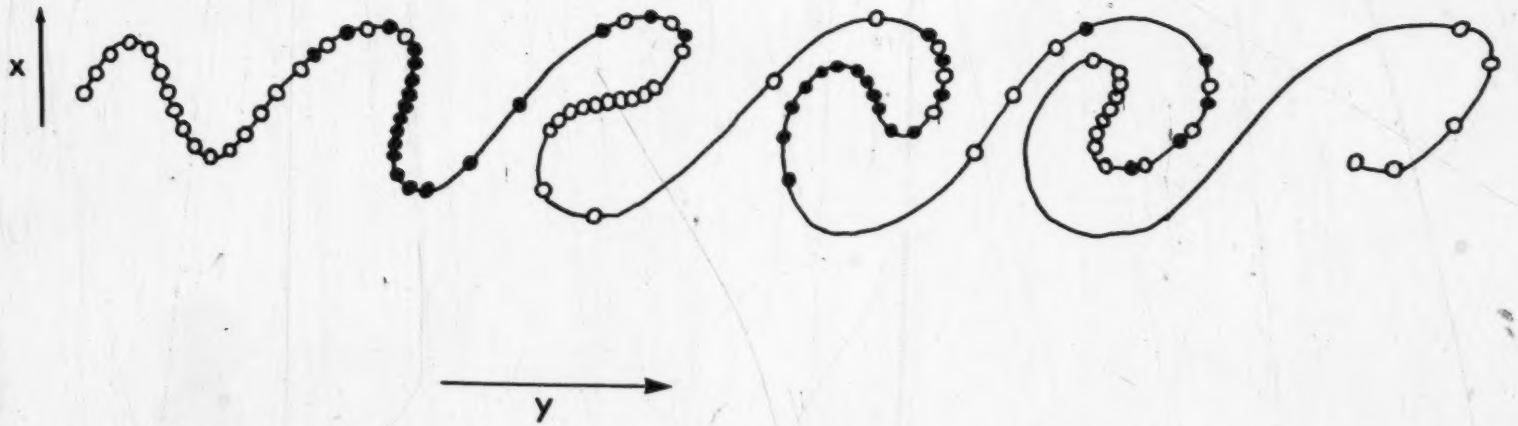

Figure 4.1 Streaklines for the nonlinear Kelvin-Helmholtz instability for the hydrodynamic case. Streaklines were derived using 5 sets of 20 points released at equal time intervals. Open and closed circles represent alternating sets of particles. (modified after Hama, 1962).

The separation of space charge leads to alternating increases and drops in the electric potential with respect to the surrounding regions, at the interface. Since under ideal MHD conditions, conductivity is negligible perpendicular to the field lines and infinite parallel to the field lines, the change in electric potential causes field-aligned currents to be drawn from the ionosphere in order to minimize the potential difference. The excess negative space charge at the centre of the spiral leads to field-aligned current out of the ionosphere. This current flows in the form of hot electrons entering the ionosphere. The space charge depletion at the wave ligament leads to field-aligned current into the ionosphere. This current is carried by cold electrons moving upward out of the ionosphere. Westward ionospheric currents flow in order to maintain current continuity. This configuration of westward ionospheric current, with associated field-aligned currents, is called the substorm current wedge.

When the upward field-aligned current reaches a threshold value of approximately $1\mu A/m^2$ (Knight, 1973), an accelerator region at an altitude of 1 Re is activated. This causes a sudden acceleration of electrons into the ionosphere, signalling the onset of the substorm expansive phase. Thus the catastrophic increases in field-aligned current associated with expansive phase onset are caused by the action of the accelerator.

Greenwald and Walker (1980) estimated a parallel current of approximately $3\mu A/m^2$ associated with the Kelvin-Helmholtz instability. Thus the field-aligned current which is generated by the Kelvin-Helmholtz instability seems to be sufficient to activate the accelerator at 1 Re which would enhance the current to magnitudes typically associated with expansive phase onset. The field-aligned current creates a small transverse magnetic field component $\underline{B}_1$. This component acts in a direction perpendicular to the initial direction of the magnetic field since

$$\mu_0 \underline{J}_1 = \nabla \times \underline{B}_1 \qquad 4.4$$

where $\underline{J}_1$ is the field-aligned current. From the instability condition (equation 4.1) we can see that the resulting magnetic field, which has a component parallel to $\underline{k}$, has a damping effect on the Kelvin-Helmholtz instability.

E. Conclusions

The identification of substorm precursory and expansive phase activity with the Kelvin-Helmholtz instability can explain the greater occurrence of substorm activity in times of southward IMF. As figure 1.5 indicates, magnetic reconnection in the magnetotail is enhanced when the IMF is directed southward. Reconnection converts the magnetic energy into particle kinetic energy, thus the plasma is driven out of the reconnection region with velocities on the order of the Alfvén velocity (Petschek, 1964). For number densities $N \simeq 1/cm^3$ and magnetic field $B \simeq 10nT$ the Alfvén

velocity is approximately 200km/sec just Earthward of the neutral line, which is ≃100Re behind the Earth. The enhancement of CPS plasma velocities makes the CPS/LLBL boundary unstable to the Kelvin-Helmholtz instability. Since the CPS plasma velocities are greater than those of the LLBL the Kelvin-Helmholtz waves travel Earthward along the boundary. This maps down to the ionosphere as a westward motion of the surge.

The observed pattern of substorm precursory activity can now be interpreted in terms of the growth of the Kelvin-Helmholtz instability at the CPS/LLBL interface. An increase in the plasma flow speed in the CPS results in increased vorticity and the growth of surface waves at the shear layer. Alternating accumulations and depletions of negative space charge at the interface result in alternating upward and downward field-aligned currents connecting the ionosphere and the velocity shear zone in the distant magnetotail. In the ionosphere,current flows from downward to upward field-aligned currents in order to maintain current continuity. A schematic diagram showing the relation of the Kelvin-Helmholtz instability to the wedge is shown in figure 4.2.

Prior to the expansive phase onset, when field-aligned current magnitudes are too low to trigger the accelerator at 1 Re, this current configuration would create the signature of a weak substorm current wedge. This is the precursory signal that was observed in each of the three events

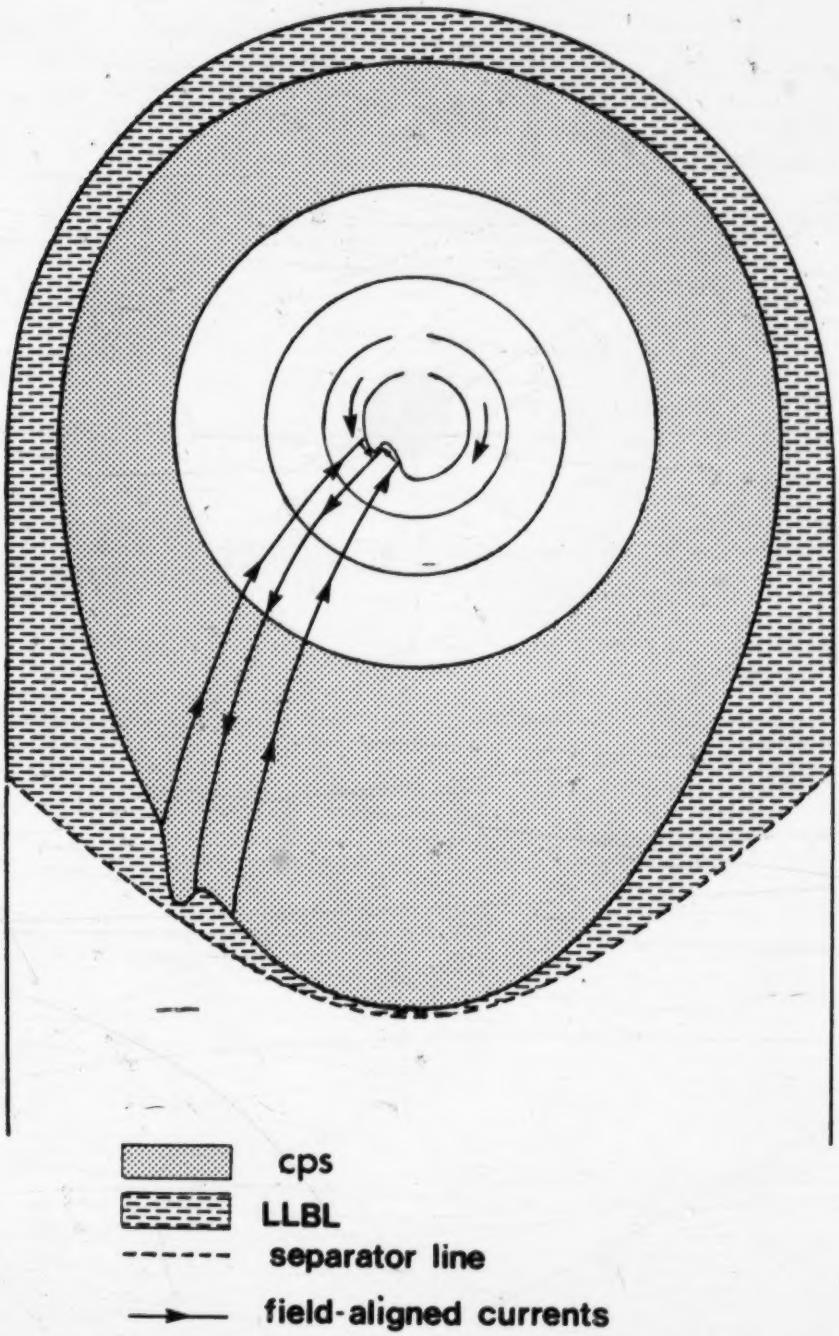

Figure 4.2 Mapping of field-aligned current created by Kelvin-Helmholtz waves from the CPS/LLBL interface to surge forms in the auroral ionosphere.

presented. The ionospheric component of the wedge was found to have a length from 10° to 15° in longitude (at approximately 68°N). This corresponds to length of 450 to 650 km which is on the order of the values of 600 to 800 km found by Tighe (1978) in a study of substorm surges. Because of the scale size of these forms, only single wedges could be observed, rather than a multiplicity of them. In the case of day 231, the border between the eastward and westward electrojets, which maps to the CPS/LLBL interface, was observed to move northward, implying the intrusion of CPS plasma into a region of space previously occupied by LLBL plasma. This suggests that for day 231, we have observed the growth of the surface wave at the CPS/LLBL boundary in the deep magnetotail.

The model gives field-aligned current densities associated with the precursory substorm current wedge of 360 mA/m for day 231 and 125mA/m for days 20 and 59. The model field-aligned currents were introduced along lines of constant geomagnetic longitude. However, field-aligned currents into the ionosphere have a greater areal extent, thus to calculate the areal densities of the field-aligned currents we assume that each of the upward and downward field-aligned currents has a longitudinal extent of 5°. This gives current densities of 1.6$\mu A/m^2$ for day 231 and .56$\mu A/m^2$ for days 59 and 20. These current densities are on the order of magnitude necessary to activate the accelerator at 1 Re. As the surface wave at the CPS/LLBL layer continues to grow,

the field-aligned currents increase, triggering the accelerator and resulting in the substorm expansive phase.

In summary, we have been able to establish current systems responsible for the geomagnetic perturbations seen just prior to onset. It was found that the precursory activity can be explained in terms of the Kelvin-Helmholtz instability at the CPS/LLBL interface. It was shown that this instability leads to the substorm current wedge and that the substorm current wedge can be observed before the time of the onset of the expansive phase.

BIBLIOGRAPHY

Akasofu,S.-I., Polar and Magnetospheric Substorms, *D. Reidel*, Dordrecht, 1968.

Akasofu,S.-I., Physics of Magnetospheric Substorms, *D. Reidel*, Dordrecht, 1977.

Arnoldy,R.L., Signature in the interplanetary medium for substorms, *Planet.Space Sci., 76*, 5189, 1971.

Axford,W.I., and C.O. Hines, A unifying theory of high latitude geophysical phenomena and geomagnetic storms, *Can. J. Phys., 39*, 1433, 1961.

Baumjohann,W., R.J. Pellinen, H.J. Opgenoorth, and E. Nielson, Joint two-dimensional observations of ground magnetic and ionospheric electric fields associated with auroral zone currents: Current systems associated with local auroral break-ups, *Planet. Space Sci., 29*, 431, 1981.

Biermann,L., Solar corpuscular radiation and the interplanetary gas, *Observatory, 77*, 109, 1957.

Boström,R., A model of the auroral electrojets, *J. Geophys. Res., 69*, 4983, 1964.

Braithwaite, K.S., and G. Rostoker, DP2 current system in the ionosphere and magnetosphere, *Planet. Space Sci., 29*, 485, 1981.

Chapman,S. and V.C.A. Ferraro, A new theory of magnetic storms, *Terr. Mag. Atmos. Elect. 36*, 77, 1931.

Coleman, P.J. and W.D. Cumming, Stormtime disturbance fields at ATS 1,*J. Geophys. Res.*, *76*, 51, 1971.

Dungey,J.W., Interplanetary magnetic field and the auroral zones, *Phys. Rev. Lett.*, *6*, 47, 1961.

Eastman, T.E., B. Popielawska, and L.A.Frank, Three-Dimensional plasma observations near the outer magnetospheric boundary, *J. Geophys. Res.*, *90*, 9519, 1985.

Greenwald, R.A. and A.D.M. Walker, Energetics of long period resonant hydromagnetic waves, *Geophys. Res. Lett.*, *7*, 745, 1980.

Hama, A., Streaklines in a perturbed shear flow, *Phys. Fluids*, *5*, 644, 1962.

Hasegawa,A., and T.Sato, Generation of field-aligned current during substorm, in *Dynamics of the Magnetosphere*, 529, ed. by S.-I. Akasofu, 1978.

Heikkila,W.J. and J.D. Winningham, Penetration of magnetosheath plasma to low altitudes through the dayside magnetospheric cusps, *J. Geophys. Res.*, *76*, 883, 1971.

Hill,T.W., Solar-wind magnetosphere coupling, in *Solar-Terrrestrial Physics*, edited by R.L. Carovillano and J.M. Forbes, 261, 1983.

Iijima,T., and T.A. Potemra, The amplitude distribution of field-aligned current at northern high latitudes observed by Triad, *J. Geophys. Res.*, *81*, 2165, 1976.

Kavanagh,L.D., Magnetospheric structure, in *Earth's Magnetospheric Processes*, edited by B. McCormac, 3, 1972.

Kisabeth, J.L., The dynamical development of the polar electrojets, *Ph.D. thesis, U of Alberta*, 1972.

Kisabeth,J.L. and G. Rostoker, Development of the polar electrojet during polar magnetic substorms, *J. Geophys. Res.*, *76*, 6815, 1971.

Kisabeth,J.L. and G. Rostoker, The expansive phase of magnetospheric substorms, 1. Development of the auroral electrojets and auroral arc configuration during a substorm, *J. Geophys. Res.*, *79*, 972, 1974.

Knight, S., Parallel electric fields, *Planet. Space Sci.*, *21*, 741, 1973.

McPherron,R.L., Growth phase of magnetospheric substorms, *J. Geophys. Res.*, *75*, 5592, 1970.

McPherron,R.L., C.T. Russell and M.P. Aubry, Satellite studies of magnetospheric substorms on August 15, 1968, 9. Phenomenological model for substorms, *J. Geophys. Res.*, *78*, 3131, 1973.

Michalke, A., On spatially growing disturbances in an inviscid shear layer. *J. Fluid. Mech.*, *23*, 521, 1965.

Ness, N.F., C.S. Scearce, and S. Cantaiano, Probable observation of the geomagnetic tail at 1000 Re by Pioneer 7, *J. Geophys. Res.*, *72*, 3769, 1967.

Opgenoorth, H.J., R.J. Pellinen, H. Maurer, F. Kuppers, W.J. Heikkila, K.U. Kaila, and P. Tanskanan, Ground-based observations of an onset of localized field-aligned currents during auroral breakup around magnetic midnight, *J. Geophys. Res.*, *48*, 101, 1980.

Parker, E.N., Interaction of the solar wind with the geomagnetic field, *Phys. Fluids*, *1*, 172, 1958.

Paschmann, G., Plasma structure of the magnetopause and boundary layer, in *Magnetospheric Boundary Layers*, edited by B. Battrick, 1979.

Pellinen,R.J., and W.J. Heikkila, Observations of auroral fading before breakup, *J. Geophys. Res.*, *83*, 4207, 1978.

Perreault,P., and S.-I. Akasofu, A study of geomagnetic storms, *Geophys. J.R. Astron. Soc.*, *54*, 547, 1978.

Petschek,H.E., Magnetic field line annihilation, NASA SP-50, Proceedings of AAS-NASA Symposium on the Physics of Solar Flares, ed. by W.N. Hess, 425, 1964.

Pu, Z.Y., and M.G. Kivelson, Kelvin-Helmholtz instability at the magnetopause: Energy flux into the magnetosphere, *J. Geophys. Res.*, *88*, 853, 1983.

Rostoker, G., Dependence of the high-latitude ionosphere fields and plasma characteristics on the properties of the interplanetary medium, in *High-Latitude Space Plasma Physics*, ed. by B. Hultquist and T. Hagfors,189, 1983a.

Rostoker,G., Triggering of expansive phase intensification of magnetospheric substorms by northward turnings of the interplanetary magnetic field, *J. Geophys. Res.*, *88*, 6981, 1983b.

Rostoker,G., The Kelvin-Helmholtz instability and its role in the generation of the electric currents associated with Ps 6 and westward travelling surges, in *Proceedings of the Chapman Conference on Magnetotail Dyanamics*, ed. by A.T.Y. Lui, in press, 1986.

Rostoker,G., H.-I. Lam, and W.D. Hume, Response time of the magnetosphere to the interplanetary magnetic field, *Can. Jour. of Physics*, *50*, 544, 1972.

Rostoker,G., and R. Boström, A mechanism for driving the gross Birkeland current configuration in the auroral oval, *J. Geophys. Res.*, *81*, 235, 1976.

Rostoker,G., S.-I. Akasofu, J. Foster, R.A. Greenwald, Y. Kamide, K. Kawasaki, A.T.Y. Lui, R.L. McPherron, and C.T. Russell, Magnetospheric substorms-definition and signatures, *J. Geophys. Res.*, *85*, 1663, 1980.

Rostoker, G., and J.C. Samson, Can substorm expansive phase effects and low frequency Pc magnetic pulsations be attributed to the same source mechanism?, *Geophys. Res. Lett.*, *3*, 271, 1984.

Rostoker,G., I. Spadinger, and J.C. Samson, Local time variations in the response of Pc 5 pulsations in the morning sector to substorm expansive phase onsets near midnight, *J. Geophys. Res.*, *89*, 6749, 1984.

Rostoker,G., Y. Kamide, and J.D. Winningham, Energetic particle precipitation into the high latitude ionosphere and the auroral electrojets, 3. Characteristics of electron precipitation into the morning sector auroral oval, *J. Geophys. Res.*, *90*, 7495, 1985.

Rostoker,G., S.-I. Akasofu, W. Baumjohann, Y. Kamide, and R.L. McPherron, The roles of direct input of energy from the solar wind and unloading of stored magnetotail energy in driving magnetospheric substorms, submitted to Space Sci. Rev.,1986.

Samson,J.C., G. Rostoker, Polarization characteristics of Pi2 pulsations and implications for their source mechanisms: Influence of the westward travelling surge, *Planet. Space Sci.*, *31*, 435, 1983.

Shawhan,S.D., C.G. Falthammar, and L.P. Block, On the nature of large auroral zone electric fields at 1-Re altitude, *J. Geophys. Res.*, *83*, 1049, 1978.

Tighe, W.G., A study of the westward travelling surge, *M.Sc. thesis*, U of Alberta, 1979.

Vasyliunas,V.M., Theoretical models of magnetic field line merging, *Rev. Geophys. Space Phys.*, *13*, 303, 1975.

Walker, A.D.M., The Kelvin-Helmholtz instability in the low-latitude boundary layer, *Planet. Space Sci.*, *29*, 1119, 1981.

Wiens,R.G., and G. Rostoker, Characteristics of the development of the westward electrojet during the expansive phase of magnetospheric substorms, *J. Geophys. Res.*, *80*, 2109, 1975.

Wolf, R.M., The quasi-static (slow-flow) region of the magnetosphere, in *Solar-Terrestrial Physics*, ed. by R.L. Carovillano and J.M. Forbes, 303, 1983.

Wolf,R.A., and M. Harel, Dynamics of the magnetospheric plasma, in *Dynamics of the Magnetosphere*, ed. by S.-I. Akasofu, 143, 1978.

APPENDIX

A. MHD Analysis of the Kelvin-Helmholtz instability

The magnetohydrodynamic (MHD) formulation describes an inviscid plasma which has infinite conductivity parallel to the magnetic field lines. The following equations, together with Maxwell's equations, describe the equilibrium state of such a plasma. They are:

the equation of motion

$$\frac{d}{dt}[\rho(\underline{r},t)\underline{v}(\underline{r},t)]=\underline{J}(\underline{r},t)x\underline{B}-\nabla p(\underline{r},t) \qquad A.1$$

the equation of mass conservation

$$\frac{\partial \rho}{\partial t}(\underline{r},t)+\nabla\cdot[\rho(\underline{r},t)\underline{v}(\underline{r},t)]=0 \qquad A.2$$

and the generalized Ohm's law

$$\eta\underline{J}(\underline{r},t)=\underline{E}(\underline{r},t)+\underline{v}(\underline{r},t)x\underline{B}(\underline{r},t) \qquad A.3$$

where $\underline{E}$ and $\underline{B}$ are the electric and magnetic field vectors, respectively, $\underline{v}$ is the fluid velocity, ρ is the plasma density, p is the particle pressure, and η is the resistivity.

The following derivation will give the growth rate and instability condition for an incompressible plasma with a tangential velocity discontinuity at a plane boundary. A cartesian coordinate system is chosen such that the boundary is in the yz plane with the velocity discontinuity occurring at x=0. Assuming that all perturbations are small the MHD equations can be linearized, i.e. all quantities can be written in the form

$$g=g_0+g_1$$

where g_0 is the unperturbed value and g_1 is the perturbation. Linearizing equation A.1 in this fashion, with the use of Maxwell's equation $\mu_0\underline{J}=\nabla x\underline{B}$ we find

$$\mu_0\rho_0\ddot{\underline{\xi}}=[(\nabla x\underline{B}_1)x\underline{B}_0+(\nabla x\underline{B}_0)x\underline{B}_1]-\nabla p_1 \qquad A.4$$

where a displacement vector ξ has been introduced which satisfies

$$\underline{v}=\partial\underline{\xi}/\partial t$$

and

$$\underline{B}_1=\nabla x(\underline{\xi}x\underline{B}) \qquad A.5$$

The dot notation indicates differentiation with respect to time. Using standard vector operations equation A.4 becomes

$$\nabla^2\tilde{p}_1=\nabla\cdot[(\underline{B}_1\cdot\nabla)\underline{B}_0+(\underline{B}_0\cdot\nabla)\underline{B}_1]/\mu_0-\nabla\cdot(\rho_0\ddot{\underline{\xi}}) \qquad A.6$$

where $\tilde{p}_1$ is the sum of the perturbed particle and magnetic pressures, given by

$$\tilde{p}_1=p_1+(\underline{B}_1\cdot\underline{B}_0/\mu_0) \qquad A.7$$

For an incompressible plasma $\nabla\cdot\underline{\xi}=\nabla\cdot\underline{v}=0$; thus, if we assume that the unperturbed plasma density is uniform (except at the boundary surface), the last term of equation A.6 drops out. Furthermore, if we assume that the unperturbed magnetic field is uniform (except at the boundary), equation A.5 becomes

$$\nabla^2\tilde{p}_1=0 \qquad A.8$$

away from the boundary surface. A non-trivial solution to this equation is

$$\tilde{p}_1=p_0\exp[-k|x|+i(k_y+k_z-\omega t)] \qquad A.9$$

where $k=(k_y^2+k_z^2)^{1/2}$. This is the equation for a surface wave in the yz plane. The perturbation goes to zero as the

distance from the boundary increases.

The plasma displacement vector is found by combining equations A.4 and A.5. In a uniform incompressible plasma $\underline{\xi}$ is given by

$$\underline{\xi}=\frac{\nabla p_1}{\rho[\omega^2-(\underline{k}\cdot\underline{v}_a)^2]} \qquad \text{A.10}$$

where $\underline{v}_a$ is the Alfvén velocity given by

$$\underline{v}_a=\underline{B}_0/\sqrt{\mu_0\rho}$$

and ρ is now used to represent the unperturbed density.

The boundary conditions are the continuity of the pressure and the normal component of the displacement across the boundary. Applying these boundary conditions to equation A.10 gives

$$\frac{1}{\rho_1}[(\omega-\underline{k}\cdot\underline{v}_0)^2-(\underline{k}\cdot\underline{v}_{a1})^2]+\frac{1}{\rho_2}[\omega^2-(\underline{k}\cdot\underline{v}_{a2})^2]=0$$

where the subscripts 1 and 2 refer to the regions $x>0$ and $x<0$, respectively. The term $(\omega-\underline{k}\cdot\underline{v}_0)$ is the Doppler shifted frequency with respect to ω, and $\underline{v}_0$ is the relative velocity between regions 1 and 2.

Assuming that time variations are of the form $\exp[i\omega t]$, the condition for instability is that ω must be complex and have a negative imaginary part. Solving the above equation for ω gives the instability condition

$$(\underline{k}\cdot\underline{v}_0)^2>(\frac{1}{\rho_1}+\frac{1}{\rho_2})[\rho_1(\underline{k}\cdot\underline{v}_{a1})^2+\rho_2(\underline{k}\cdot\underline{v}_{a2})^2] \qquad \text{A.11}$$

for the Kelvin-Helmholtz instability. The growth rate for the instability is then given by

$$\gamma^2=\frac{\rho_1\rho_2(\underline{k}\cdot\underline{v}_0)^2}{(\rho_1+\rho_2)^2}-\frac{\rho_1(\underline{k}\cdot\underline{v}_{a1})^2+\rho_2(\underline{k}\cdot\underline{v}_{a2})^2}{\rho_1+\rho_2} \qquad \text{A.12}$$

Thus the growth rate for the Kelvin Helmholtz instability is

proportional to the wave number in an incompressible plasma featuring a tangential velocity discontinuity.